NOVEL OPERATIONAL CONDITION MONITORING TECHNIQUES FOR WIND TURBINE BRAKE SYSTEMS

by

Mani Entezami

A thesis submitted to

The University of Birmingham

for the degree of

DOCTOR OF PHILOSOPHY

School of Electronic, Electrical and Computer Engineering

College of Engineering and Physical Sciences

University of Birmingham

July 2013

Abstract

In the event of important component failure or during conditions where wind speed is over the design limit, it is crucial for wind turbines to stop operating. A failure in the braking system of wind turbines may result in loss of the whole structure.

This thesis addresses the problem of automatic detection and diagnosis of faults within wind turbine brake systems. The main aim is to develop a cost effective and non-intrusive condition monitoring solution that could cover the existing lack of automatic health monitoring systems on brake systems. This can be used to either enhance safety or achieve a more affordable current level of safety.

The use of an induction motor as a sensor to identify faults within the hydraulic unit of the brake system has been explored. The braking event was also used as an input to an analysis which identified faults within blade systems. The use and further development of appropriate fault detection and diagnosis methods within electrical machines using several detailed case studies to monitor the condition of wind turbine brake systems has been demonstrated.

In conclusion, it is shown that the results of the analyses of laboratory and field trial experiments with the proposed approaches and simulations have the potential to develop a comprehensive commercialised condition monitoring application for wind turbine brakes.

Acknowledgments

I would like to thank the following for their priceless contribution to this PhD work:

Stuart Hillmansen for being an excellent supervisor, Welsh companion, friend and especially for monitoring my passport and driving me back home with no drowsiness.

Clive Roberts and Edd Stewart for their outstanding support, supervision, friendship, conga dancing, problem solving and drinking skills.

Paul Weston for his appreciated discouragements, disapprovals and criticisms along with extraordinary technical and mathematical support.

Mayorkinos Papaelias, Fausto Pedro García Márquez and NIMO project (Development and Demonstration of a Novel Integrated Condition Monitoring System for Wind Turbines, FP7-ENERGY-2008-TREN-1: 239462) for managing and organising conferences and the industrial trials, and the funding.

Jon Tutcher, Gremmie Yeo and Gemma Nicholson for their delightful friendship and supplementary tea and biscuits they provided during this work.

Mary Winkles for tracking me down for deadlines and reports and more importantly reporting my presence to the UK border agency.

Claire Davis and Pietro Tricoli for their valued supervision and appreciated clarifications.

Katherine Slater for anglicising this thesis.

Adnan Zentani and Andy Dunn for their technical disagreements on health and safety issues.

My ex for leaving me in peace.

My family, especially my mum and sister for their love and support.

My friends and every individual in the railway group for their friendship and care.

Finally, the wonderful lovely old witch, Nutmeg, from whom I have been provided nothing but love.

Contents

LIST OF FIGURES ..... **V**

LIST OF TABLES ..... **X**

CHAPTER 1 INTRODUCTION **1**

1.1 Overview 1

1.2 Wind turbine fundamentals 3

1.3 Induction machines and wind turbines 8

1.4 Faults and failures 9

1.5 Failures in wind turbines 10

1.6 Wind turbine brake systems 11

1.6.1 Aerodynamic brakes *12*

1.6.2 Mechanical brakes *13*

1.6.3 Electrodynamic brakes *14*

1.6.4 Braking design considerations *15*

1.7 Thesis outline 17

1.7.1 Objectives *17*

1.7.2 Summary *18*

1.7.3 Structure of the thesis *19*

CHAPTER 2 RESEARCH METHODS **22**

2.1 Introduction 22

2.2 Fault detection and diagnosis approaches 22

2.2.1 Quantitative models *23*

2.2.2 Qualitative models *26*

2.2.3 Process history methods *27*

2.3 The three-phase induction motor 28

2.4 State of art on induction machine condition monitoring 29
2.4.1 Vibration monitoring 30
2.4.2 Thermal monitoring 30
2.4.3 Magnetic flux 31
2.4.4 Electrical measurements 31
2.4.5 Comparison and summary 32
2.5 Applied fault detection and diagnosis approaches in this work 35
2.5.1 Fast Fourier transform 35
2.5.2 Spectrogram 37
2.5.3 Park's vector 37
2.5.4 Envelope analysis 41
2.5.5 Parameter estimation 42
2.6 Data acquisition in condition monitoring systems 45
2.6.1 Fault tolerance data acquisition approach 46
2.7 Summary 48
CHAPTER 3 EXPERIMENTAL CONDITION MONITORING OF LABORATORY INDUCTION MACHINES 49
3.1 Introduction 49
3.2 Data acquisition system 49
3.3 Measurements and analysis 53
3.3.1 A 3 HP with excitation – power lab 53
3.3.2 Fatigue machine - hydraulic power unit 62
3.3.3 Ventilation fan system 67
3.3.4 1.1 kW induction motor 74
3.4 Summary 84
CHAPTER 4 NEG MICON 750 BRAKE HYDRAULIC POWER UNIT 86
4.1 Introduction 86
4.2 Measurements and analysis 88
4.2.1 Data acquisition 88

4.2.2 Data analysis *90*

4.3 SIMULATION OF THE HYDRAULIC POWER UNIT 93

4.4 SUMMARY 99

CHAPTER 5 V47 AND AW1500 HYDRAULIC POWER UNIT 101

5.1 INTRODUCTION 101

5.2 VESTAS V47-660 HYDRAULIC POWER UNIT CONDITION MONITORING 101

5.2.1 Introduction *101*

5.2.2 Instrumentation *102*

5.2.3 Data Analysis *104*

5.3 ACCIONA AW1500 HYDRAULIC SYSTEM CONDITION MONITORING 109

5.3.1 Introduction *109*

5.3.2 Instrumentation *110*

5.3.3 Data analysis *111*

5.4 SUMMARY 117

CHAPTER 6 BLADE TIP MONITORING 118

6.1 INTRODUCTION 118

6.2 DATA ANALYSIS 119

6.3 MODELLING 121

6.4 SUMMARY 128

CHAPTER 7 CONCLUSIONS 130

7.1 INTRODUCTION 130

7.2 KEY ACHIEVEMENTS 130

7.3 FURTHER AREAS FOR INVESTIGATION 132

7.4 PUBLICATIONS 132

REFERENCES 134

APPENDIX A - BLUEBEAR CONFERENCE POSTER 149

APPENDIX B - CM2011 CONFERENCE PAPER 150

APPENDIX C - PHM SOCIETY DOCTORAL CONSORTIUM 162

APPENDIX D - RENEWABLE ENERGY JOURNAL PAPER 165

APPENDIX E - IET CONFERENCE POSTER 173

APPENDIX F - MEG III CONFERENCE POSTER 174

List of Figures

Figure 1.1: Main components of a typical wind generator 4

Figure 1.2: Total global installed wind capacity 6

Figure 1.3: Common design technology for HAWT 8

Figure 1.4: Sub-system failure rates for a Swedish wind power plant (2000-2004) 10

Figure 1.5: NEG Micon 750 blade tips 12

Figure 1.6: Hydraulic unit of Vestas V47-660 kW wind turbine 13

Figure 1.7: NEGM750 hydraulic/accumulator system 14

Figure 1.8: Experimental electromagnetic brake on a NEG Micon 750 15

Figure 2.1: Quantitative process model approach 24

Figure 2.2: An example of a fault tree diagram 27

Figure 2.3: Fourier Transform of a phase of a healthy motor current 36

Figure 2.4: Spectrogram of one phase of a healthy motor current 37

Figure 2.5: Ideal simulated three-phase current 38

Figure 2.6: Ideal Park's transform of the simulated three-phase 39

Figure 2.7: Simulated-three phase with 5^{th} harmonic and 2 kHz sampling rate 39

Figure 2.8: Park's Transform of the simulated three-phase with 5th harmonics 40

Figure 2.9: FFT of the simulated current with the 5^{th} harmonic 40

Figure 2.10: Example of Hilbert transform in generating the envelope signal 42

Figure 2.11: A mass spring damper system 44

Figure 2.12: Overview of a fault tolerant embedded system 48

Figure 3.1: Overview of the developed condition monitoring system 52

Figure 3.2: Finalised data processing unit prototype for NIMO project 52

Figure 3.3: Power lab traction system 53

Figure 3.4: Two cycles of the line to line voltage measured from the PWM generator 54

Figure 3.5: FFT analysis of the PWM generated voltage for the motor 55

Figure 3.6: Current measurements from the three-phase motor ran by a PMW system 56

Figure 3.7: FFT analysis of the three-phase current 56

Figure 3.8: Filtered current measurements from the PWM driven motor 57

Figure 3.9: FFT analysis of the motor three phase currents with 2 kHz RC filter 57

Figure 3.10: Voltage measurements of the system 58

Figure 3.11: Current measurements of the system 58

Figure 3.12: Spectrogram of the 0-1500 rpm experiment 59

Figure 3.13: Current measurements from a no-load to full-load situation 60

Figure 3.14: Spectrogram of the current measurement for no-load to full-load 60

Figure 3.15: Three-phase current measurements from a no-load to half-load situation 61

Figure 3.16: Spectrogram of the current measurement for no-load to full-load 61

Figure 3.17: 1.1 kW hydraulic power unit driving a fatigue machine 62

Figure 3.18: Current measurement at 150 bar 63

Figure 3.19: Current measurement from 0 - 150 bar 64

Figure 3.20: Spectrogram of the measured current at 10 kHz sampling rate 65

Figure 3.21: Spectrogram of the measured current at 2 kHz sampling rate 65

Figure 3.22: Characteristics of a third order Butterworth filter 66

Figure 3.23: Spectrogram of the measured current at 2 kHz 66

Figure 3.24: Spectrogram analysis for higher frequency range 67

Figure 3.25: Wiring diagram of the ventilation fans 68

Figure 3.26: Installed sensor within the control box 68

Figure 3.27: 1.1 kW ventilation fan located at the railway centre traction lab 69

Figure 3.28: Sampled experiment of the running ventilation fan 69

Figure 3.29: Zoomed windows of the starting and end point of the fan operational period 70

Figure 3.30: Park's transform of the sampled event 70

Figure 3.31: Park's transform of the current without the starting peak 71

Figure 3.32: Park's transform of an abnormal situation 72

Figure 3.33: Spectrogram of the measured signal with the possibility of impulsive noise 72

Figure 3.34: Spectrogram of a healthy measurement 73

Figure 3.35: Stator current FFT analysis (100-1000 Hz) 74

Figure 3.36: 1.1 kW three-phase motor 75

Figure 3.37: Measured three-phase current from the starting point until it stopped 76

Figure 3.38: Voltage measurements of the motor 76

Figure 3.39: Fast Fourier of the healthy condition measurements 77

Figure 3.40: Time-Frequency spectrogram analysis of the healthy condition 77

Figure 3.41: Park's transform of the healthy condition 78

Figure 3.42: Envelope of the original signal using peak detection method 78

Figure 3.43: Envelope of the original signal using Hilbert transform 79

Figure 3.44: Comparison of one phase from a healthy and a faulty measurement 79

Figure 3.45: FFT of the healthy and faulty conditions 80

Figure 3.46: Spectrogram of the faulty condition 81

Figure 3.47: Park's transform of the healthy and faulty condition 81

Figure 3.48: Hilbert transform of the healthy and faulty condition 82

Figure 3.49: Envelopes of the healthy and faulty condition 82

Figure 3.50: Frequency analysis of faulty and healthy condition voltages 83

Figure 3.51: Spectrogram of the voltage in healthy condition 83

Figure 3.52: Spectrogram of the voltage in faulty condition 84

Figure 4.1: SIME-Industry mechanical brake system installed on NEG Micon 750 86

Figure 4.2: Hydraulic system of NEG Micon 750 87

Figure 4.3: The main control panel of the NEG Micon and the UoB data logging system 89

Figure 4.4: Automatically recorded data from the hydraulic unit by UoB data logging unit 89

Figure 4.5: FFT of the current of the recorded event 90

Figure 4.6: Spectrogram of the captured current 91

Figure 4.7: Current data from 5 different events 92

Figure 4.8: FFT spectrum of the 5 current samples 93

Figure 4.9: Model of the hydraulic brake system in Simulink 94

Figure 4.10: Current envelope of the simulation and real data and their categorisation 95

Figure 4.11: FFT spectrum of a phase from the simulation 96

Figure 4.12: Spectrogram of the current from the simulation 96

Figure 4.13: Envelope curve of the three simulated conditions 97

Figure 4.14: FFT spectrum of the three simulated conditions 97

Figure 4.15: Moving RMS for every 5 cycles of the faulty and healthy conditions 98

Figure 4.16: Simulated three-phase current with one faulty phase to ground line 99

Figure 4.17: Park’s transform of a simulated healthy condition and a faulty phase situation 99

Figure 5.1: Terna Energy wind farm, Evia, Greece 102

Figure 5.2: V47 nacelle control panel 102

Figure 5.3: Instrumentation used for remote monitoring of the V47 hydraulic power 103

Figure 5.4: Overview of the condition monitoring system for the V47 turbine 103

Figure 5.5: Captured event from the V47 hydraulic unit 104

Figure 5.6: The event of pumping up to 250 bar 105

Figure 5.7: Performance duration of the recorded events 106

Figure 5.8: Final peak of the current values 106

Figure 5.9: Park's vector of a healthy and the faulty conditions 107

Figure 5.10: Spectrogram of the current from the V47 hydraulic unit in healthy condition 107

Figure 5.11: Spectrogram of the current from the V47 hydraulic unit in faulty condition 108

Figure 5.12: Filtered and zoomed form of the faulty current data 108

Figure 5.13: Filtered and zoomed form of a healthy current data 109

Figure 5.14: AW1500 hydraulic power system 110

Figure 5.15: Installation of current clamps within the control box of the AW1500 111

Figure 5.16: Wind speed measurement from the day of the trial 111

Figure 5.17: Shaft speed along with hydraulic pressure of the AW1500 112

Figure 5.18: Hydraulic pressure in normal and intentional fault conditions 113

Figure 5.19: Increase in hydraulic pressure and current envelope 114

Figure 5.20: Current data, starting hydraulic pressure 174 bar and ending around 228 bar 114

Figure 5.21: Spectrogram of the current 115

Figure 5.22: Hydraulic pressure for the 100 seconds from the starting point 116

Figure 5.23: Current data for the hydraulic pressure sections 116

Figure 6.1: NEG Micon 750 with applied brake tips 118

Figure 6.2: Shaft speed sensor 119

Figure 6.3: High-speed shaft data in three wind speed conditions during braking 120

Figure 6.4: FFT analysis of the shaft speeds 121

Figure 6.5: The process of IMF 124

Figure 6.6: IMF level 1 of the shaft speed data 125

Figure 6.7: Simulink model of the shaft speed with the use of estimated parameters 125

Figure 6.8: Measured high speed shaft velocity versus simulated data 126

Figure 6.9: FFT of the measured data and the simulation output 126

Figure 6.10: FFT of the simulated fault versus the measured data 127

Figure 6.11: Simulated icing fault and healthy measured data 128

List of Tables

Table 1.1: Induction motors used in NEG Micon 750 wind turbines 9

Table 2.1: Faults in induction machine and efficacy of condition monitoring methods 32

Chapter 1 Introduction

1.1 Overview

Progress in electrical, mechanical, civil and control engineering has continued to drive enhancements within the wind energy industry. This has resulted in more powerful and efficient components, such as larger towers, blades, electrical machines and power electronics. At present, wind energy is the most developed renewable technology with a vast number of wind turbines used across the world, as well as the many projects currently in progress [1]. In 2010, 10% of the UK's electricity was generated by wind turbines; the UK government has set a target of 15% by 2015 [2].

Due to the immense increase in production and implementation of wind turbines, reliability and operational maintenance have become ever more important. New technologies and complexity within the design of the turbines have increased the possibility of faults occurring, which requires improvements in the consistency of production and reliable health monitoring systems. Analyses of wind farm maintenance costs show that up to 40% of the outlay is related to unexpected component failures which lead to costly unscheduled repairs. Wind farm operators constantly seek to minimise these expenses. Moreover, situations involving major failures often result in catastrophic damage, jeopardising investments, reputations and confidence in wind energy [3].

Three-phase induction machinery has been widely used in commercial and industrial applications. This is due to its simple structure, virtually maintenance free operation and the ability to be driven directly from the grid or standard power lines. Induction machines are

commonly used in wind turbines as actuators for a range of subsystems, therefore their operation and maintenance is important for wind farm operators.

Within a wind turbine there are a vast number of subsystems. The design of a wind turbine integrates many different engineering disciplines, for example, aerodynamics, structures, machines and transmissions. The overall system reliability is therefore affected by the interaction between these different aspects. Mindful system integration is required to minimise the probability of system failure and the associated downtime [4].

In the design of a wind turbine, the wear and lifetime of the components are critical, but geographical and environmental studies are also required. Wind gusts, lightning, icing, wildlife (such as bird collisions) and changes in climate are all examples that should be considered when a wind farm is being planned. These can all cause structural damage and, consequently, failures that lead to loss of revenue [5].

Early fault detection via regular inspection of the system components helps to prevent and reduce the number of major breakdowns. The use of condition monitoring systems within wind turbines has been significantly increased by wind farm operators. This is due to the ease of scheduled maintenance, possible improvement in fault detection and diagnosis of the whole system and optimisations [6]. Existing condition monitoring systems are normally based on a supervisory control and data acquisition. A variety of sensors, such as temperature, voltage, current, vibration and speed are installed within different components [7].

Monitoring almost every single component of a wind turbine can be costly. Transferring data to the processing and control centre and its subsequent analysis requires a huge amount of data processing procedures, which are expensive and time consuming. Therefore, using a condition monitoring system that can look only at the critical components might be more

desirable to the operators. An appropriate choice of sensors and data processing unit would also help to maintain the effectiveness and lower the cost of the monitoring system.

Adaptivity of condition monitoring systems, for those existing wind turbines that suffer a lack of a suitable monitoring system, has also been of interest to operators. Thus a condition monitoring approach that can be retrofitted, installed and maintained easily would be advantageous for the wind industry [8].

This thesis primarily addresses the development of retrospective condition monitoring systems which can be fitted to existing wind turbines to improve their performance. A key requirement of such a system is that it should be effectively non-intrusive and use simple sensors. The main focus of the work is on the rotating machinery within a turbine. This includes both the induction machines used for actuation and the main power generating equipment.

1.2 Wind turbine fundamentals

Wind is the movement of air mass from a high pressure area to a low pressure area and is mainly caused by differences in temperature within the atmosphere. A high difference in pressure increases the velocity of the wind. Changes in the weather, location, region and altitude are all factors that have a significant effect on wind speed and direction [9]. A wind turbine is a rotating machine that converts the kinetic energy of the wind to mechanical energy, resulting in the production of electricity using electrical generators. The rotary part can be either vertical or horizontal, which classifies the two different types of turbine: vertical and horizontal axis wind turbines (VAWT and HAWT).

The most commonly used wind turbines are horizontal-axis with two or three blades. Having the rotor positioned on the top of the tower creates a more efficient system, as more wind energy is produced compare to VAWTs. These turbines also have housing held up by the

tower, called the nacelle, which contains the gearbox and generator. A yaw system, which turns the nacelle and rotor to face the wind, enables the turbine to capture the highest amount of energy by facing the direction of the wind. Additionally, some wind turbine blades have moveable blade tips, which are used as air brakes. Figure 1.1 illustrates the components involved in a three bladed horizontal-axis wind turbine [9].

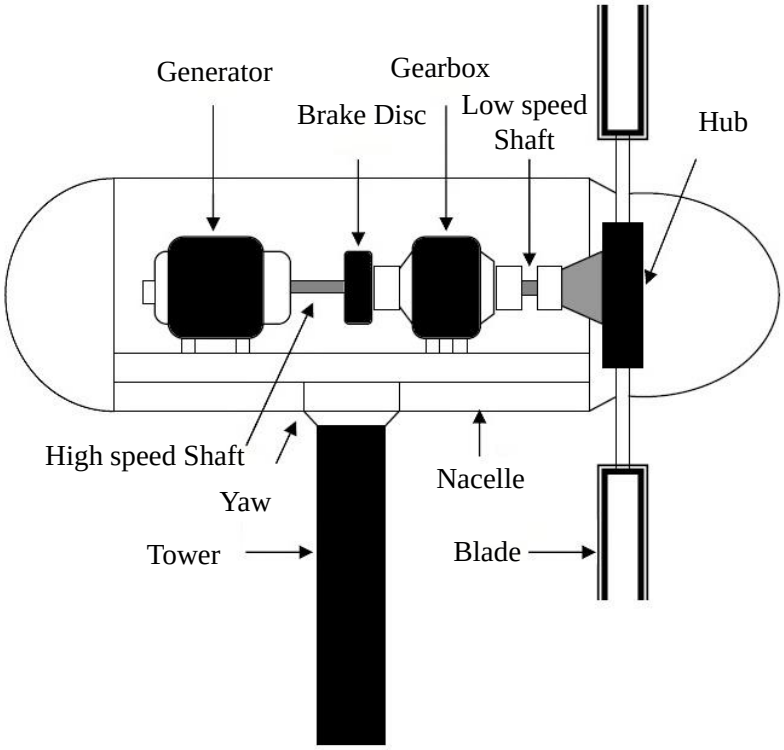

Figure 1.1: Main components of a typical wind generator
adapted from [10]

Here are brief descriptions of wind turbine components a selection of which are shown in Figure 1.1 [11]:

- Blades: capture the wind energy, are made of advanced composite materials, normally fibre reinforced plastics.
- Rotor: the blades, hub, low-speed shaft and bearing together are known as the rotor.
- Pitch: controls the direction of the blades to face the wind.

- Mechanical brake: disk-based brake that applies force to stop the rotation during emergencies, it is also known as the parking brake during maintenance.
- Low-speed shaft: a shaft that is rotated by the rotor.
- Gearbox: increases the speed of the low-speed shaft to a suitable value that is required in electricity generators.
- Generator: an electrical machine that converts the mechanical energy to electrical energy.
- Controller: starts and stops the turbine in specific wind speeds to ensure safety.
- Anemometer: measures the wind speed and conveys it to the controller.
- Wind vane: calculates the wind direction and communicates with the yaw system.
- Nacelle: a large cover on the top of the tower to protect the electrical and mechanical transmission system.
- High-speed shaft: drives the generator from the gearbox.
- Yaw drive: allows the rotor to face the wind as wind direction changes.
- Yaw motor: moves the yaw drive.
- Tower: made from steel lattice or tubular steel. Taller towers capture more energy and generate more electricity as wind speed increases with height.

The main advantage of vertical-axis wind turbines is that the gearbox and transmission systems are placed at ground level; this allows easy access for maintenance. Another advantage is their ability to capture the wind regardless of the wind direction, therefore no yaw system is required. However, maintenance of these turbines is not straightforward, as removal of the rotor is often required. The maximum power rating of this type of turbine is reported to be about 4 MW [12]. Due to the aerodynamic design, the capture of energy is not efficient; in circumstances such as lower wind speeds they will require assistance to start. For higher power rated VAWTs, larger landscape is required as guy-wire is necessary for

supporting the structure. VAWTs, in range of 2 to 10 kW, are mainly used for grid independent situations and in the places where the wind often changes direction [13].

The annual worldwide generated wind turbine energy output has significantly improved since the late 1990s. Figure 1.2 shows the increase in global wind energy capacity since 1997. In spite of the fact that recent wind turbines are constructed to high technical standards, there are still research areas that require further development, particularly in medium to large size turbines (500 kW and above) and maintenance methods. Within the last few years, wind turbine manufacturers and operators have focused on developing advanced condition monitoring systems in order to evaluate the structural condition of wind turbines, as well as the operational state. This has led to a significant enhancement in early fault detection and reduction in maintenance time.

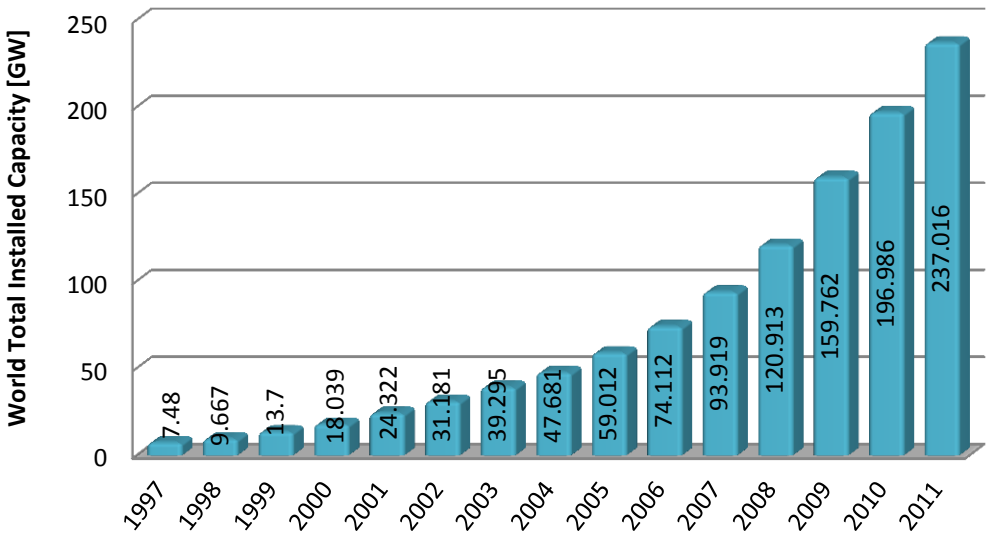

Figure 1.2: Total global installed wind capacity [1]

HAWTs can be categorised in two ways: fixed and variable speed.

In the fixed-speed category, there are two main types of design. In the first type, the turbine does not have a pitch system and the design of the blade stalls the wind speed at a certain velocity and produces an assured torque; this type is also known as passive stall. The generated torque passes through a gearbox and produces a speed for the high-speed shaft that will be suitable for an asynchronous generator and therefore a direct connection to the grid. However, in the second type, known as active stall, a simple pitch unit has been implemented in order to optimise the efficiency of the captured energy by small changes within the blade angles at different wind speeds [14].

The most advanced wind turbines are able to operate at variable rotor speeds. This allows for flexible operation and the most efficient power generation. One of the existing configurations is variable slip, which uses a wound rotor induction motor. This consists of windings, which allow the resistance of the rotor to be changed to produce a suitable torque in different wind conditions. The most common configuration is the pitch-controlled system, which has a hydraulic unit that drives the pitch and changes the blade direction to face the wind, thus optimising the output energy [14]. Figure 1.3 demonstrates the common configurations in wind turbine design.

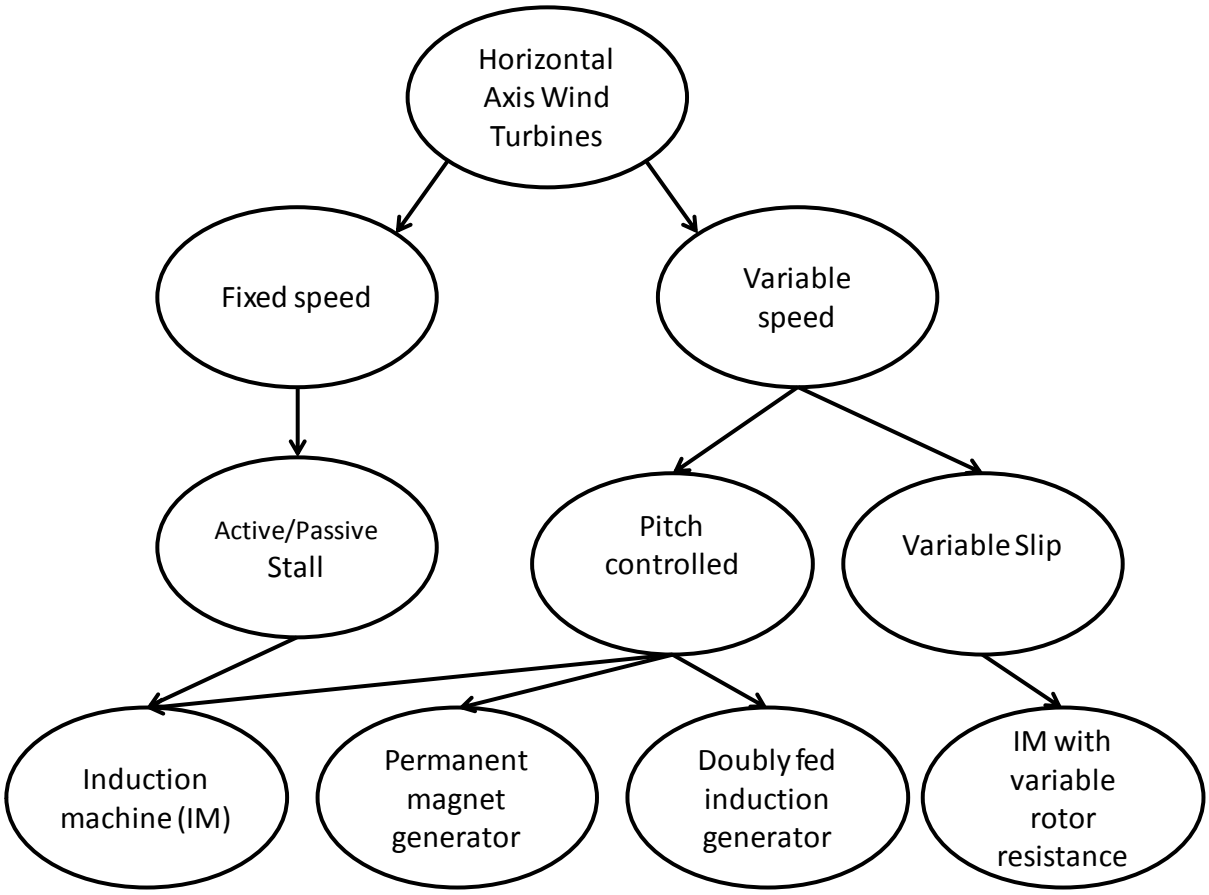

Figure 1.3: Common design technology for HAWT [14,9].

1.3 Induction machines and wind turbines

There are several uses of induction machinery within wind turbine actuator devices. One of the main parts of a wind turbine is the generator, which is an induction machine. The yaw system is also driven by three-phase induction motors. Maintaining pressure within hydraulic units, brake and pitch systems are other uses of three phase machines in wind turbine design. For example, in the NEG Micon 750 wind turbine (NM48/750, 48 m blade diameter and 750 kW nominal output power) up to 10 induction motors are used.

Place of use	Type of Motor	Quantity
Generator	Asynchronous 750/200 kW	1
Yaw	Asynchronous 0.37 kW	3-4
Brake Hydraulic	Asynchronous 0.37 kW	1
Gear Oil Pump	Asynchronous 1.1 kW	1
Water Cooling	Asynchronous 0.53 kW	1
Service Crane	Asynchronous 0.55 kW	1
Gear Oil Cooling Fan	Asynchronous 0.55 kW	1

Table 1.1: Induction motors used in NEG Micon 750 wind turbines [15]

Operation and maintenance of these systems are critical for wind farm operators. Thus, placing a suitable condition monitoring system on each unit in order to detect and diagnose faults in early stages is beneficial.

1.4 Faults and failures

The engineering definition of the term ‘fault’ is an unpermitted abnormality or deviation of any system parameters from an acceptable condition. When a fault within a system prevents normal operation, a malfunction, this stops the system functioning, thus causing a failure. A failure to operate is a breakdown [16,17]. Detecting the fault type, magnitude, time of occurrence and location in a system are the main factors involved in fault detection and diagnosis systems. In a fault detection and diagnosis system the following tasks are followed [16]:

- Fault detection: *Indicates that a fault has occurred in the system.*
- Fault diagnosis: *Determines the type of fault. This could lead to finding the possible location (component) of the failure*.
- Fault identification: *Extracts the characteristics of the fault such as seriousness and significance. It also determines the exact location of the failure.*

1.5 Failures in wind turbines

When a failure occurs inside the wind turbine, for example oil temperature exceeding a critical threshold in the gearbox, the control unit either logs the failure directly or registers the consequences of the fault. It then responds, depending on the type of malfunction. Sometimes, in order to avoid safety hazards or main system breakdowns, the turbine has to be shut down. Often they are restarted because of erroneous failure detection, which could be caused by noise within the system. If the failure is serious, a visual inspection has to be made which can be carried out by the operators. Finally, whenever a major failure has happened, a report is written.

Figure 1.4 describes the failure rates within the main components. This pie chart is an example of component failures that have happened in a wind farm in Sweden.

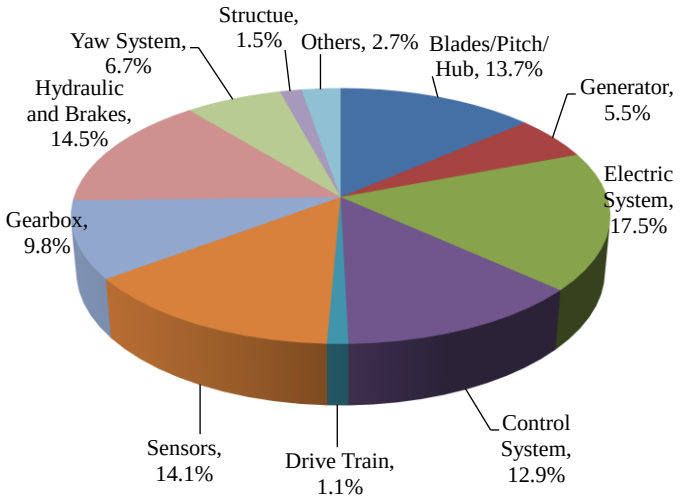

Figure 1.4: Sub-system failure rates for a Swedish wind power plant (2000-2004) [18]

1.6 Wind turbine brake systems

It is essential for wind turbines to stop operating in the case of failure of critical components and at wind speeds over a critical limit. Failure to brake the wind turbine rotation may result in loss of the whole structure [19].

Wind turbine brake systems are generally monitored by manual inspections and observations by the operator. Automated online performance and condition monitoring of braking systems leads to early fault detection of the system components and also helps to minimise the number of major breakdowns, reducing downtimes.

Within this thesis the braking mechanisms of a passive stall and a pitch-controlled wind turbine are discussed. The present study explores an online condition monitoring approach of the braking system hydraulic power currents and the speed of the high speed shaft as a comprehensive method of brake system fault diagnosis. Measurements of the high-speed shaft and electrical currents in the hydraulic unit can be used to effectively monitor the condition of the brakes and lead to successful detection of faults.

According to the International Electrotechnical Commission standard, EN 61400-1:2004, wind generators must have at least one braking system that can stop the turbine completely from any operating speed. In order to meet DS472 (Danish Standard) requirements, each turbine has to have at least two fail-safe brake units [20,21].

The three main types of braking system are: aerodynamic, mechanical and electrical (generator).

Aerodynamic braking (feathering and blade tips) and electromagnetic, if available, are mainly applied for the first few moments to reduce the speed and then a combination of these with the mechanical brake are used to bring the turbine to a complete stop [22].

1.6.1 Aerodynamic brakes

Aerodynamic braking varies depending on the type of wind turbine. In active stall and pitch controlled wind turbines, aerodynamic braking generates an aerodynamic torque that acts against the rotor torque by rotating the blades by 90° from their normal position. In stall wind turbines, aerodynamic braking is mainly applied by the blade tips [20]. Figure 1.5 is a photograph of a NEG Micon 750 wind turbine blade in operation and before installation.

Figure 1.5: NEG Micon 750 blade tips
upper image captured while blade tip brake was activated; lower image is the blade tip part (foreground) to be installed on a blade [Author's collection]

Blade tips are mounted flaps at the end of the blades. The application of blade tips causes a force against the normal rotation direction of the rotor and consequently reduces the speed. They usually have to be reset to the normal position by the operator as the occurrence of blade tip braking is normally caused by a failure or very high wind speed. Within this work it has been discovered that currently the condition monitoring of wind turbine blade tips is often based on the operator's observations [23].

In pitch controlled wind turbines, aerodynamic braking is applied by changing the angle of pitch to face the wind against the normal direction and adjusting the angle of pitch to a position in which no mechanical torque would be transferred. Pitch systems are usually driven by a hydraulic unit via a cylinder connected to each blade. In some turbines the same

hydraulic unit drives other parts as well, such as the mechanical brake, for example the Vestas V39/V4x/V90 [24]. Figure 1.6 shows a V47 turbine hydraulic unit installed in the nacelle.

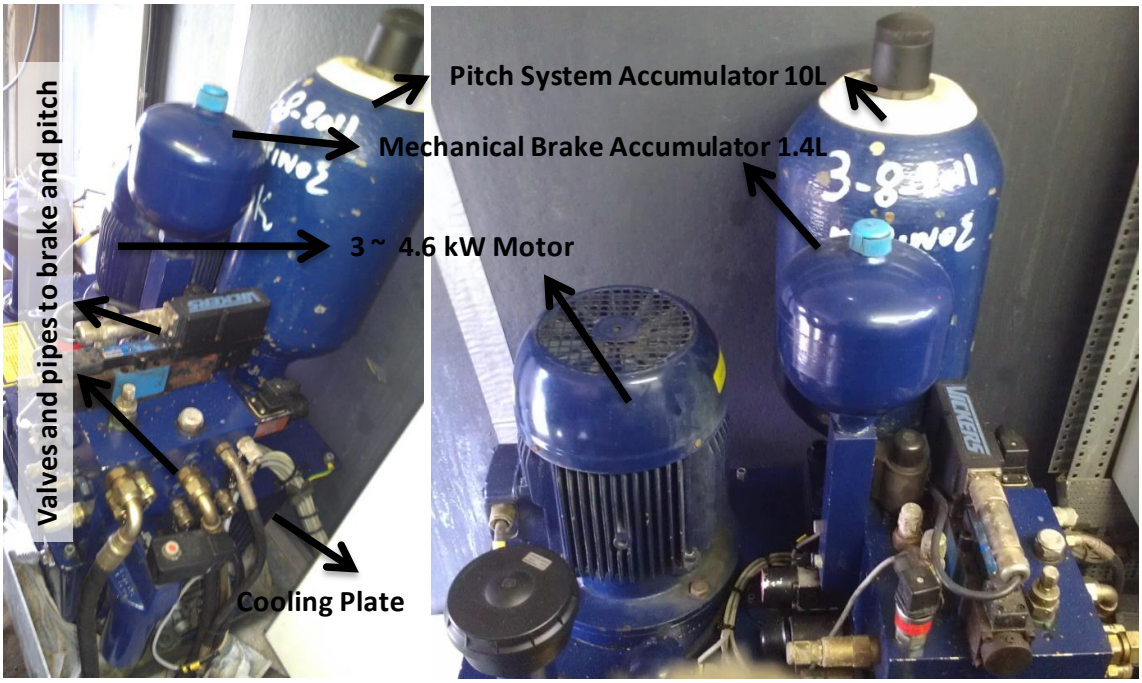

Figure 1.6: Hydraulic unit of Vestas V47-660 kW wind turbine
located in the nacelle; on the left valves and pipes along with the 4.6 kW three phase motor and two accumulators can be seen, on the right is the same unit from a different angle [Author's collection].

1.6.2 Mechanical brakes

Mechanical brakes are usually fail-safe brakes that are installed on the high-speed shaft, due to the lower torque needed compared to braking the low-speed shaft.

In stall wind turbines, the mechanical brake is usually applied after the release of the blade tips, while in pitch controlled turbines the mechanical brake will only be applied during emergencies or maintenance of the critical components.

The requirement to apply mechanical braking during operation may be almost eliminated thanks to improvements in aerodynamics, hydraulic soft braking and electrodynamic braking

methods [25]. However, to meet safety requirements, the installation of a fail-safe mechanical brake must be considered within the design [21].

The mechanical brake system hydraulic pressure is usually monitored and controlled by the main controller. Remarkably, the other parts are not automatically monitored and the maintenance and condition monitoring are based on the operator's regular inspections and observations. Figure 1.7 is the hydraulic unit and brake disc of a NEG Micon 750 wind turbine.

The hydraulic power unit keeps the wind turbine brakes disengaged. Pads are mounted on the callipers that apply force when the hydraulic pressure is released; this creates friction between the pads and the disc, thus causing braking to occur. During normal operation of the wind turbine, the hydraulic power, provided by the gear pump, is used periodically to maintain the pressure in the accumulator to release and keep the pads off the brake disc.

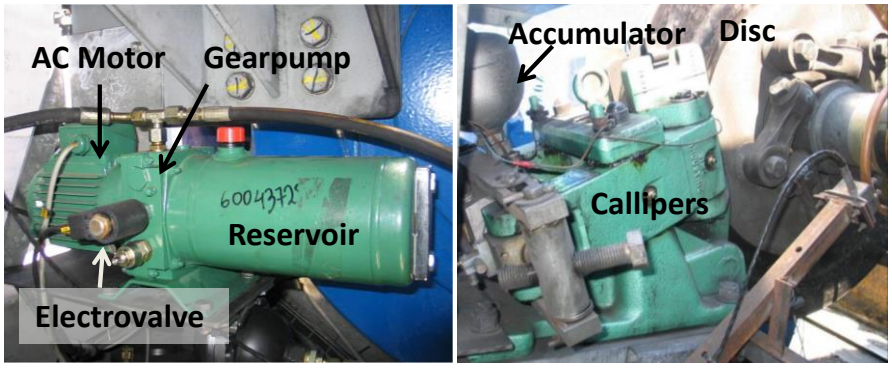

Figure 1.7: NEGM750 hydraulic/accumulator system
consisting of a 0.37 kW induction machine, which drives a gear pump and consequently maintains the pressure to release the disc and callipers. The electrovalve is to prevent the unit from exceeding its pressure limits [Author's collection]

1.6.3 Electrodynamic brakes

Electrodynamic braking loses rotational energy by reconfiguring the generator to feed a resistor bank. This is expensive compared to traditional mechanical brakes, but to maintain

resistor banks, due to their structure and design, is less costly. The self-excitation of the generator is the main part of this method, which can reduce its lifetime [26].

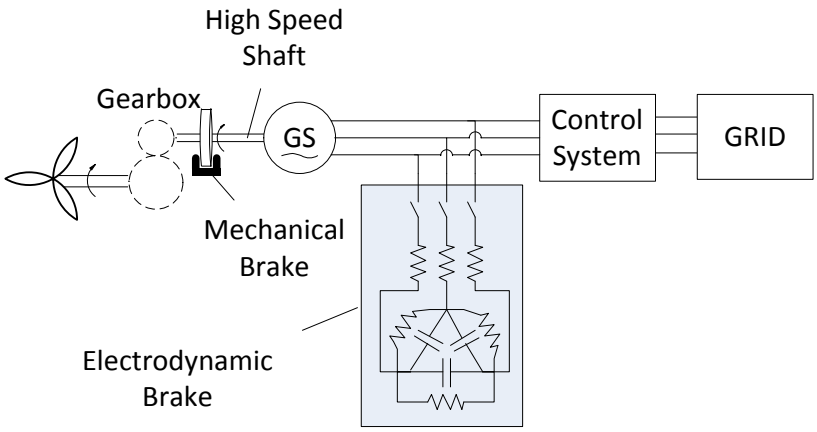

Figure 1.8: Experimental electromagnetic brake on a NEG Micon 750
[26]

In general, the use of an electromagnetic braking system could provide a safe and efficient method of stopping rotation. An electromagnetic brake system uses a three-phase rectifier connected to a DC line and can store the generated energy in capacitors. In some designs, the capacitors have been used as an emergency power source to control the blades and the brake unit. Moreover, recharging the DC line slows down the rotation and helps the braking procedure [27].

Electrodynamic braking is mainly applied to small size wind turbines, as dumping the lower power into a small resistor bank stops the rotation. Therefore, installation of mechanical brakes can be avoided [28].

1.6.4 Braking design considerations

Wind turbine mechanical brakes apply a large constant retarding torque close to the design load of the high-speed shaft without allowing for the speed and the torque that is being generated by the rotor blades. Therefore, in a high speed situation, a sudden high torque against the normal rotation would place stress on the gearbox, generator, blades and tower.

However, the torque generated by aerodynamic braking is less harmful to the gearbox and shaft than that produced by mechanical braking, as it acts directly on the blades. This is why aerodynamic braking is generally used to reduce the speed before the mechanical braking is applied [28].

Grid power line faults, such as power brownout or unbalanced phases, may trigger any type of fail-safe braking systems, for example, mechanical brakes. Frequent application of the mechanical brake results in structural damage, as the load on the gearbox and blades during the braking is extremely high and can exceed the design specification limits. Having full control of the mechanical brake and limiting its operation to emergency situations such as overspeed and maintenance could be a solution to the problem [29]. Recently, the idea of soft braking has been studied. In this method a hydraulic system is used to control the mechanical braking torque generated by the brake disc, taking into account the current speed of the shaft, while bringing the speed of rotation of the turbine to zero [19,30].

Mechanical braking is carried out by the use of friction between the pads and the disc, which applies a large force on both sides; this can generate temperatures up to 600 °C [31]. Thus special metal alloys are used in brake disc manufacture, capable of withstanding temperatures of up to 700 °C [32]. Temperature sensors added to the brake disc allow for better monitoring to prevent overheating of the pads and disc by disengaging and engaging the callipers when the temperature reaches a predefined threshold [33,34].

Fire protection systems have always been required in wind turbines. This is due to the use of sound-proofing foam layers, which are highly flammable. Sparks arising when worn brake pads are applied to the brake disc may cause sound-proofing foam or other flammable parts to catch fire. The use of thermal blankets has been proposed for passive fire protection purposes [35].

A recent catastrophic example of brake failure in the UK was a wind turbine that collapsed during high wind speeds (around 50 mph) due to freewheeling and failure in braking. This happened in Coldingham, Scotland, in December 2011 [36,37].

Case studies from one wind farm with turbines less than 1 MW show the response of the mechanical brake to a power loss can take up to 10 seconds. Due to lack of electrical load, the rotor accelerates and consequently it will place a greater load on the mechanical brake. Appropriate electrical braking of the wind turbine in such a situation can reduce the speed of the shaft and therefore reduce the load on the mechanical brake and allow smoother braking [38].

In mechanical braking, the friction force is used to stop the rotation. Therefore, while the high-speed shaft is at its highest speed, mechanical braking is not recommended as it will take longer to stop and consequently raise the temperature, which decreases the effectiveness of the brake pads. Thus having two or three braking stages to stop the turbine would be advantageous.

In some variable speed wind turbine designs an emergency battery backup system is installed to keep the blade pitch system active during grid power failures. One of the drawbacks is the effect of uncontrolled ambient temperature on battery life, which is an additional safety issue [39].

1.7 Thesis outline

1.7.1 Objectives

The central hypothesis addressed in this work is whether it is possible to develop a retrospective and non-intrusive condition monitoring system to improve certain aspects of the performance of wind turbine systems.

The proposed work is delivered through the completion of several objectives:

- Initial review of wind turbine failure modes and faults to identify a suitable sub-system for later studies.
- A general review of fault detection and diagnosis literature focused on model-based approaches.
- To design, develop and evaluate a low-cost and non-intrusive condition monitoring system to acquire and process data from wind turbine sub-systems.
- To develop a model of a selected sub-system with a suitable level of abstraction to enable fault detection and diagnosis algorithms to be tested with simulated faults.
- To determine the performance of the condition monitoring system and improvement of the models using laboratory-based tests and field trials.

1.7.2 Summary

The work presented in this thesis has been undertaken as part of a European Union (EU) project: the Development and Demonstration of a Novel Integrated Condition Monitoring System for Wind Turbines (NIMO), which applies new methods of condition monitoring to wind turbines and aims to detect faults and failures at the early stages [40].

This thesis reviews wind turbine failure modes and focuses on fault diagnosis and identification of a brake system for several detailed case studies. It also covers the use of appropriate fault detection and diagnosis methods within electrical machinery. This includes model-based approaches, such as parameter estimation and signal models.

Within the case studies, the development of a model of a brake system has been carried out. A suitable level of abstraction to enable fault detection and diagnosis algorithms to be tested with simulated faults is also considered.

Extension of the model and algorithms to consider a wind turbine braking event to monitor the blade structural health has been implemented.

This thesis addresses the problem of automatic detection and diagnosis of faults within wind turbine brake systems. The central theme is to use induction motors as a sensor to identify faults within the hydraulic unit, which drives the brake system. It also uses the braking event as a technique to detect structural faults within blades.

During the development of this work, a requirements specification for a wind turbine condition monitoring system, based around a distributed embedded system has been considered. Techniques in fault-tolerant design and performance of the condition monitoring system during field trials have been demonstrated.

1.7.3 Structure of the thesis

The structure of the following chapters of this thesis is described below.

Chapter 2 - Research methods

A literature review was carried out in three main sections:

- Fault detection and diagnosis approaches and their application.
- Induction machines and state of art on their condition monitoring.
- The importance of data acquisition systems.

Motor current signature analysis and related methods are introduced and explained.

Chapter 3 – Experimental condition monitoring of laboratory induction machines

A set of laboratory-based experiments were performed in this work. The application of the fault detection and diagnosis methods on condition monitoring of induction machines was performed on collected data from the laboratory trials to assess the methods.

Monitoring and understating the behaviour of different induction machines by the use of current signature were studied.

Data acquisition and requirements for real industrial tests were studied, tested and verified.

Chapter 4 - NEG MICON 750 Brake Hydraulic Power Unit

This chapter presents a case study of real wind turbine condition monitoring. An induction machine was used to monitor a sub-system within the turbine.

The collected data from the real turbine was used for further modelling approaches. The model was then used to explain the behaviour of the hydraulic unit and to simulate a number of faults. The data processing methods were performed to study the behaviour of the hydraulic unit.

This chapter concludes with how to monitor a complex system using a low-cost and non-intrusive approach.

Chapter 5 - V47 and AW1500 Hydraulic Power Unit

This chapter describes how a confirmation of the applied methods in the previous chapter was carried out by performing the same approaches on two other wind turbine hydraulic systems. This is followed by an explanation of how historical data processing approaches can be applied, and how the collected current data from the hydraulic system can be matched with the existing hydraulic pressure recorded by the wind farm operator.

An induced fault, made by the operator during the trial, was used to demonstrate the fault detection and diagnosis methods and their efficacy.

Chapter 6 - Blade Tip Monitoring

This chapter presents a simple approach to monitor the operation of the blade tips by use of existing measurements provided by the wind turbine operators. The provided data were also used to design a dynamic model of the behaviour of the high-speed shaft at the event of braking. The work also demonstrates the use of parameter estimation to improve the model. The model was to evaluate the methodology and also used to simulate a number of faulty conditions.

Chapter 7 - Conclusions

In this chapter, the results of the case studies are reviewed. It concludes that the condition monitoring system and the applied fault detection and diagnosis approaches presented in this work perform sufficiently to address the problems.

The strengths and limitations of the methods and areas of future work are discussed. The need to develop more accurate models is addressed, particularly by the use of a higher quality of qualitative analysis.

A summary of the publications that were carried out within this PhD work is also presented.

Chapter 2 Research methods

2.1 Introduction

The use of condition monitoring and fault detection and diagnosis techniques has recently been increasing in industrial applications. The common reasons are:

- to reduce the cost of maintenance
- to achieve early fault detection and prediction applications
- to provide performance optimisation and improvements in reliability

In this chapter, an overview of fault detection and diagnosis and its methodologies is provided.

In the previous chapter, the use of induction machines in wind turbine design was discussed. This chapter continues by exploring the condition monitoring techniques used for induction machines and discusses a number of examples of their use within the wind energy industry. A comparison of the relevant condition monitoring methods is provided.

Additionally, the use of parameter estimation on a simple second order dynamic system has been explored for further condition monitoring and modelling purposes.

Finally, fault detection and diagnosis methods plus stages in the design of a fault tolerant data acquisition unit used within this work are described.

2.2 Fault detection and diagnosis approaches

Two major approaches to fault detection and diagnosis are model-free and model-based.

Examples of model-free methods include the following [16]:

- *Physical Redundancy*: In this approach, sensors are installed for measuring the same physical quantity, therefore differences between the measurements can be indicated as a sensor fault. Detection of sensor faults is a benefit of this approach, however one of the disadvantages of this method is that it leads to additional hardware, cost and weight.
- *Checking limits*: In this method, measurements are compared automatically. Whenever the measurement exceeds the threshold a fault is deemed to have occurred. Two significant drawbacks of this method are:
    - Since the plant variables may vary widely due to normal input variations, the test thresholds need to be set quite conservatively.
    - A fault in a single component could affect the other variables, resulting in difficulties in diagnosis of the faulty component.

In model-based methods, the mathematical behaviour of the system is implemented in the form of various equations or similar transformed representations. This can be used as a facility to develop designs or improve control algorithms. It also provides a better way of understanding particular system behaviours. An acceptable model will lead to valuable outcomes and conclusions. In order to achieve a mathematical model of a dynamic system, the following tasks should be considered: finding subsystems, representing the equations, analysis and interpretations, and tests and examinations [41].

The model-based approaches can be categorised into three main types: quantitative, qualitative and process history [17].

2.2.1 Quantitative models

Quantitative models can be subcategorised into two types: process models and signal models.

2.2.1.1 Process models

In quantitative process model methods, a mathematic model, which represents the behaviour of the system, is required. This model is used to provide analytical redundancy, which is relied upon for most of the process model-based fault detection and diagnosis methods.

Measurements from real sensors and computed results from models are used in the comparison of generated quantities. The differences between the modelled and measured quantities are called 'residuals'. If the residuals exceed pre-defined threshold levels then it indicates faults within the system [16]. This method, illustrated in Figure 2.1, can be represented in three stages: mathematical (behavioural) model, residual generation and evaluation, and decision making.

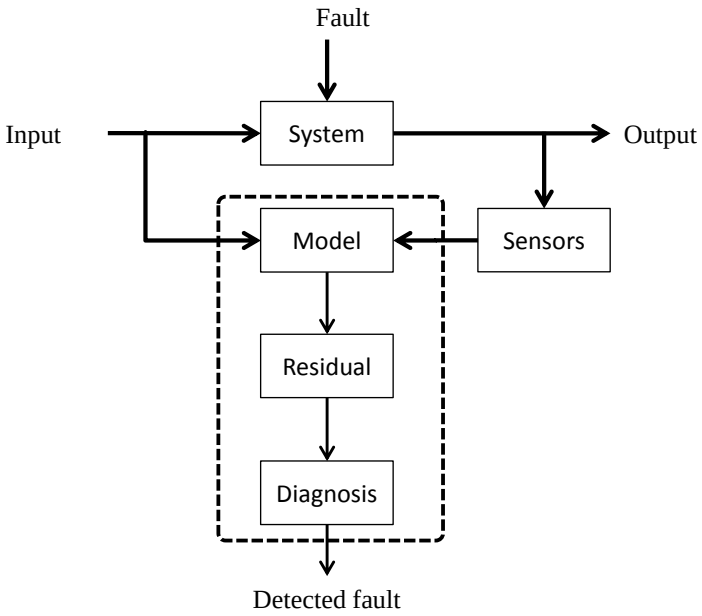

Figure 2.1: Quantitative process model approach

Common residual based techniques are:

- *System identification (estimated parameters)*: In this approach the system parameters are considered in the set values, e.g. a second order system and its parameter matrix. The set values are compared with inputs and outputs and any difference that exceeds

certain thresholds indicates a fault [42]. This method has been successfully implemented and is considered well developed, especially in linear processes [42].

- *Observer based*: Estimation of the outputs from measurements by use of algorithms such as Kalman filters [16]. In this approach, a model is used to estimate the behaviour of the system in advance by considering the past, present and expected computed results from the model. For example, Kalman filters have often been used for noise reduction and to generate a more acceptable signal from the sensor measurements. A Kalman filter can be applied to allow the estimation of position during sudden loss of an otherwise prevalent global positioning system signal and also to eliminate any anomalies in the received positioning data [43].
- *Parity relations*: Multiple sensors for measurements of the system will increase the reliability of the collected information. A fault within any of the sensors can be incorporated into a set of linear parity equations, generating a set of residuals which can then be used in fault detection and diagnosis [17,44].

2.2.1.2 Signal models

In this approach the output of the system is analysed. Changes within the output signal can be related to a particular processing fault. Thus, analysis of the changes may result in fault detection and diagnosis. This method is commonly used in rotating machineries, especially vibration and current analysis [42]. The approaches mainly used in fault detection and diagnosis systems using signal models are [45]:

- Spectrogram analysis: This is based on frequency and time domain analysis by using techniques such as Fourier and Wavelet transformations to characterise the behaviour of the system in order to extract abnormalities and faults.

- Envelope analysis: This can be based on time and/or frequency domain analysis, where the signal is characterised within suitable domains. For example, in time domain analysis, norms, peaks and total duration illustrate various behaviours of the system that the signal is measured from.

In these methods, use of filters such as low-pass, band-pass or high-pass filters helps to limit a certain bandwidth of the signal to pass for further amplitude and frequency analysis.

2.2.2 Qualitative models

Qualitative models are mainly knowledge-based expert systems. These can be used to generate residuals. The residuals allow detection of changes in the system behaviour and lead to fault detection and possible diagnosis. This represents the knowledge of a human expert by classifying a sequence of rules from which conclusions can be made. This could consist of simple *if* and *then* statements implemented in a computer program [46]. Thus, an alarm can be generated after indication of a fault using the defined rules. However, unknown behaviours cannot be dealt with.

For this type of fault detection and diagnosis, methods using expert systems, fault trees and abstraction by quantisation are commonly used:

- Expert systems: A simple *if* and *then* statement in a computer program is an example of an expert system based on the designer and operator knowledge:

  if condition 1 *and* 2 *then*
  State A is occurred.
  end if

  if State A *and* B
  Fault class *x* has happened.
  Alarm activation.
  end if

- Fault trees: In this approach, a set of possible symptoms that lead to a failure is shown by a series of block diagrams. It has levels of nodes, each of which represents a threshold of a possible fault and connects to the previous levels by logic operators such as ‘AND’ or ‘OR’. Figure 2.2 illustrates an occurrence of a fault within a system using a combination of seven other faults which are measurements and thresholds within system components and characteristics.

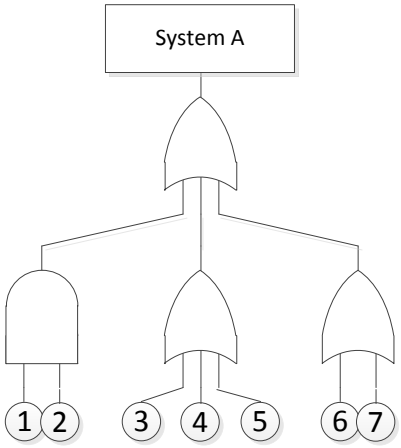

Figure 2.2: An example of a fault tree diagram

- Abstraction by quantisation: Inputs and outputs are measured by an analogue to digital convertor within a digital processor unit, where a suitable level of quantisation is chosen. Thus, the data sets are considerably reduced and it helps with reductions in data communication buses within the condition monitoring system.

2.2.3 Process history methods

In this method, instead of using knowledge of system behaviour in advance, a large quantity of historical data is used to implement *a priori* knowledge using qualitative or quantitative methods. Qualitative shape analysis, artificial intelligence techniques (such as neural network

and fuzzy logic) and statistical feature extraction are the common methods in this approach [17].

In a system where the parameters are not attainable, analysis of the historical behaviour of the system can help to study changes over time and to observe system performance. This will lead to detection of an abnormality within the system behaviour which will lead to further fault detection and diagnosis investigation [17].

2.3 The three-phase induction motor

In Chapter 1 it was mentioned that the majority of industrial machinery is driven by induction motors. In this section, the principle of three-phase motors is described. Furthermore, it addresses the common fault detection and diagnosis approaches within induction motors and finally explores the methods used in this thesis.

Induction motors consist of two main parts: a stator and a rotor.

The stator has a set of windings which generates a rotating magnetic field in the air gap between rotor and stator by using the supplied current. The induced magnetic field in the rotor winding or bars (dependent on the design of the motor) opposes the magnetic field of the stator according to Lenz's and Faraday's laws. Consequently, this opposition generates torque on the rotor. However, in normal operation, the speed of the rotor (n_r) is slightly less than that of the stator field (synchronous speed) (n_s), thus induction motors are classified as asynchronous machines. Slip is related to the difference between the speed of the stator field and the rotor speed. Equation (2.1) shows how slip can be calculated from the synchronous and rotor speeds [47].

$$s = \frac{n_s - n_r}{n_s} \tag{2.1}$$

The synchronous speed is a function of the number of poles within the stator winding and the supply frequency. As magnetic poles come in pairs, north and south, the number of poles (p) is always an even number. The stator field speed, which is also known as synchronous angular speed, can be calculated in revolutions per minute (rpm) using equation (2.2).

$$n_s = \frac{120 \times f}{p} \tag{2.2}$$

where f is the stator supply frequency in Hz.

Slip speed ($n_{slip} = n_s - n_r$), which is the difference between rotor and synchronous speed, along with equation below can be used to determine the slip frequency [48]:

$$f_{slip} = sf \tag{2.3}$$

Slip analysis in induction machine condition monitoring is commonly used and this is demonstrated further in this chapter.

2.4 State of art on induction machine condition monitoring

The low-cost, simple design, robustness, direct connection to the power line and reliability of induction motors are the main reasons for their popularity in industry. They are used in a variety of engineering systems, such as hydraulic power units, compressors, water pumps and cooling fans [47]. Due to their vast contribution to the working of industrial machinery, the reliability and maintenance of induction motors have become of significant importance for manufacturers and operators [49]. Faults within induction motors can usually be categorised as either electrical or mechanical. Electrical faults include stator windings faults and three-phase power issues, such as unbalanced voltage or brown out in any of the phases [50]. Bearing failures, broken rotor bars, misalignment, bent shafts, air gap eccentricity and faults caused by the load are the most notable mechanical failures [51]. In induction motor

condition monitoring, methods such as vibration, thermal, flux and electrical analyses have been carried out. A brief description of the aforementioned methods is set out below.

2.4.1 Vibration monitoring

Vibration monitoring is the measurement of periodic oscillations of machinery motion due to outer and inner forces, which could be mechanical, electrical or magnetic [52]. All rotating machinery vibrates at a certain level. However, improvements in mechanical and electrical designs have increased the life and reduced the vibrations of the induction motors. Thus, in this approach, high sensitivity vibration sensors are mainly required. Detection of bearing faults, unbalanced rotor and faulty gears are possible uses of this method [53,54]. Filtering, combined with spectral analysis, are the main methods used in fault detection and diagnosis for vibration measurements, but this technique requires high frequency sample rates (40-50 kHz), creating a large volume of data which can be difficult to handle. Moreover, the cost of a vibration sensor depends on its resolution, and in some circumstances it can be expensive in comparison to the cost of the induction motor. The main disadvantage of this method is access to the machinery. For example, in order to perform vibration measurement on a wind turbine hydraulic unit, a journey to the nacelle by a specialist technician plus a fast and reliable communication bus to transfer the data are required. Additionally, any failure within the sensors creates an extra maintenance cost for the installed system [55].

2.4.2 Thermal monitoring

Thermal monitoring is performed by the installation of temperature sensors locally or by using thermographic cameras, and can be used to detect overloading, stall situations, and unbalanced operation of an induction motor (causing excess heat). For example, research has shown that changes in stator winding insulation can radically decrease the lifetime; an

approximate 5°C increase would reduce the lifetime by 8 years [56]. In order to perform this method, the installation of temperature sensors in rotor and stator windings is essential, which therefore makes this method an intrusive approach, which is best fitted during the manufacture of the motors. On the other hand, thermal cameras measure and analyse the temperature gradients by taking high quality images, and these have often been used in more hazardous conditions [57]. The disadvantages of an accurate thermal camera are the cost and complexity of analysis. Another drawback is that the use of the rise in temperature to detect fault is not prompt enough to achieve an early fault detection and diagnosis system, as the fault is already progressing [55].

2.4.3 Magnetic flux

This approach, in order to perform fault detection and diagnosis methods, measures and monitors the axial leakage flux of the machine by use of search coils. These coils are usually installed on the end of the shaft. Changes in the flux can be monitored by the induced voltage within the coil. Unbalanced voltage and rotor bar faults can successfully be detected using this method [58,59]. However, mechanical faults such as bearing failures cannot be detected at early stages using this method [51]. Other drawbacks of this method include the limitation of retrofitting and also accessing the machinery. This is usually restricted by operators due to health and safety concerns, and issues which may void a warranty provided by the manufacturers.

2.4.4 Electrical measurements

Electrical or mechanical faults affect the magnetic field within the induction machines. The effect can be extracted from the current measurements within the stator. This method, by analysing the measured current signals, can detect faults within the motor and any existing

failures in power electronic or invertor systems. Motor current signature analysis is a non-intrusive online monitoring method often used for fault detection and diagnosis of induction machinery [60]. Motor current signature analysis has been used in this work.

Spectral analysis and signal processing approaches such as Fast Fourier Transform, Wavelet Transform, Park's Vector, Hilbert Transform and Envelope Analysis of the measured signals are often used to determine faults within induction machine systems [55]. One of the advantages of this method is that access to the machinery is not needed. Split-core clamp current transducers can be used to avoid any inference in electrical wiring. This method is also able to identify faults that develop gradually over time, knowledge of which can be used for better maintenance scheduling and to prevent further damage and longer downtimes [60]. In this method, no parameter estimation is needed [61].

2.4.5 Comparison and summary

Table 2.1 shows a comparison of the aforementioned fault detection and diagnosis methods and the efficacy of the approaches in some of the studied faults in induction motors.

Table 2.1: Faults in induction machine and efficacy of condition monitoring methods [62]

		Condition monitoring approaches			
		Vibration	Thermal	Flux	Electrical
Faults	Winding Insulation Fault		✓		✓
	Winding short circuit	✓	✓	✓	✓
	Broken rotor bar	✓		✓	✓
	Air gap eccentricity	✓			✓
	Bearing fault	✓			✓

In this work, a number of experiments on condition monitoring of induction motors and the use of motor current signature analysis have been carried out. This is due to the advantages of this method in comparison to others, including:

- accessibility to the machinery is not needed
- it is non-intrusive
- the use of cost efficient sensors
- manageable amount of data
- implementable sampling frequencies and data processing by low–cost small embedded systems
- reliability and background work that has been done by other researchers and manufacturers

Moreover, as motor current signature analysis is able to detect external faults within coupled gearboxes and external mechanical loads [55], the concept of using an induction motor as a sensor for fault detection and diagnosis in the hydraulic unit of the wind turbine brake system, which is driven by an induction machine, has also been studied.

As an example, if frequency analysis is used, faults can be detected through the analysis of frequency sidebands.

- Unbalanced rotor or broken rotor bar [63]

$$f_b = (1 \pm 2s) f_1 \tag{2.4}$$

- Stator winding – short circuit [55,64]

$$f_{sc} = f_1 \left[k \pm \frac{n}{p} (1 - s) \right] \tag{2.5}$$

- Air gap eccentricity [65,66]

$$f_{ag} = f_1 \left[(nR \pm n_d) \frac{(1-s)}{p} \pm k \right] \quad (2.6)$$

- Bearing fault [65]

$$f_{bearing} = \left| f_1 \pm n \frac{N_b}{2} f_r \left[1 \pm \frac{D_b}{D_c} cos\beta \right] \right| \quad (2.7)$$

- Gearbox faults [55,67]

$$f_{gr} = f_1 \pm m \frac{f_1}{gr(\frac{p}{2})} \quad (2.8)$$

where,

f_b is the broken bar frequency

f_{sc} short circuit frequency

f_{ag} Air gap eccentricity frequency

$f_{bearing}$ Bearing frequency

s is the slip

f_1 is the supplied frequency

f_r is the rotor frequency

p is the number of pole pairs

$k = 1, 3, 5$ ... (order number of stator current harmonics)

$n, m = 1, 2, 3$ ...

R is the number of rotor bars

D_b is the diameter of the bearing ball

D_c is the diameter of the bearing pitch

β is the contact angle of the balls on the inner and outer races

gr is the gear ratio

2.5 Applied fault detection and diagnosis approaches in this work

In this section the motor current analysis approaches considered in this work are presented. System identification methods, used for parameter estimation and fault detection and diagnosis by looking at the second order system (mass spring damper) and analysis of its natural frequency, are discussed. The use of frequency domain analysis with regards to current signature and a few common failure modes are also illustrated.

2.5.1 Fast Fourier transform

The Fourier transform is a mechanism for considering a time-domain signal in the frequency-domain. This allows consideration of the different frequencies within the signal and facilitates harmonic spectral analysis. The Discrete Fourier transform in digital signal processing systems is often used for frequency-domain analysis in order to analyse the condition of the electrical machinery and is consequently a powerful tool for fault detection and diagnosis.

Below is the Discrete Fourier transform of a sampled signal $x(n)$ with a sampling frequency of ω_s:

$$X(\omega) = \sum_{n=-\infty}^{+\infty} x(n) e^{-j2\pi(\frac{\omega}{\omega_s})n} \tag{2.9}$$

The number of complex multiplications is proportional to N^2, where N is the number of samples in a chosen section of $x(n)$. Therefore using DFT is time consuming for applications such as digital signal processors and computer based systems. To overcome this issue in real-

time signal processing systems,the Fast Fourier Transform (FFT) is used. The FFT is a more efficient and faster alternative using fewer calculations. In the FFT the number of calculations is reduced to $N \log_2 N$. This is due to storing the repeated calculations and re-using them [68].

In induction machinery, stator current analysis is used to detect static eccentricity and in the application of performing early fault detection. This is normally preceded by FFT analysis of the current [69].

Figure 2.3 is the FFT result, produced in Matlab, of a healthy three-phase motor. The experiment was conducted using a 2 kHz sampling frequency and had a duration of 2 seconds. It was based on a 1.1 kW three-phase motor powered by the grid and operated in steady state. The x-axis represents the frequency while the y-axis is the amplitude and is related to the number of points within the time-domain signal.

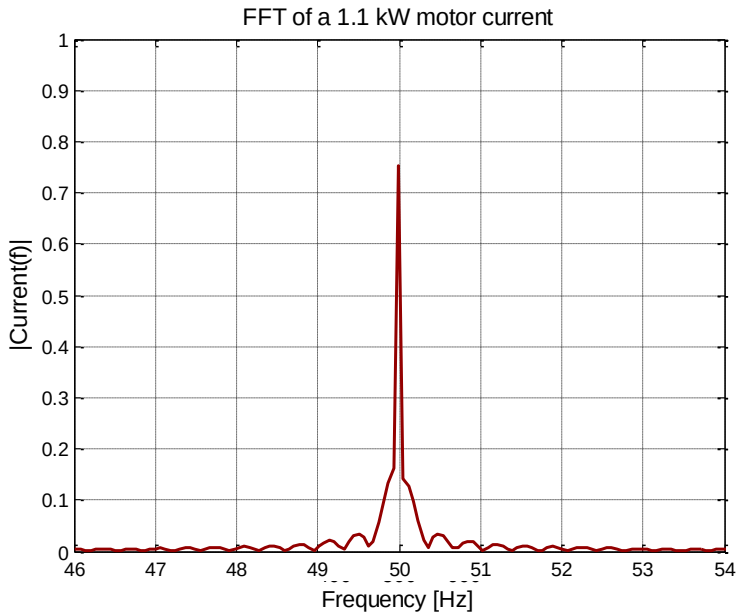

Figure 2.3: Fourier Transform of a phase of a healthy motor current

2.5.2 Spectrogram

A time-frequency domain analysis that represents the signal with a spectral density that varies in time is often used to study the temporal changes in the harmonic content of waveforms. This method is a form of short time Fourier transform [69]. A window of the signal is selected and represented in 2D/3D, and follows the next window with a suitable overlap [55]. The spectrogram of the motor current shown in Figure 2.3, with no temporal changes, is shown in Figure 2.4.

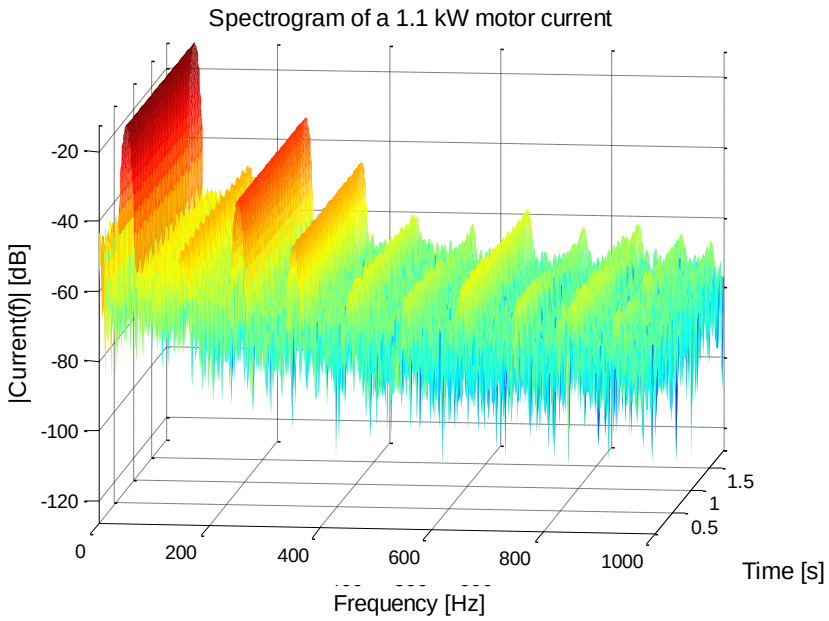

Figure 2.4: Spectrogram of one phase of a healthy motor current

2.5.3 Park's vector

In condition monitoring of balanced three-phase machinery, a simplified method using two dimensional axes instead of three phases is often used. The two axes represent a circle, which can often be used to determine healthy and faulty machines [70].

The Park's transformation, direct-quadrate zero, often applies on induction motor stator current. The transformation produces two components i_d, i_q out of three stator current lines ($i_a, i_b \; and \; i_c$), demonstrated in (2.10) and (2.11).

$$i_d = \frac{1}{\sqrt{6}}(2i_a - i_b - i_c) \tag{2.10}$$

$$i_q = \frac{1}{\sqrt{2}}(i_b - i_c) \tag{2.11}$$

$i_d \; and \; i_q$ are simplified DC representors of the three-phase. The Park's vector approach has been applied in fault detection and diagnosis systems in order to detect faults such as bearing faults, unbalanced load, airgap eccentricity and broken rotor bar [55,70].

Figure 2.5 and Figure 2.6 show a simulated three-phase current and its Park's transform. The three-phase has been created with no harmonics and considering a non-discrete system, which shows the effect of data acquisition errors.

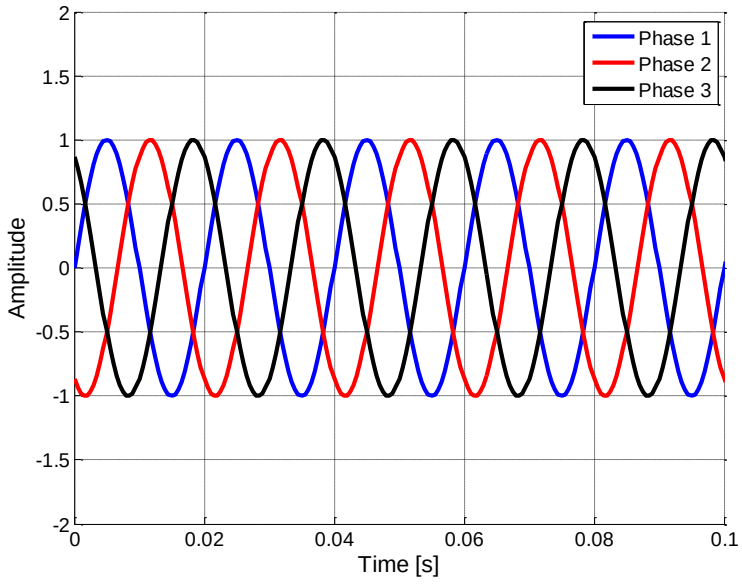

Figure 2.5: Ideal simulated three-phase current

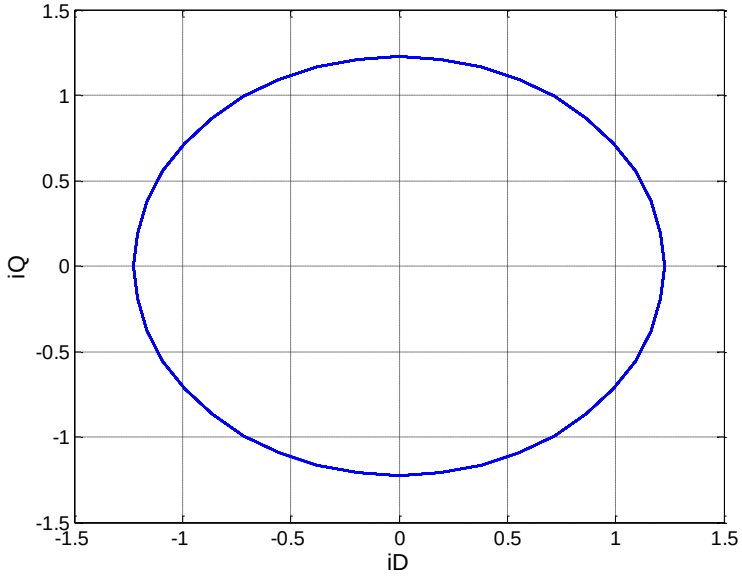

Figure 2.6: Ideal Park's transform of the simulated three-phase

Figure 2.7 is the three-phase simulated current along with its 5th harmonics, with a ratio of 10% - 20% and sampling frequency of 2 kHz. Figure 2.8 is the Park's transform of the measured currents at 2 kHz and includes 1% Gaussian noise representative of sensor error.

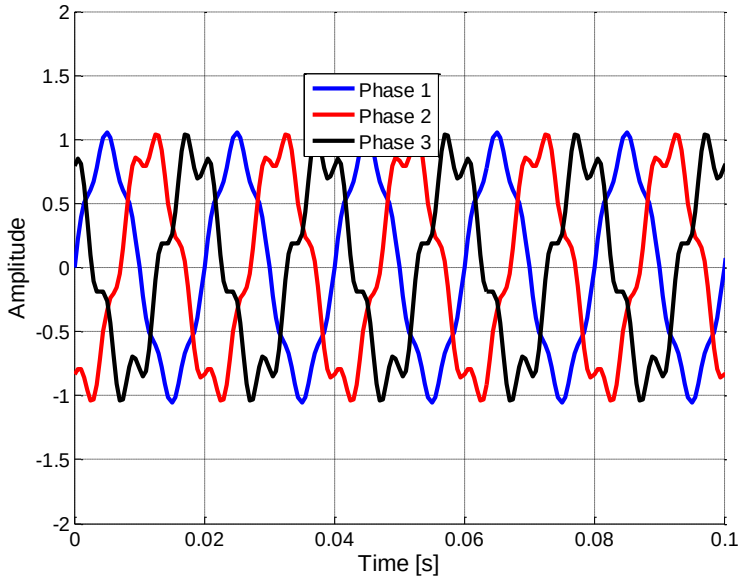

Figure 2.7: Simulated-three phase with 5th harmonic and 2 kHz sampling rate including 1% noise in the measurement

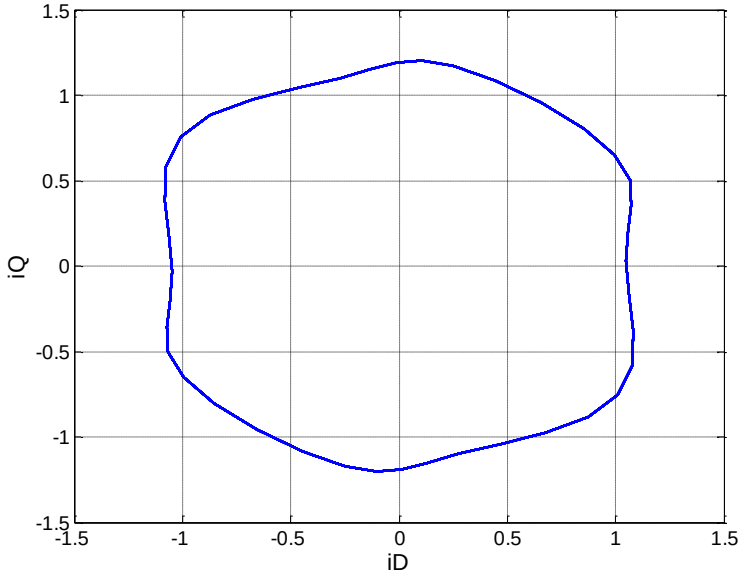

Figure 2.8: Park's Transform of the simulated three-phase with 5th harmonics and measurement error at 2 kHz sampling rate.

Figure 2.9 illustrates the frequency analysis of the simulated signal. The fundamental 50 Hz is followed by the 5th harmonic.

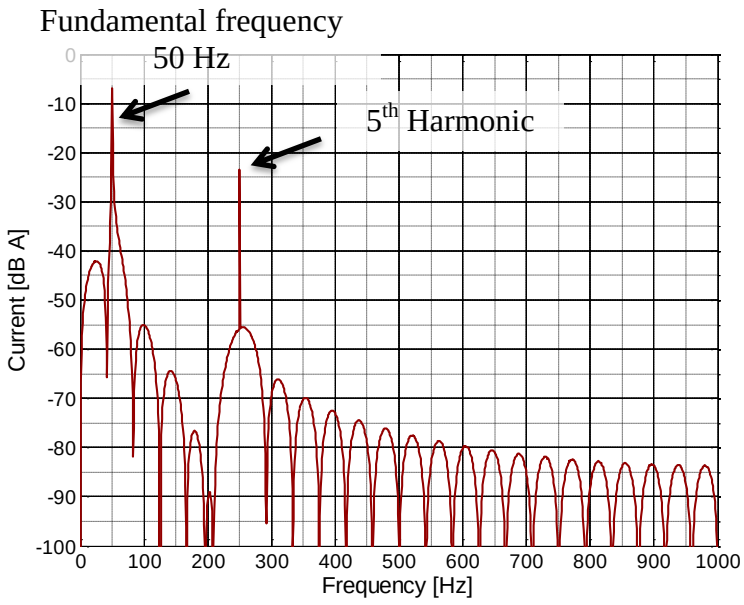

Figure 2.9: FFT of the simulated current with the 5th harmonic

2.5.4 Envelope analysis

A current analysis of an induction machine, in the time domain, can be categorised by its average amplitude, duration and starting peaks. The shape of the connected peaks of a time variant signal is called the envelope of the signal, which is similar to the upper envelope in amplitude modulation in radio frequency engineering. The envelope can be produced through the use of methods such as the Hilbert transform, or peak detections followed by interpolation functions [71,72].

2.5.4.1 Hilbert transform

The Hilbert transform is a transformation of a signal from time-domain to time-domain. Positive frequency and negative frequency components are shifted by +90 and -90 degrees, respectively. The Hilbert transform of the time signal $x(t)$ is shown as $H(t)$. The analytical signal, $a(t)$, is the envelope of the original signal.

$$H(t) = \int_{-\infty}^{+\infty} \frac{x(\tau)d\tau}{t-\tau} \tag{2.12}$$

The complex result can be shown as:

$$H(t) = x(t) + iy(t) \tag{2.13}$$

Therefore the $|H(t)|$ represents the analytical signal $a(t)$ and it is the magnitude of the envelope of the original signal.

$$a(t) = \sqrt{x^2(t) + y^2(t)} \tag{2.14}$$

Figure 2.10 is an example of use of the results of the above equations in producing the envelope of the original signal.

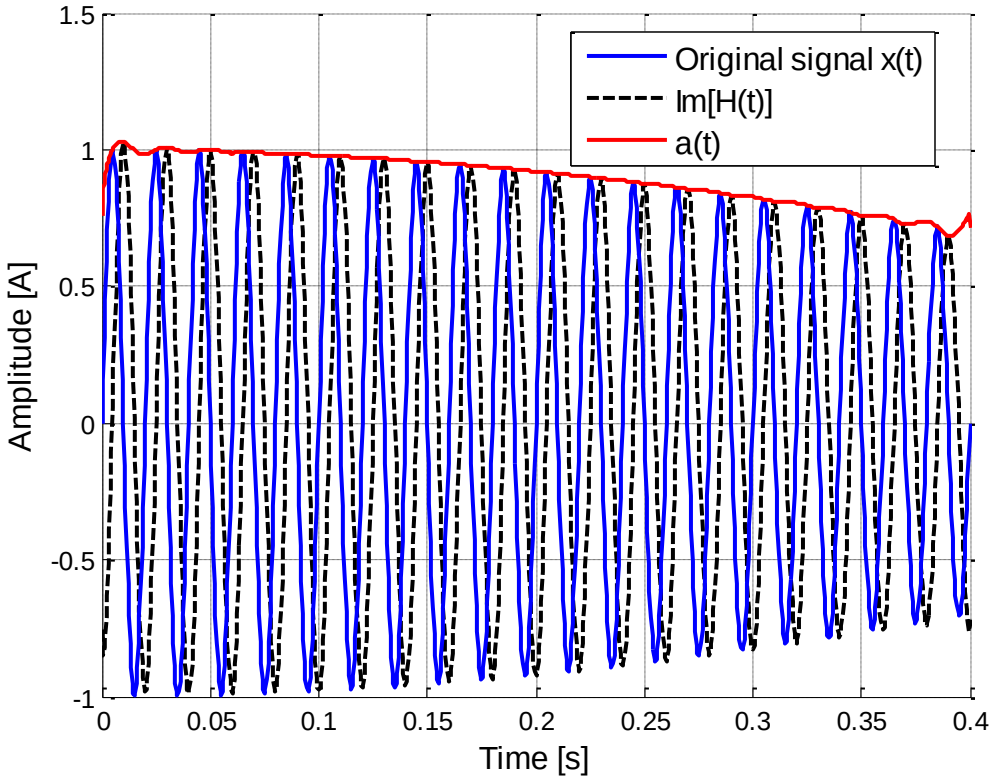

Figure 2.10: Example of Hilbert transform in generating the envelope signal

2.5.5 Parameter estimation

In order to estimate the parameters of a linear time-invariant discrete dynamic system with a single-input single-output, an autoregressive model is considered.

An autoregressive (AR) model is a subcategory of the autoregressive-moving average (ARMA) model, which is an elaboration of the past values of a linear system. These models can be used to determine time variant system parameters by using its current and past values. This can be used to predict the system behaviour. Thus, comparison of estimated AR-based model results and measurements with the real plants generates residuals, which counts as a model-based fault detection and diagnosis method [73].

In order to undertake the parameter estimation using the AR model, DC offset within the signal must first be removed. This can be performed by subtracting the mean from the time series. The "mean-adjusted series" can be calculated by:

$$y_t = Y_t - \bar{Y}, \quad t = 1, \dots N \tag{2.15}$$

where Y_t is the measured value at time *t* (data sample), $\bar{Y}$ is the mean of the existing samples, and y_t is the generated mean-adjusted series. The number of past values is the order of the AR model. Here is the equation for the first-order autoregressive, AR(1):

$$y_t = -a_1 y_{t-1} + e_t \tag{2.16}$$

where y_{t-1} is the series at the time *t-1*, a_1 is the autoregressive coefficient, and e_t is the error. This shows that in AR(1) model y_t regresses to its old value.

Complexity in autoregressive models can be achieved by higher-orders, which include more detailed y_t. The n^{th} order autoregressive model, AR(*n*):

$$y_t - a_1 y_{t-1} - \cdots - a_n y_{t-n} = e_t \tag{2.17}$$

where a_1 up to a_n are the autoregressive coefficients on lags *1* to *n*.

In this thesis, the method is carried out by the Matlab/Simulink 'ARX' command (System Identification Toolbox) that processes the AR model by considering the orders, which must be set manually [74] .

A simple second order model consisting of mass, spring and damper can be shown to yield a series that follows a particular form of an AR model. By using the AR(2) model with the input and output of the mass spring damper model, the system transfer function can be identified.

As an example, the transfer function for a second order system is described in this section.

Figure 2.11 shows a simple mass spring damper system. The relation between forces within the system can be described by applying Newton's third law to the system:

Motion of the Mass (F) = – Restoring Force (k) – Damping Force (C)

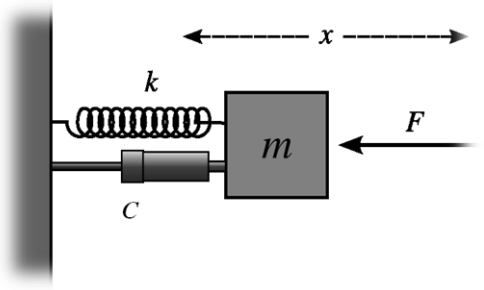

Figure 2.11: A mass spring damper system
x = displacement [m], f = external force [kg×m×s^{-2}], m = mass of the block [kg], c = damping constant [kg×s^{-1}], k = force constant of spring [kg×s^{-2}]

According to Newton's second law (2.18), damping force (2.19) and the fundamental spring equation (2.20) the motion of the mass is illustrated in equations (2.21) and (2.22).

$$F = ma = m\frac{dv}{dt} = m\frac{d^2x}{dt} = m\ddot{x} \tag{2.18}$$

where 'm' is the mass of the block [kg], 'a' is the acceleration [ms^{-2}] of the mass and x is the displacement [m] of the mass relative to a reference point.

$$F = -cv \tag{2.19}$$

where 'c' is the damper coefficient and v is the velocity [ms^{-1}].

$$F = -kx \tag{2.20}$$

where 'k' is the spring constant [kgs^{-2}].

$$m\frac{d^2x}{dt} + c\frac{dx}{dt} + kx = f(t) \tag{2.21}$$

$$m\ddot{x} + c\dot{x} + kx = f(t) \tag{2.22}$$

In order to model the motion of the mass in Matlab, the transfer function is needed. This can be derived from the Laplace transform of the equation (2.22), which is represented by equation (2.23).

$$L\{f(t)\} = F(S) = ms^2X(s) + csX(s) + kX(s) = (ms^2 + cs + k). \quad (2.23)$$

Therefore, the transfer function can be shown as below:

$$G(s) = \frac{X(s)}{F(s)} = \frac{1}{ms^2 + cs + k} \quad (2.24)$$

The ARX function will provide the zeros and poles in the Z transfer function (discrete system) and can be converted to S domain (continuous) in order to be compared with the real system.

2.6 Data acquisition in condition monitoring systems

In order to perform analysis on signals in real life, an interface is needed to convert continuous signals to discrete signals; this is an application of analogue to digital converters. The converted discrete signals are suitable for data analysis programs on computer systems.

Sampling rate and resolution are two of the important parameters of data acquisition systems, and should be correctly chosen [75]. The Nyquist-Shannon sampling theorem declares that the sampling rate must be at least twice as high as the maximum possible frequency in the analogue signal [76]. Therefore, if a spectrogram of 0-1000 Hz is desirable for data analysis, then a minimum sampling rate of 2 kHz will be required. For ease of data processing, low sampling frequency (for example 200 – 3000 Hz) rates can be used in motor current signature analysis [77,78]. In order to achieve an appropriate digitised sample of the analogue signal, it is necessary to use sampling rates considerably higher than the Nyquist frequency. Digital and anti-aliasing filters can be applied to enhance the suitability of the signal for frequency

analysis. Sampling in higher frequencies will generate much larger data blocks and consequently require more time consuming calculations and complex firmware. The resolution of analogue to digital converters determines the accuracy of the measurements, being the minimum quantifiable change. Depending on the input signal range, a desirable resolution can be selected by the number of output bits of the converters [75].

Induced noise into the sensors or a sensor failure has always been of concern. Solutions such as Kalman filters and parity relation approaches are applicable for fault detection and diagnosis in data acquisition systems [79]. Moreover, complexity in embedded system software can also increase the risk of faults within the software; application of watchdog timers can help to prevent program halts.

The condition monitoring system process unit must contain suitable hardware components, such as a central processing unit, memory modules, such as a random access memory for main calculation and a larger, portable memory for storage. Component reliability and lifespan are vital. For example, in some circumstances the use of inferior quality computer hard disks can add vulnerability to the system, therefore this should be avoided [80].

2.6.1 Fault tolerance data acquisition approach

In order to design a data acquisition unit for a condition monitoring system, its reliability and fault tolerance must be considered. Errors and inaccuracies within data processing units can lead to incorrect diagnosis and thus less certainty in the fault detection and diagnosis system.

In this work, to avoid failures within the data acquisition and processing system, two methods have been applied: passive and active.

Choice of appropriate electronic components and a suitable circuit design that can survive in diverse conditions, such as high electromagnetic fields, noisy zones or different climates, is the passive approach to a robust condition monitoring system.

Application of modular design and the consideration of suitable fault detection and diagnosis methods within a real time program are an active approach to a fault tolerant condition monitoring system. For example, the use of two different timestamp systems, emergency storage units, and parity checking in calculations and measurements within the program are redundant tactics to achieve a fault tolerant system. Multiple redundant sensors can also be effective in order to detect sensor faults and provide a more reliable data acquisition system. For instance, in the motor current signature analysis approach, measurement of two phases in a three-phase induction machine is sufficient. However, the use of a third sensor not only allows the system to detect sensor faults, but also leads to the use of some other approaches, such as Park's vector. In terms of software, the idea of using recursive functions or referencing within the program should be carefully carried out, as an inappropriate code can cause the system to fail due to non-returnable routines or loss of address within the functions. For reconfigurability, especially system structure, alternative functions and watchdog systems should always be considered. Modular design within hardware and software is also effective in the case of maintenance and debugging. These are illustrated in Figure 2.12, which demonstrates the states within a fault-tolerant design of an embedded system.

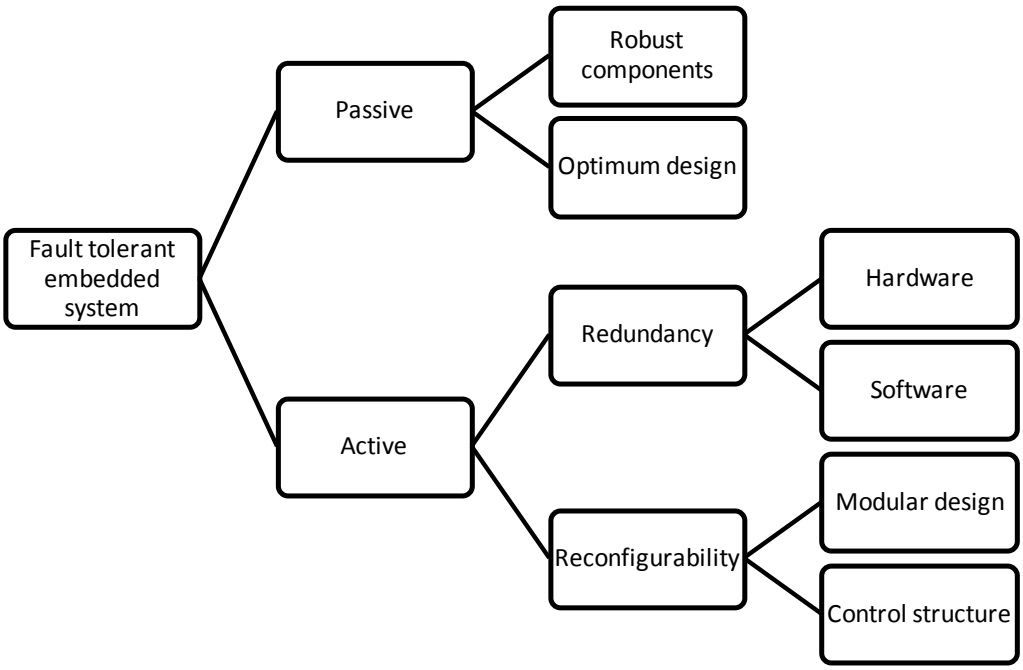

Figure 2.12: Overview of a fault tolerant embedded system
[81]

2.7 Summary

In this chapter, the concepts of fault, and fault detection and diagnosis have been introduced. State-of-the-art in induction motor condition monitoring and the importance within industrial applications have also been reviewed.

The methods that are used in this thesis were explored. The consideration of a fault-tolerant data acquisition system is carried out.

The next chapter describes and demonstrates the use of the methods on laboratory based equipment. A summary of a design of the embedded data logging system, along with sampling strategies, are also provided.

Chapter 3 Experimental condition monitoring of laboratory induction machines

3.1 Introduction

This chapter introduces the instrumentation steps and approaches in analysis, using the aforementioned research methods in Chapter 2. Measurements from different test rigs have been carried out to validate the logging system and used to apply motor current signature analysis methods for induction machine condition monitoring.

The experiments were established at the University of Birmingham laboratories:

- A 3 HP (2.2 kW) drive train located in the power laboratory at the Birmingham Centre for Railway Research and Education (BCRRE).
- A 1.1 kW hydraulic power unit driving a low cycle fatigue machine within the School of Metallurgy and Materials to apply pressure on different materials up to 100 kN.
- A 1.1 kW ventilation fan located within the traction laboratory at the BCRRE.
- A 1.1 kW induction motor.

3.2 Data acquisition system

Induction motors in industrial machinery can work continuously or run for a certain time, depending upon a demand from a control system to complete a task; this could range from seconds to hours. For example, within hydraulic powered systems the control unit tries to maintain the pressure at a certain level. This level is measured by a pressure sensor and as

soon as the pressure reaches the lowest assigned margin, the hydraulic pump will run, driven by an induction motor.

In this thesis, the idea of using small embedded systems to monitor the three-phase current of induction machines has been considered. Figure 3.1 illustrates the main design of the developed condition monitoring system for this work.

Within the design requirements, certain features were taken into account:

- Fault-tolerant: an internal watchdog timer (WDT) within the processor unit and parity checking approach in sensor measurements have been applied to the main design concepts. The WDT is used to prevent the processing unit from being halted in case of a software malfunction, which will restart the whole system [82].
- Auto triggering system: during the time that induction motors function, there are moments when they are not in use. Thus, storing data from the period when the motor is not running is unnecessary and an inefficient use of the storage unit. Moreover, extra data processing time is needed to extract the real data from the measurement.
- Cost: design of a simple printed circuit board with an adequate level of components to reach a suitable accuracy was taken into consideration to carry out the measurements from current sensors. The use of an appropriate digital signal processing chip instead of the existing expensive computer units (such as National Instrument kits) in order to perform the logging on an external SD card, and basic envelope and frequency analyses, has reduced costs.
- Communication system: ability to communicate with a standard specification PC using a USB or TCP/IP port has also been considered within the design and applied for the NIMO project in order to transfer information to the wind farm central supervisory control system.

- Mobile storage unit capability: to provide an opportunity to transfer data with no need to remove the installed system, or in the event of loss of data communication between the embedded system and the supervisory control and data processing centre. This has been accomplished by the use of an SD card.
- Sensors: within the final design, a low cost current transformer with an accuracy of 1% and the ability to clamp over the phases were used [83]. However, to verify the accuracy of the results, a set of more accurate inline current transducers were temporarily used and compared [84] .
- Accuracy: to achieve a suitable level of accuracy a set of components were chosen and the result tested with certified and advanced existing laboratory equipment, such as a NI USB-6210 data acquisition module [85]. In this work, a 16-bit analogue to digital convertor for an input range of ±5 V is used [86], which applies approximately a ±1 mA reading error from the output of the sensors.
- Frequency of sampling: the device is able to collect data up to 4 kHz sampling frequency; this is to attain an acceptable digitised signal for further data analysis purposes. To verify that the sampling is adequate for the work, a number of experiments were carried out, which are explained in this chapter. Sampling at higher frequency rates, such as 10 kHz and 50 kHz, using the NI data acquisition system, was also used to validate the results from data analysis of a lower sampling rate.
- Anti-aliasing filter: for the 50 kHz and 10 kHz sampling rates, 25 kHz and 5 kHz anti-aliasing filters were applied, respectively. However, in order to be able to study the aliasing effect, the anti-aliasing filter of 5 kHz was used for the rest of experiments in this work.

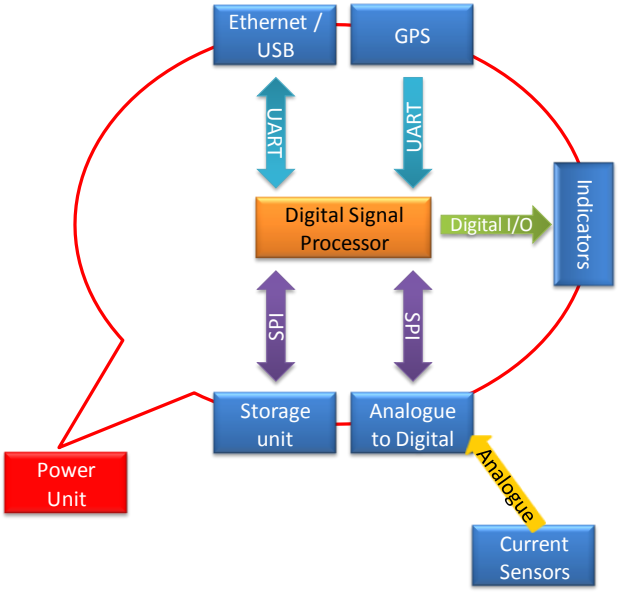

Figure 3.1: Overview of the developed condition monitoring system

The steps in design and assembly of the logger have been carried out using the BCCRE facilities. Figure 3.2 is a photograph of the last prototype of the University of Birmingham (UoB) data processing unit that was installed on a NEG Micon 750 wind turbine to monitor the condition of the hydraulic brake, by measuring the three-phase current driving the hydraulic unit.

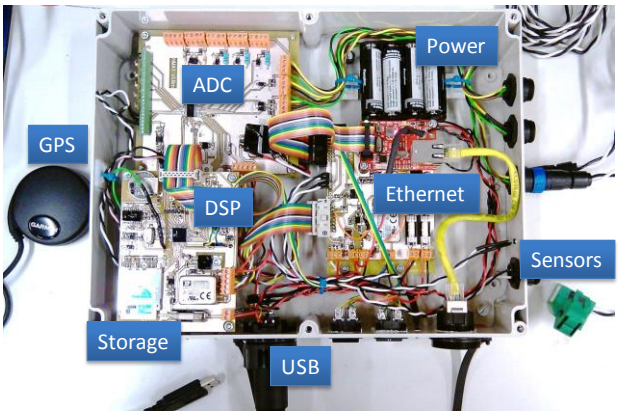

Figure 3.2: Finalised data processing unit prototype for NIMO project
[Author's collection]

3.3 Measurements and analysis

3.3.1 A 3 HP with excitation – power lab

A three-phase, 2.2 kW asynchronous motor drives a 4 kW DC motor, which acts as a generator, is located within the BCCRE power laboratory facility. The unit is driven by a 50 Hz/240 V three-phase with a pulse width modulation (PWM) control system, suitable for educational usage. This includes power electronic equipment and circuitries for speed and torque control of the AC machine.

Figure 3.3: Power lab traction system
AC motor in blue (left) and DC generator in read (right) [Author's collection].

The three-phase current of this system was monitored to evaluate the data acquisition unit and study the use of motor current analysis on induction machines. The analyses from the experiments were used to develop a suitable filter for the data acquisition unit in some circumstances; for example a PWM controlled power system often generates high energy harmonics because of the structure of a square wave form output. The harmonics from the PWM system can affect the fundamental frequencies of the motor that are valuable to motor current signature analysis [87]. These experiments were also used to test the development within data logging unit prototypes and to validate the measurements and behaviours of the AC machine in various modes. To discover the PWM frequency an experiment with a sampling rate of 50 kHz was carried out. A set of accurate industrial sensors was used for the measurements in this experiment. Three LEM LA 25-NP [84] current transducers measured

the current of each phase and two LEM AV 100-2000 [88] voltage transducers were used to monitor the line to line voltages of the supply three-phase. In this experiment the PWM was producing 55 Hz voltage output to drive the motor. The output voltage of the PWM generator can be seen in Figure 3.4.

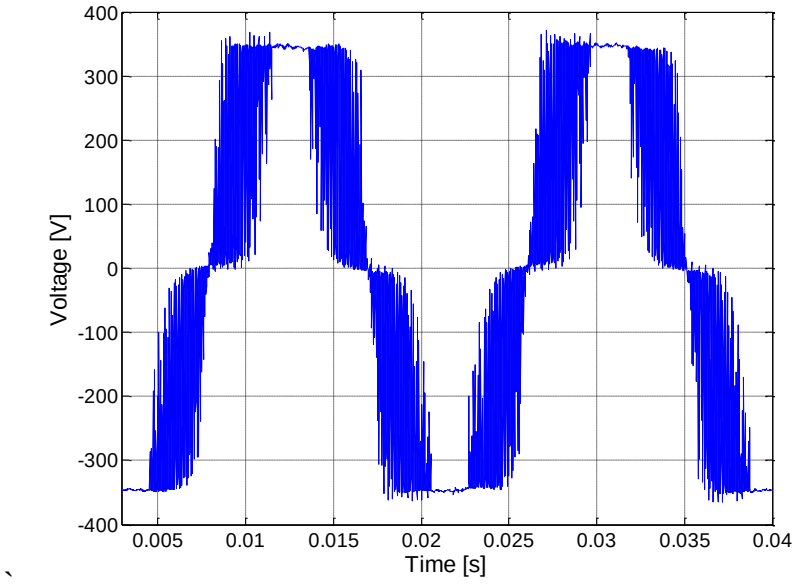

Figure 3.4: Two cycles of the line to line voltage measured from the PWM generator

The frequency analysis confirms the fundamental frequency of 55 Hz. It also shows the PWM carrier frequency is around 11.8 kHz. Figure 3.5 is the FFT spectrum of the generated voltage with the PWM system. The two main peaks caused by the PWM carrier frequency are due to the unipolar design of the PWM system which leads to total harmonic reduction [89],

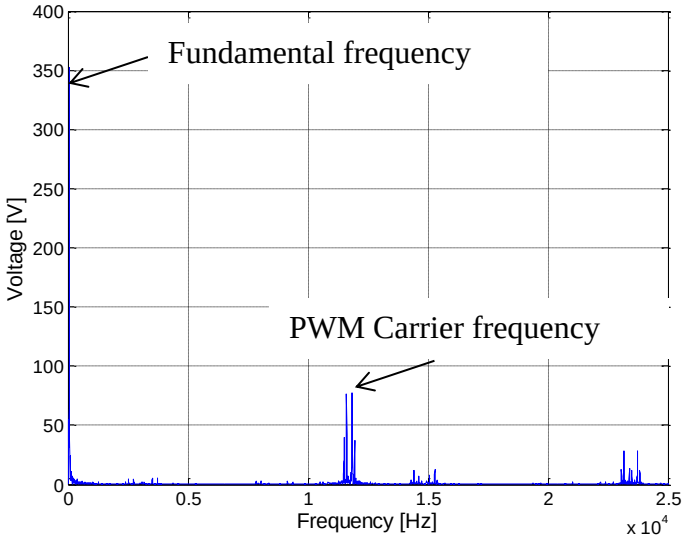

Figure 3.5: FFT analysis of the PWM generated voltage for the motor
showing the fundamental frequency of 55 Hz and around 11.8 kHz carrier frequency

As the PWM output is a square wave based signal, the signal is a combination of all odd harmonics of the fundamental frequency [90]; these affect the current signature.

An RC low-pass filter [91], with a cut-off frequency of 2 kHz, was designed and implemented within the data acquisition unit, which provides sufficient frequency band for current signature analysis and also reduces the harmonics related to the PMW. To demonstrate how an insufficient sampling rate and an inadequate ant-aliasing filter could be problematic, 1 kHz sampling frequency was chosen and with the anti-aliasing filter of 2 kHz. Figure 3.6 shows the measured three-phase current signals driving the motor without filtering. The frequency analysis of the measured signal can be seen in Figure 3.7. Figure 3.8 and Figure 3.9 are the measured signal and its FFT analysis after the filter was applied. The number of the eliminated harmonics and the shape of the current sine-wave have been enhanced. The figures demonstrate the advantage of using filtering, clearly showing a reduction in PWM related harmonics.

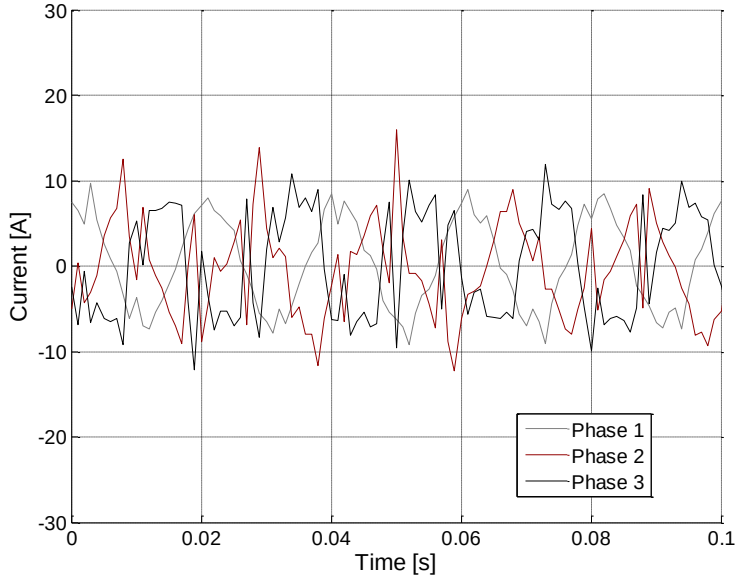

Figure 3.6: Current measurements from the three-phase motor ran by a PMW system

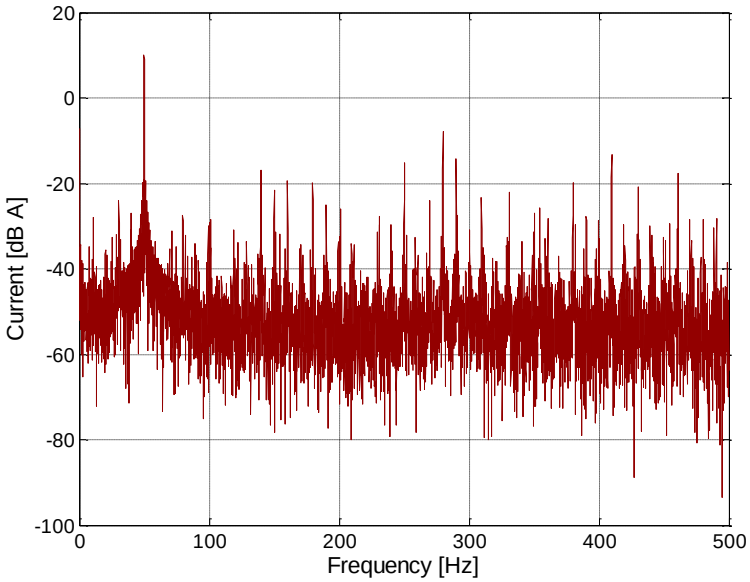

Figure 3.7: FFT analysis of the three-phase current
motor was driven by a PWM system

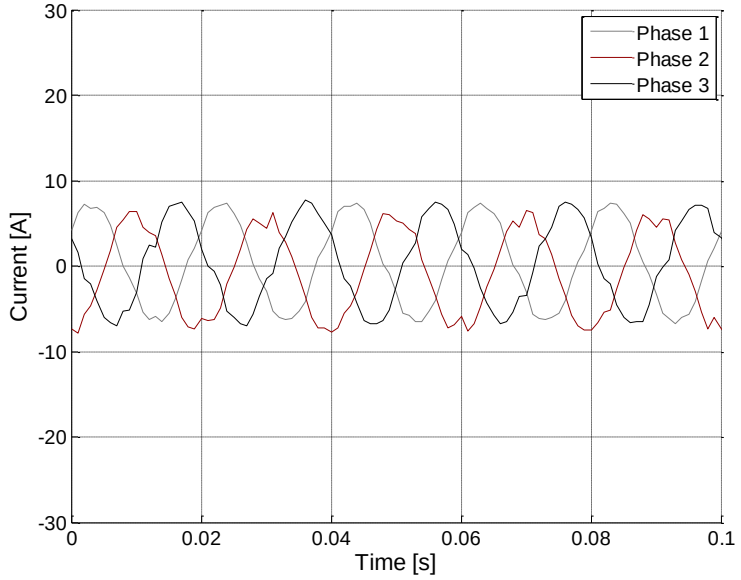

Figure 3.8: Filtered current measurements from the PWM driven motor

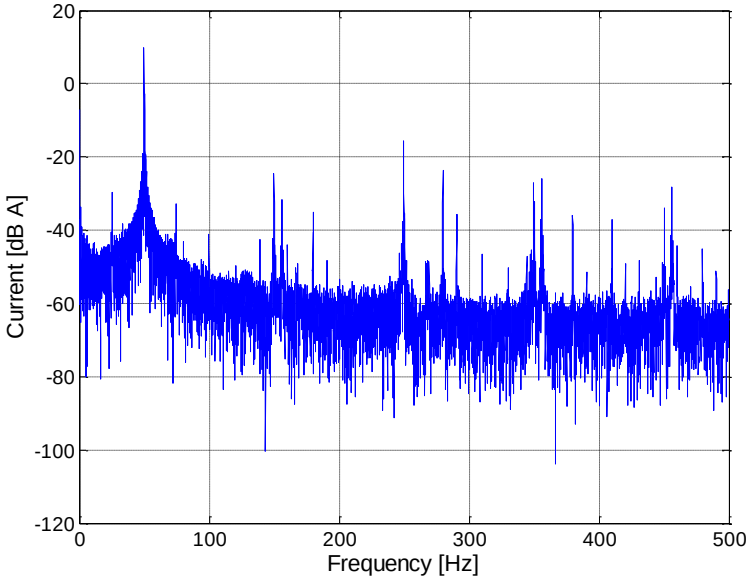

Figure 3.9: FFT analysis of the motor three phase currents with 2 kHz RC filter

In the time-frequency domain, where the frequency components of the system can be studied with time, a low sampling rate can cause observation of false harmonics, which is called an aliasing effect [92]. A test was run to demonstrate the behaviour of the motor and its power performance. Figure 3.10 and Figure 3.11 show the voltage and current measurement of an experiment in which the motor was run from 0 rpm to 1500 rpm with no load. As can be seen in the graphs, after the starting point (when the rotor starts rotating), whenever the current is

higher, the voltage is lower and vice versa. This is followed by P=VI, where P is the electrical power, V is the voltage and I represents the current of the motor. These graphs do not show the exact cycles of each phase, but illustrate the overall magnitude and envelope.

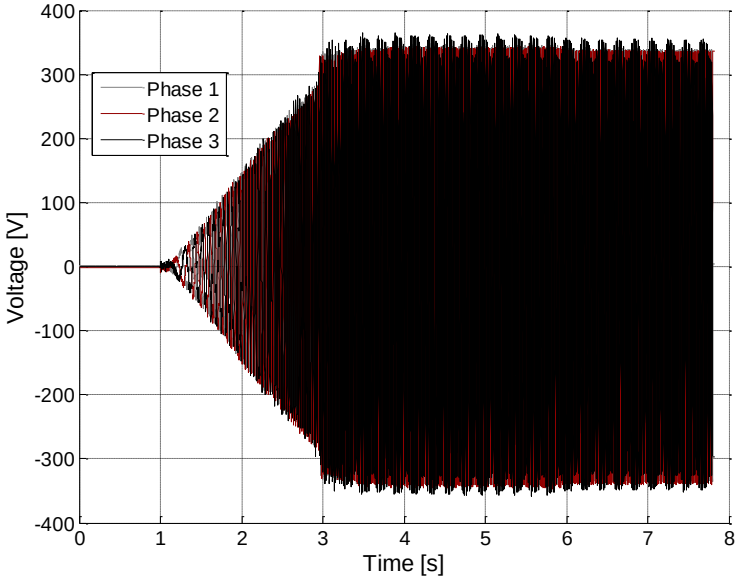

Figure 3.10: Voltage measurements of the system
in which the motor speed was from 0 rpm to 1500 rpm

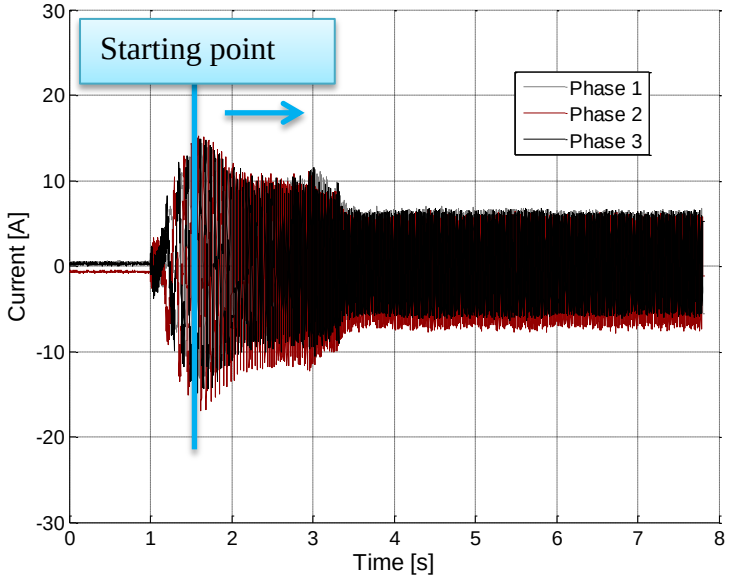

Figure 3.11: Current measurements of the system
in which the motor speed was from 0 rpm to 1500 rpm

In Figure 3.12, frequency changes within the time domain are illustrated. In order to find out what harmonics could represent the mechanical behaviour of the system, a test with variable

torque applied to the shaft was run. Torque was generated by the excitation of the DC motor. The speed of the motor was controlled by the input frequency; the fundamental harmonics from 0 to 55 Hz show that after almost 3.5 seconds the final speed is reached. In a healthy Y-connection of a three-phase wiring, the 3rd harmonic should be considerably lower compared to the 5th harmonic [93,94]. The existence of the 3rd harmonic in this example could be the aliasing effect caused by an inadequate sampling rate and an unsuitable anti-aliasing filter, which were 1 kHz and 5 kHz respectively.

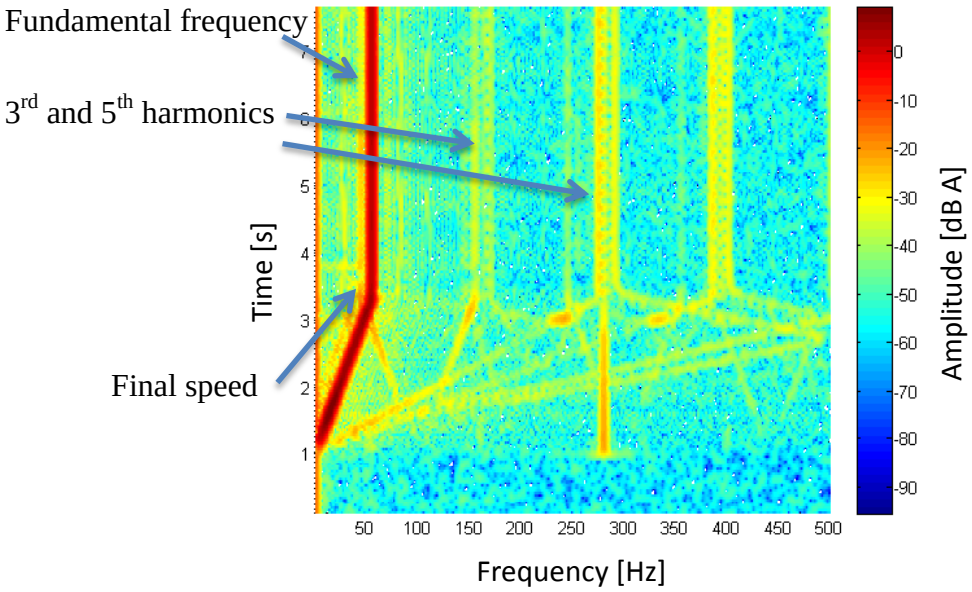

Figure 3.12: Spectrogram of the 0-1500 rpm experiment

Figure 3.13 and Figure 3.14 show the current amplitude and spectral analysis of the test where it changed from no-load to full-load condition; load was applied after 2 seconds of the operation with no load. Figure 3.14 shows harmonics around 290 Hz were moving to 340 Hz at the same time that the load was applied.

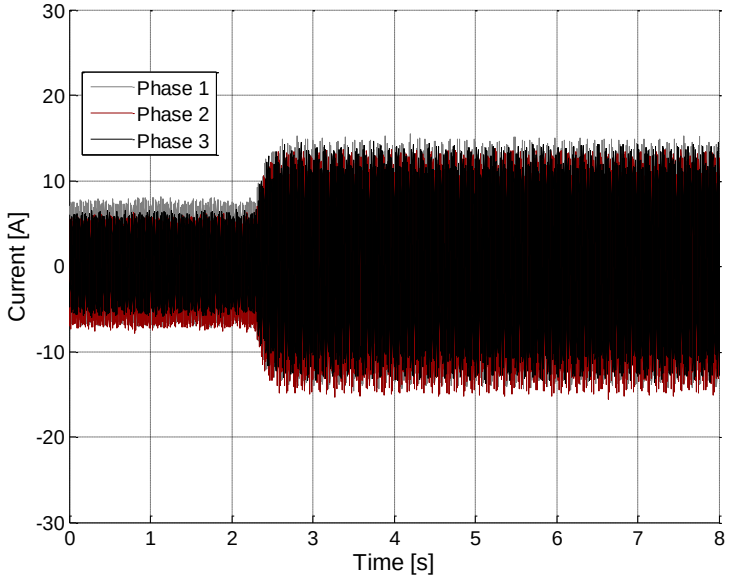

Figure 3.13: Current measurements from a no-load to full-load situation with 1 KHz sampling frequency

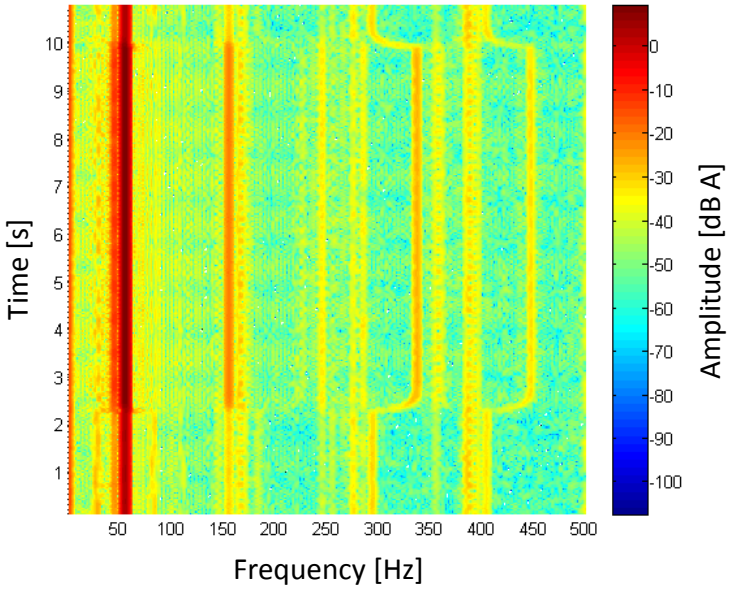

Figure 3.14: Spectrogram of the current measurement for no-load to full-load sampled at 1 kHz

To investigate whether the behaviour of the harmonics were correct, a higher sampling rate, 2 kHz, was applied to a similar experiment. The differences between the two experiments can be accounted for by the manual nature of the experimental procedure.

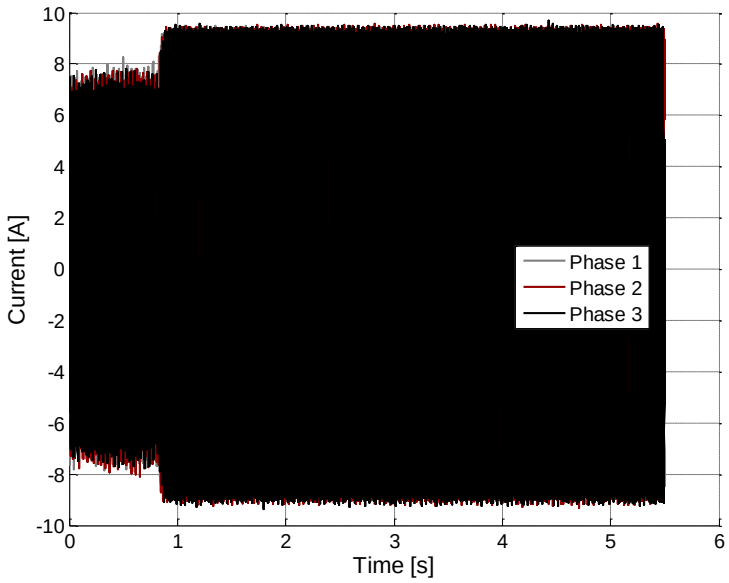

Figure 3.15: Three-phase current measurements from a no-load to half-load situation with 2 kHz sampling frequency

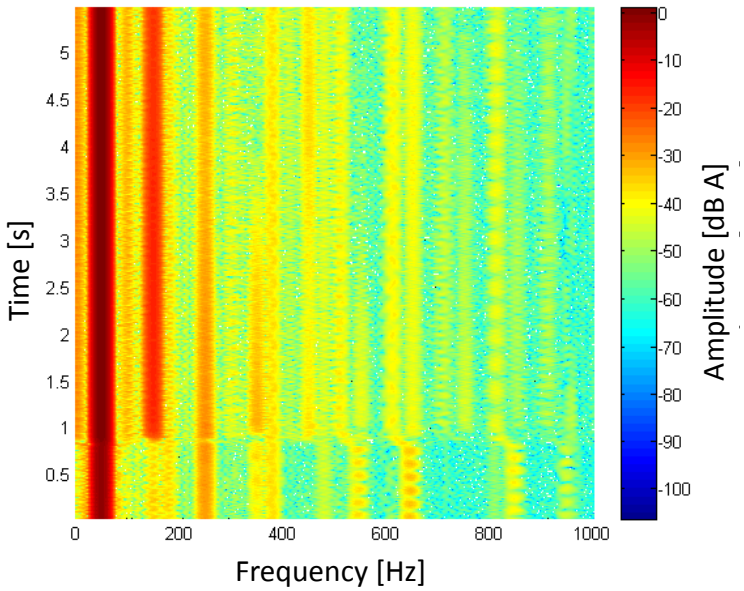

Figure 3.16: Spectrogram of the current measurement for no-load to full-load sampled at 2 kHz.

Figure 3.16, in contrast with Figure 3.14, shows that the frequency of the harmonics related to the load decrease. In the next section it can be seen that due to the high load and torque, the speed decreases and therefore the frequency components related to the load and speed fall.

Thus, an inadequate sampling rate could cause misinterpretation of the behaviour of the machine.

3.3.2 Fatigue machine - hydraulic power unit

A fatigue machine is used to test various stresses on different materials. This machine uses the hydraulic pressure to perform the stress force. A 1.1 kW induction motor drives the hydraulic power unit, which maintains the pressure at around 150 bar [95]. The motor is driven by 50 Hz/400 volts three-phase with a nominal current of 2.64 A. This experiment was mainly used to validate and calibrate the measurements. An NI data acquisition kit and UoB logger have been used to collect data and the analysis showed the same results.

In this experiment, measurement of one of the three phases was collected. Using one phase current data would be enough to carry out motor current signature analysis. However, methods such as Park's vector cannot be used because the measurements of all three phases are required.

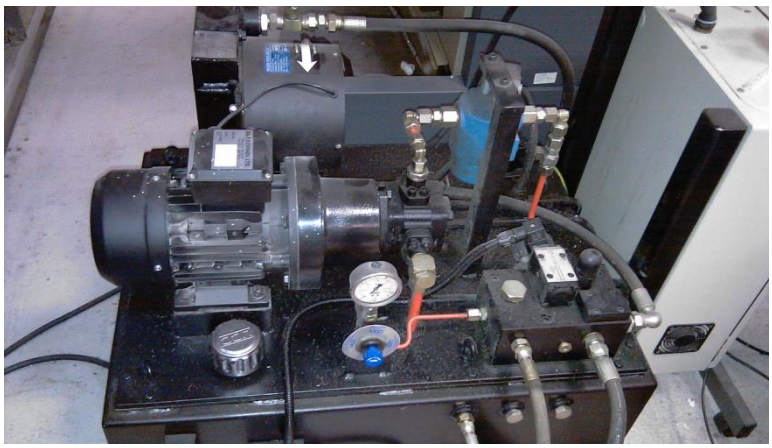

Figure 3.17: 1.1 kW hydraulic power unit driving a fatigue machine [Author's collection]

The current was sampled with frequencies of 10 kHz and 2 kHz, both with a 5 kHz anti-aliasing filter; this was to choose a suitable sampling rate for further analyses. Figure 3.18 is a comparison of the two sampling rates. Six cycles at the sampling rate of 2 kHz resulted in

240 sample points; for a 10 kHz sampling frequency 1200 points were collected. The measurements in time domain analysis are almost identical, apart from a larger data size (approximately five times greater) in the 10 kHz test.

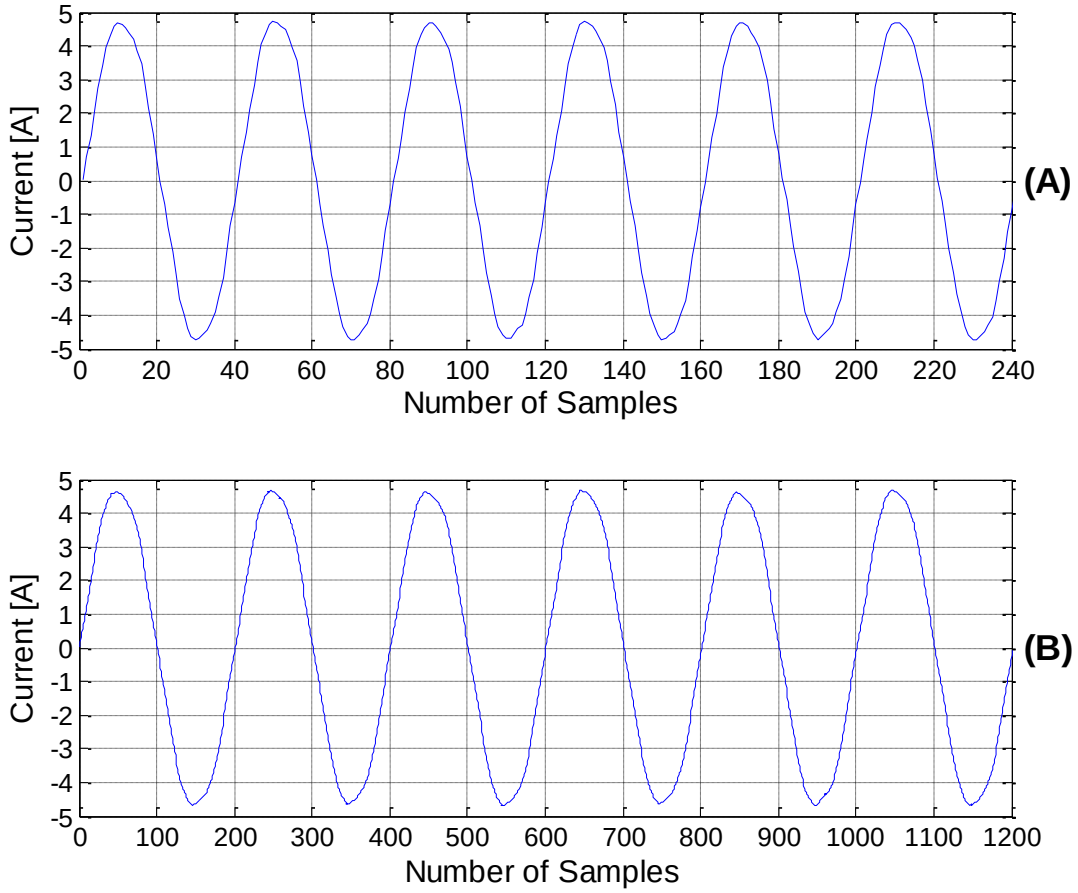

Figure 3.18: Current measurement at 150 bar
(A) at 2 kHz sampling rate (B) at 10 kHz sampling rate

To compare the frequency domain analysis and importance of the sampling rate, spectrograms of the signals are used. In this experiment, the hydraulic unit started from 0 bar and stopped at 150 bar. The hydraulic pump, driven by an induction machine, maintains the pressure for the fatigue machine and the effect of applied torque appears on the current signature, which can be seen within the spectrogram between 400 – 600 Hz. The current also increases over time as more power is needed to maintain higher pressure values. Figure 3.19 illustrates the current measurement and shows how the current increases.

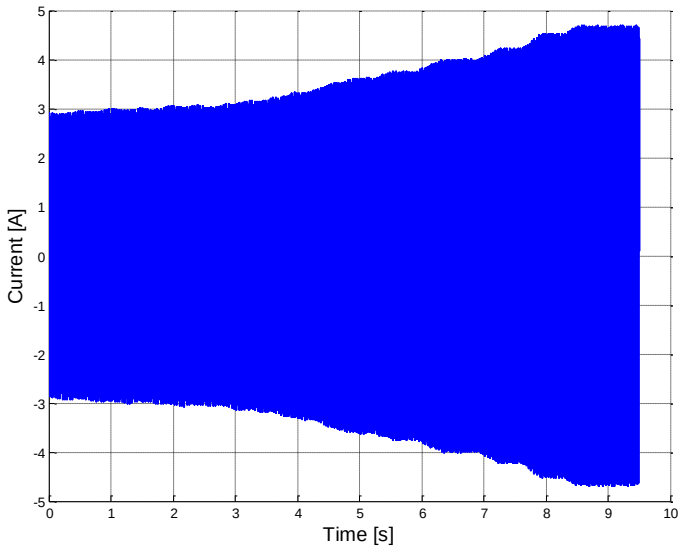

Figure 3.19: Current measurement from 0 - 150 bar

The results of the time-frequency domain, with 10 and 2 kHz sampling rates are shown in Figure 3.20 and Figure 3.21. Harmonics related to changes in pressure and increases in current can be seen in both figures. However, by the use of digital filtering, the harmonics can be observed more clearly. A 400 Hz third order high-pass Butterworth filter was applied; the characteristic of the filter is illustrated in Figure 3.22 [96]. The results of this filter can be seen in Figure 3.23. The harmonic analyses up to 1 kHz are identical to the analyses from 2 kHz sampled data. At a 10 kHz sampling rate, analysis of the current signature from 1 kHz up to 5 kHz, shown in Figure 3.24, does not provide any significant information with regards to harmonic analysis and system behaviour. Therefore, higher frequency measurements are not considered. Consequently, this results in smaller data size thus saving time in processing and space in storing.

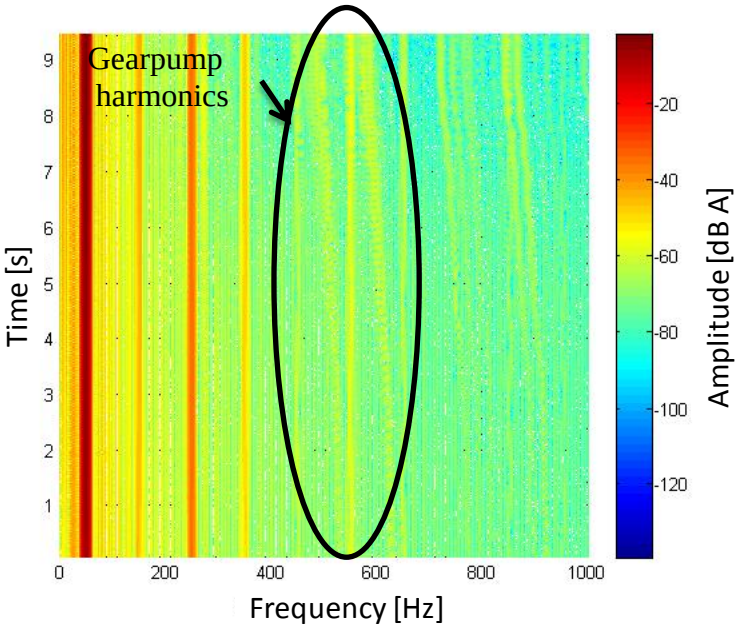

Figure 3.20: Spectrogram of the measured current at 10 kHz sampling rate

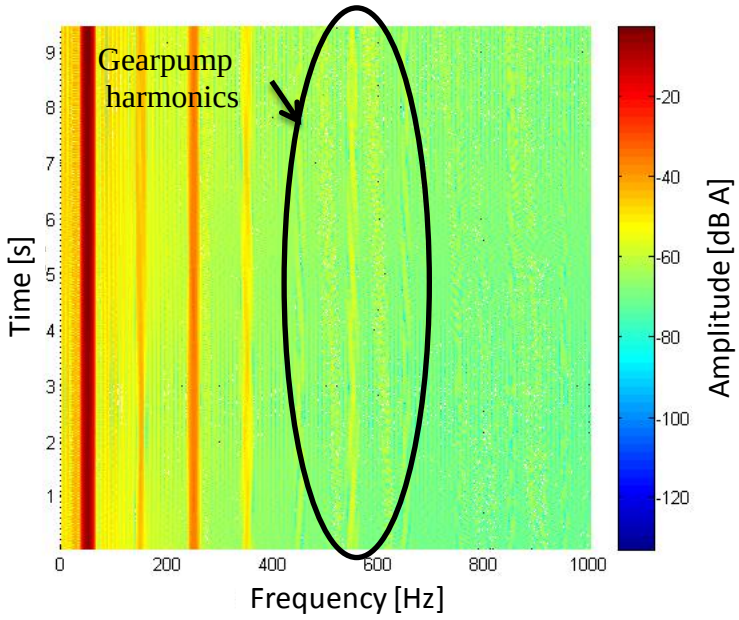

Figure 3.21: Spectrogram of the measured current at 2 kHz sampling rate

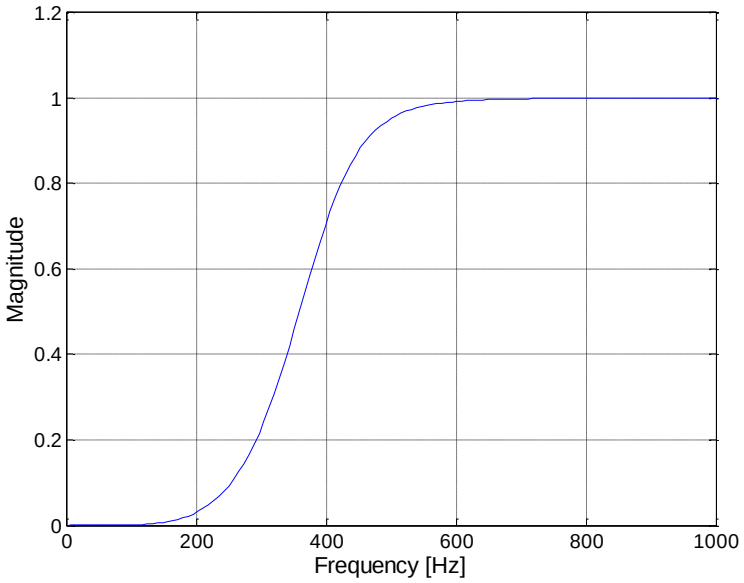

Figure 3.22: Characteristics of a third order Butterworth filter

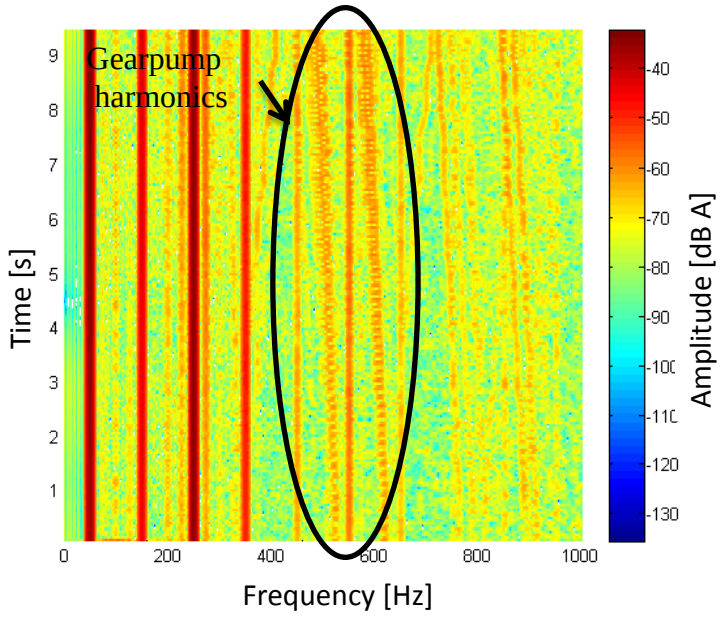

Figure 3.23: Spectrogram of the measured current at 2 kHz after being passed through a 400 Hz Butterworth filter

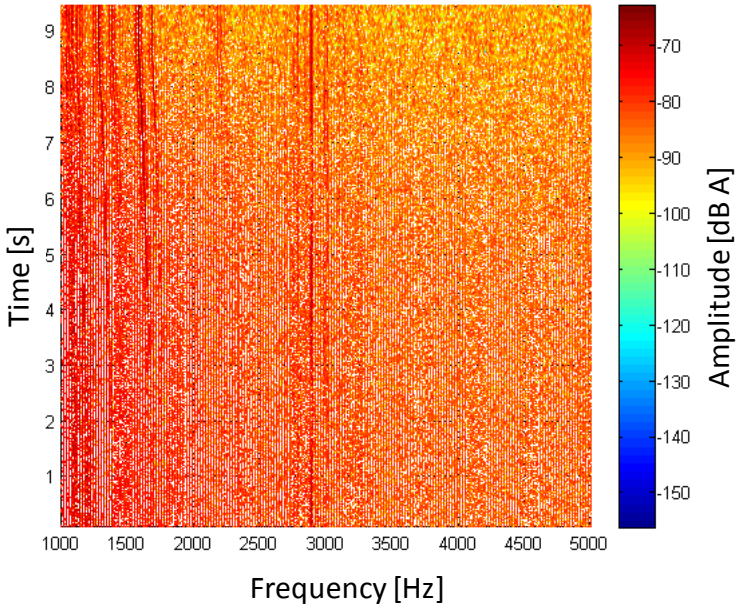

Figure 3.24: Spectrogram analysis for higher frequency range
1 kHz – 5 kHz

3.3.3 Ventilation fan system

A 1.1 kW induction motor driving a ventilation fan system, located at the railway traction laboratory facility, was used to test the automatic data logging, auto triggering system. In order to monitor the three phases providing power to the ventilation fans an understanding of the wiring diagrams and components within the main control panel was required. Figure 3.25 is a copy of a wiring diagram from the system drawing documents [97]. Figure 3.26 shows the current transformers clamped over the fan wiring, noted in the drawing document, within the main control panel. The use of current clamps is a non-intrusive approach, which avoids interfering with the existing wiring.

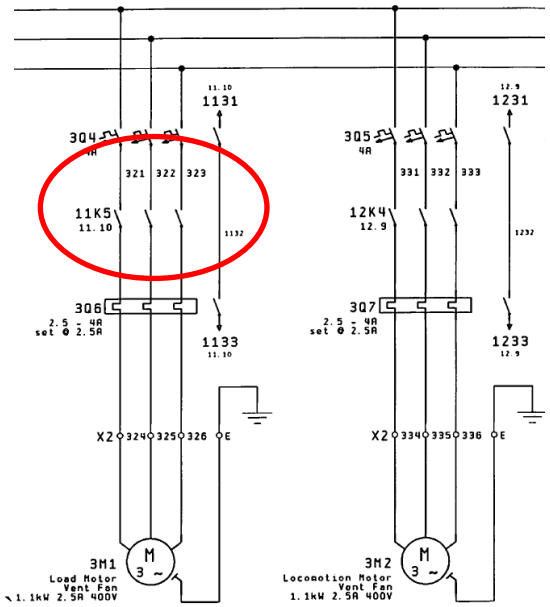

Figure 3.25: Wiring diagram of the ventilation fans
from the control panel confidential documents

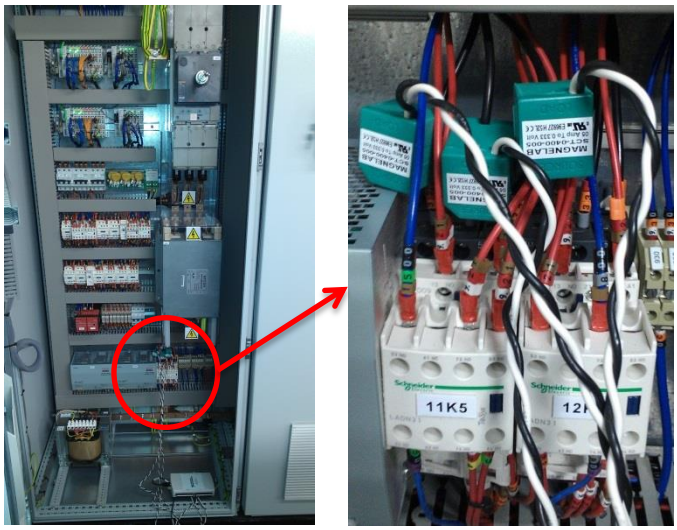

Figure 3.26: Installed sensor within the control box
[Author's collection]

Figure 3.27 shows the ventilation fan within the BCCRE traction laboratory. The fan is driven by a 1.1 kW three-phase induction machine; rated for 50 Hz, 360-480 volts and 1.97-3.00 Amps nominal current, with speed of 2800 rpm.

Figure 3.27: 1.1 kW ventilation fan located at the railway centre traction lab
[Author's collection]

The data logging system was designed to be able to detect the exact period that the motor is running, including starting peak. This is to avoid collecting data while the motor is not operating, which saves storage space and processing time. Figure 3.28 presents the automatically recorded event of the running fan.

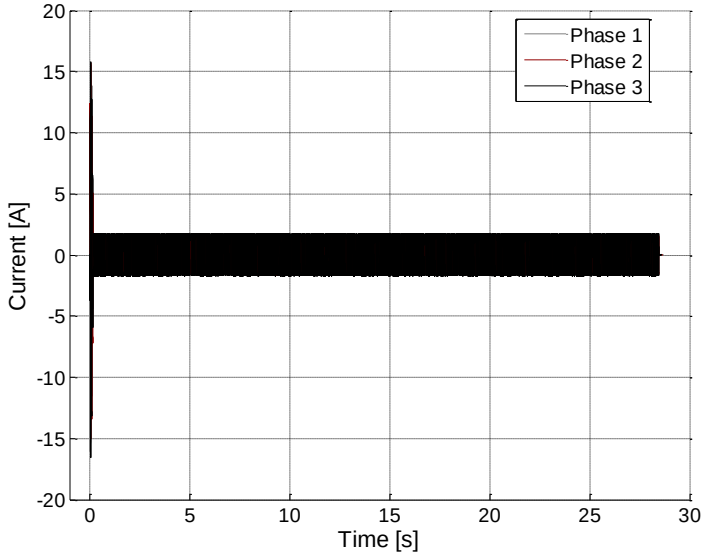

Figure 3.28: Sampled experiment of the running ventilation fan

Figure 3.29 shows the start and end points of the sampling period zoomed in. The system is able to buffer up to a few hundred milliseconds before and after predefined threshold levels. The auto-triggering system is designed such that false starts caused by random inputs or sensor noises are avoided. Appendix A provides a detailed explanation of how the triggering system performs.

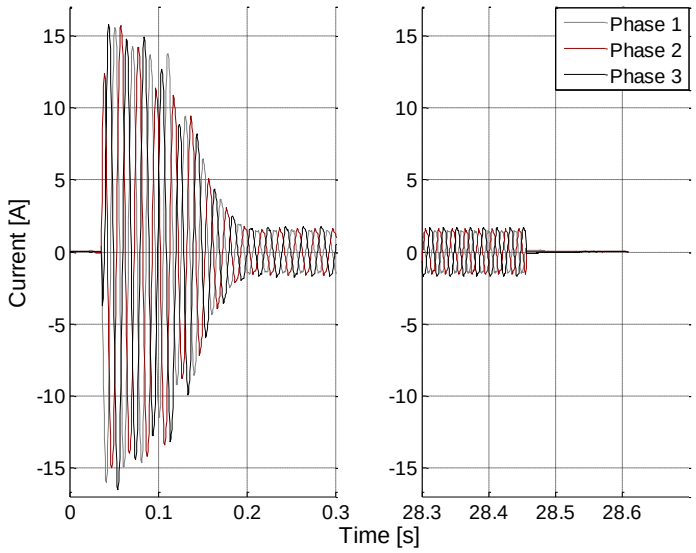

Figure 3.29: Zoomed windows of the starting and end point of the fan operational period

All three phases were measured, therefore Park's transform method was also tested on the measured data. The Park's vector approach could lead to possible fault detection and diagnosis [98]. Applications of use of Park's vector are usually used in systems that are continuously running, so the starting peaks are mainly not considered within Park's analysis. Figure 3.30 illustrates the Park's transform of the shown event including the start-up of the motor.

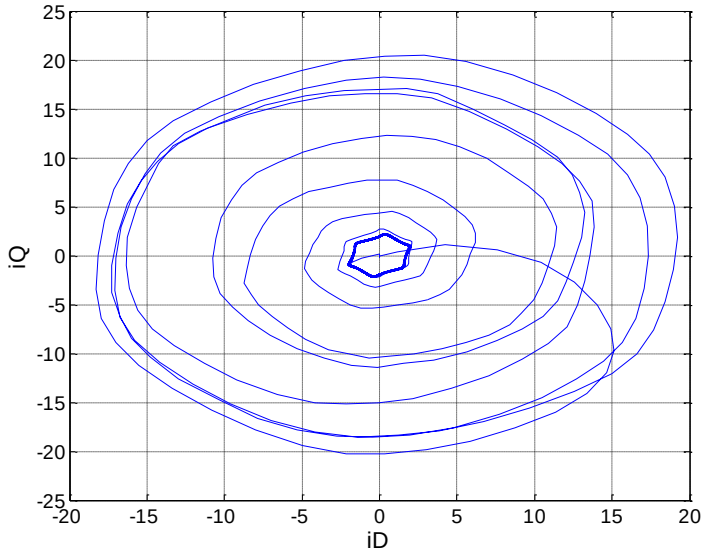

Figure 3.30: Park's transform of the sampled event

As the starting peaks are not usually considered in this method, the Park's transform of the event without starting peak is demonstrated in Figure 3.31.

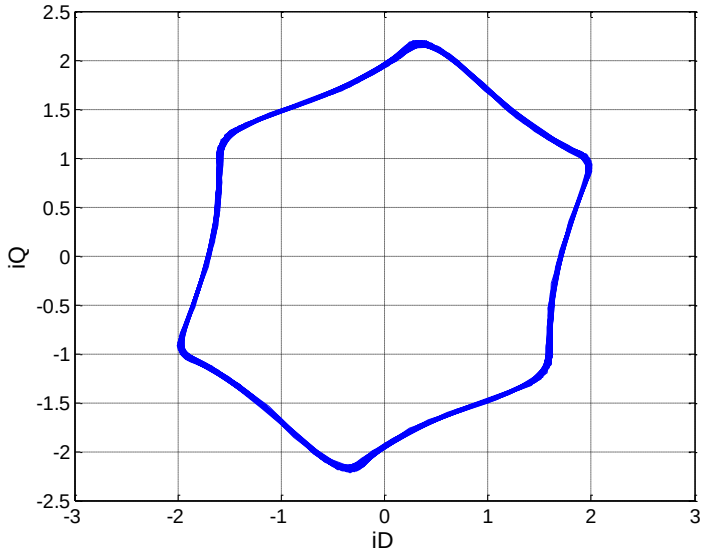

Figure 3.31: Park's transform of the current without the starting peak and slightly before the end of the operation

Within the test, there was an abnormality within the Park's transform curve, which may represent a fault. Figure 3.32 is the Park's transform of the irregular condition. However, the frequency analysis does not show any interesting harmonic, shown in Figure 3.33. The irregularity within the Park's transform can be related to measurement noise or impulsive noise [99].

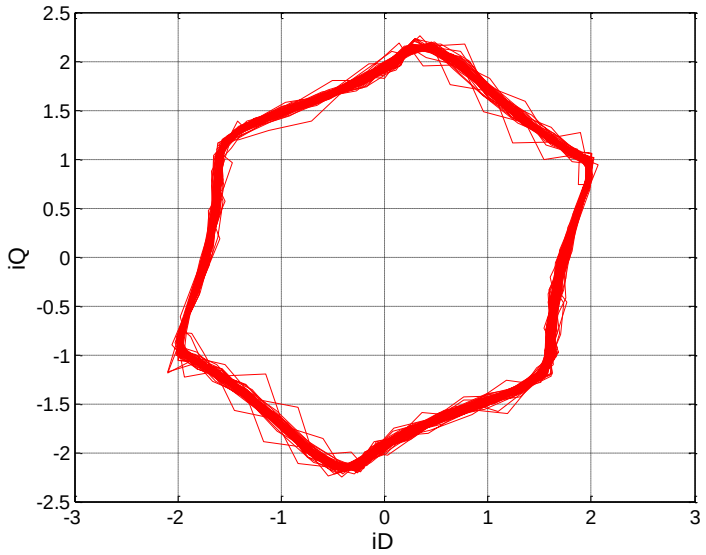

Figure 3.32: Park's transform of an abnormal situation

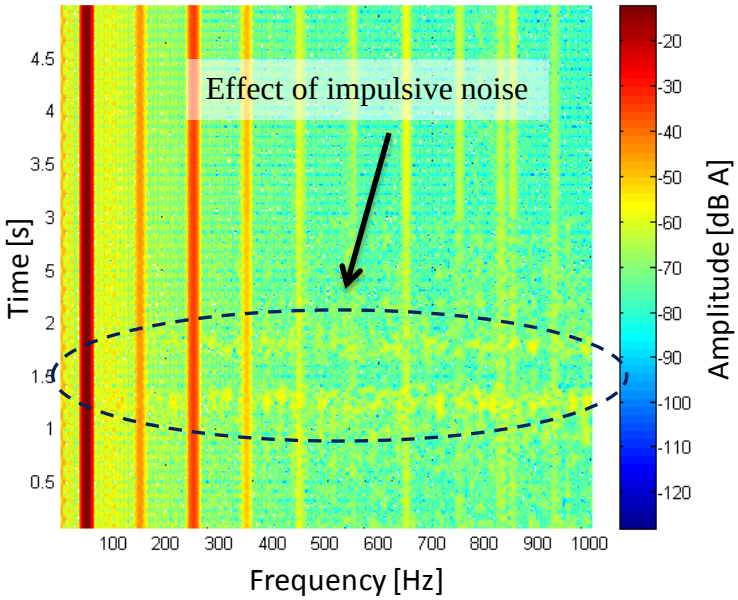

Figure 3.33: Spectrogram of the measured signal with the possibility of impulsive noise

Figure 3.34 illustrates the spectrogram of normal operation of the ventilation fans. In order to show how the blades effect can be seen on the spectrogram analysis, the number of blades were counted; the effect can be calculated as follows:

Motor nominal speed = 2800 rpm, Supply frequency = 50 Hz, Number of blades = 40

Equations (3.1) and (3.2) calculate how long it takes for a single blade to carry out one complete revolution, T.

$$T = \frac{\theta}{\omega} \tag{3.1}$$

$$\theta = \frac{2\pi}{n} \tag{3.2}$$

where ω is the angular speed $[rad.s^{-1}]$ of the motor, θ is the angular position of a blade $[rad]$ and n is the number of blades.

Using the motor specification, equations (3.1) and (3.2) T is 5.357 milliseconds. Therefore the frequency is around 1866 Hz. As the sampling rate is 2 kHz and the anti-aliasing filter is 5 kHz, the alias effect of this frequency has been measured at about 927 Hz, shown in Figure 3.35. This could represent the sub-harmonic of the original 1854 Hz, which is the effect of the blades on the stator current.

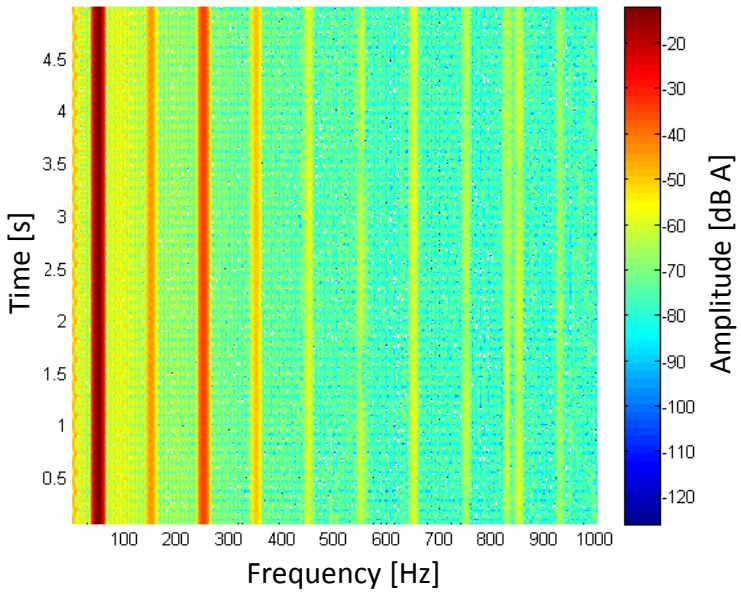

Figure 3.34: Spectrogram of a healthy measurement

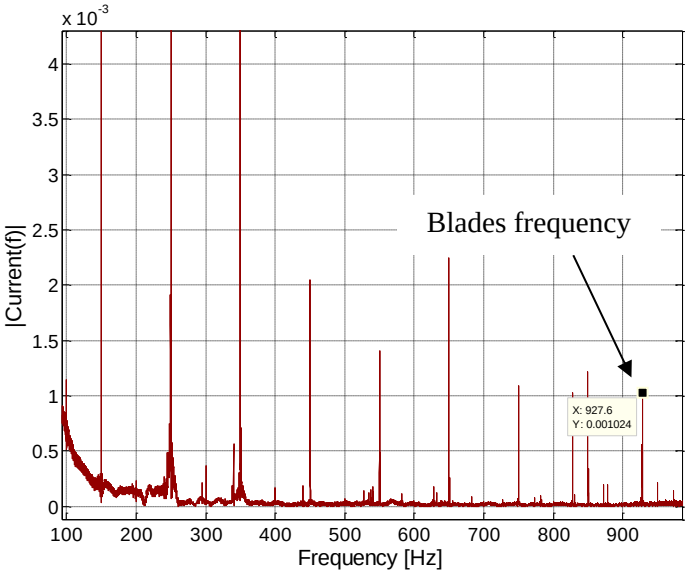

Figure 3.35: Stator current FFT analysis (100-1000 Hz)

3.3.4 1.1 kW induction motor

This experiment was run to explore a no load condition of a three-phase motor, and also to discover the behaviour of a fault on the rotor bar, which was applied by impulsive forces to the shaft. Additionally, measurement of the three-phase voltage was carried out. In order to measure the voltages, two LEM AV 100 voltage transducers were used; these sensors should be physically connected to the main power lines, which is supplying power for the motor [88]. The voltage measurements and analysis showed that nothing significant could be seen to study the behaviour of the system. This eliminates the need for voltage sensors and avoids the invasiveness of the main approaches.

In this test a 1.1 kW induction motor, shown in Figure 3.36, was used; rated for 415 volts, 2.54 Amps nominal current and speed of 1410 rpm.

Figure 3.36: 1.1 kW three-phase motor
[Author's collection]

To begin, the measurement of a healthy condition was carried out. Figures 3.37 and 3.38 show the current and voltage measurements, which illustrate the general overview of the signal envelope of the abovementioned induction motor. The FFT, spectrogram, envelope (using peak detection method and Hilbert transform) and Park's transform analyses of the healthy condition were performed and the results are shown in Figures 3.39, 3.40, 3.41, 3.42 and 3.43. Using Hilbert transform to carry out envelope analysis indicates all peaks as positive values; this is due to the square root of the squared values of the imaginary and real part in the H(x) signal.

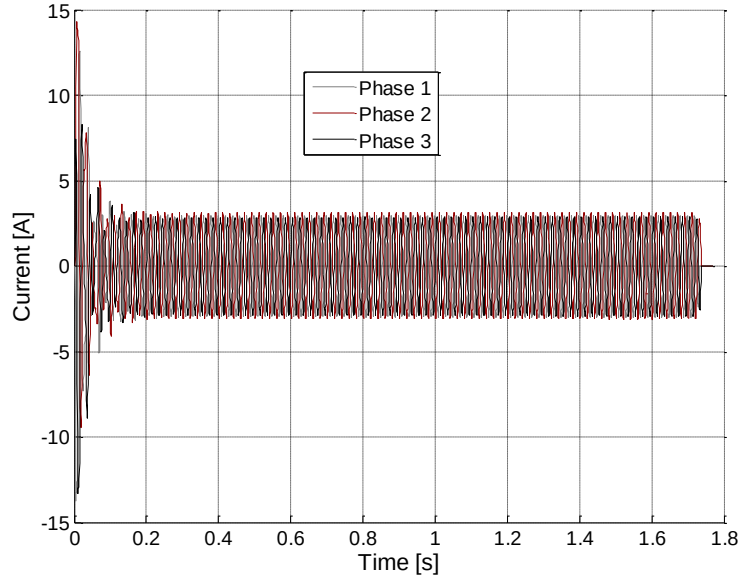

Figure 3.37: Measured three-phase current from the starting point until it stopped

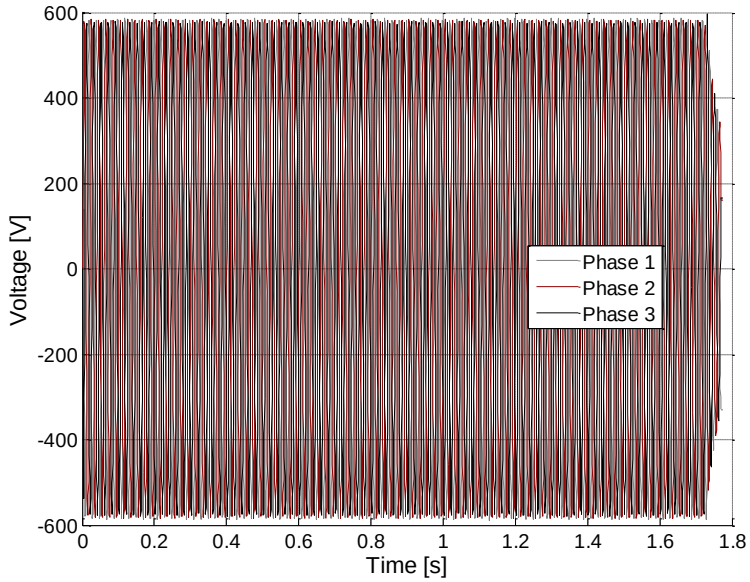

Figure 3.38: Voltage measurements of the motor

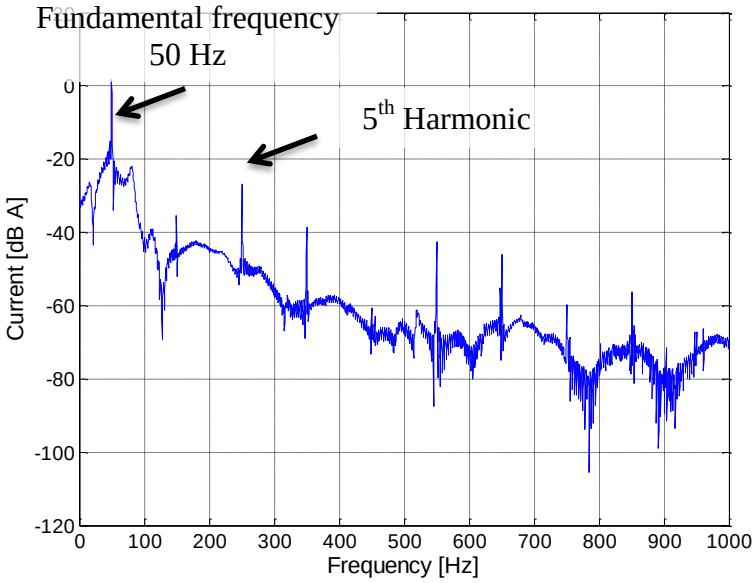

Figure 3.39: Fast Fourier of the healthy condition measurements

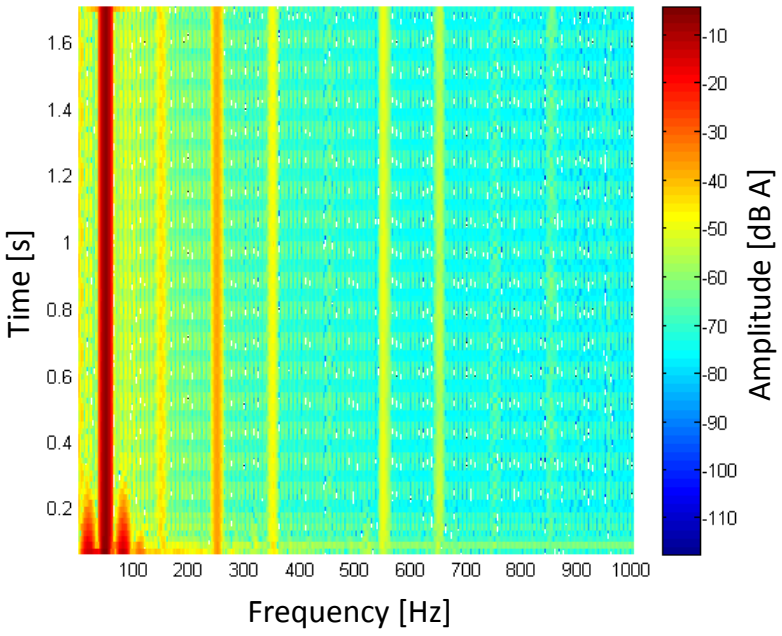

Figure 3.40: Time-Frequency spectrogram analysis of the healthy condition

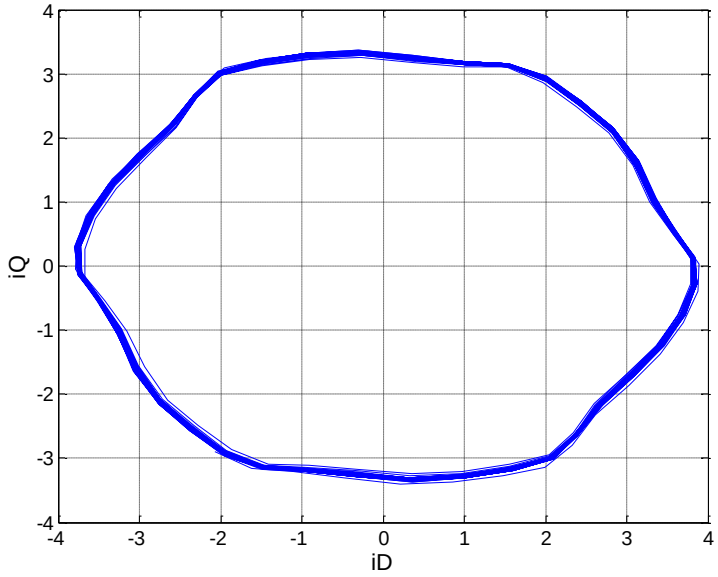

Figure 3.41: Park's transform of the healthy condition
starting peak is eliminated in this figure

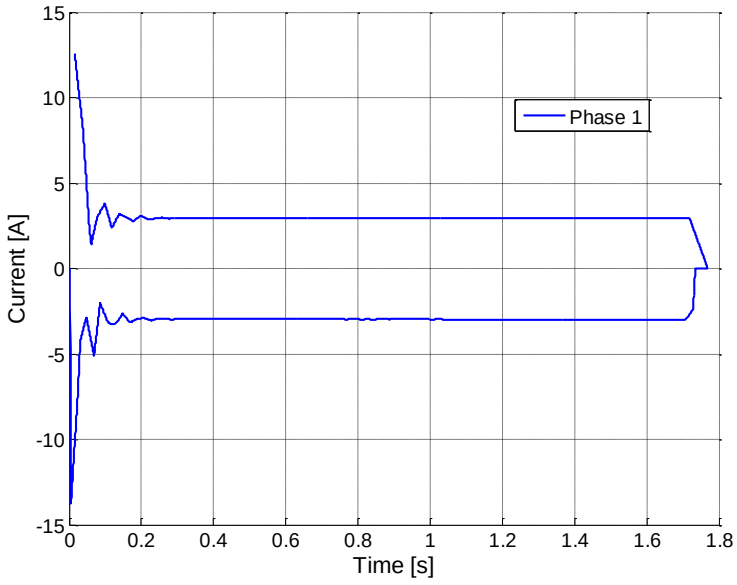

Figure 3.42: Envelope of the original signal using peak detection method

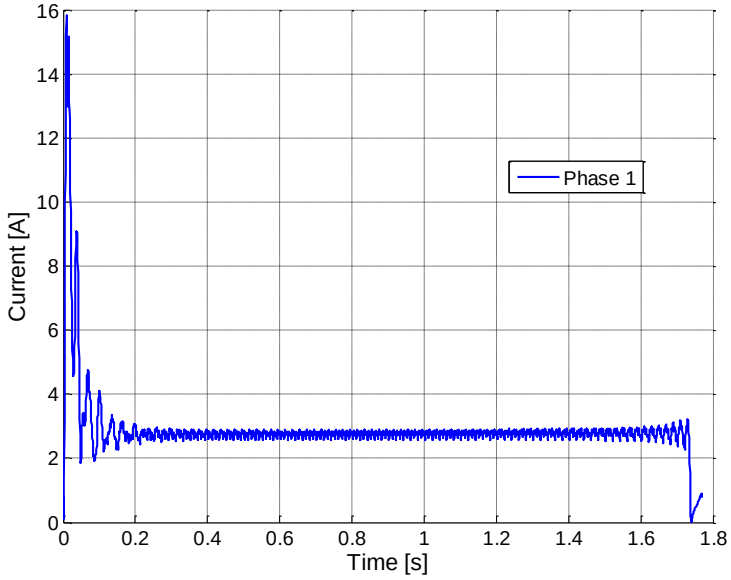

Figure 3.43: Envelope of the original signal using Hilbert transform

After having the healthy condition results, an impulsive force on the output shaft for every revolution - was applied and the results were compared within 2500 samples from each experiment, which is about 1.25 s.

In Figure 3.44, the original signals from both experiments are shown. A number of spikes within the faulty condition can be seen, which are related to the faulty situation.

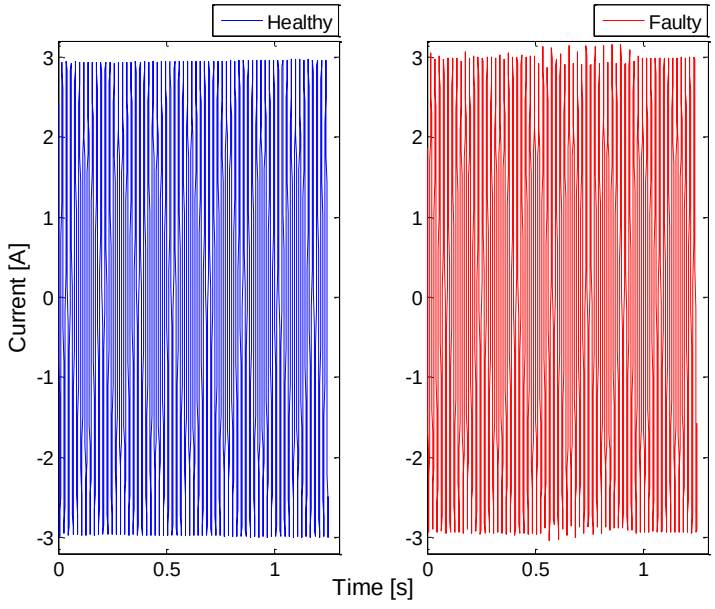

Figure 3.44: Comparison of one phase from a healthy and a faulty measurement
blue illustrates the heathy condition and red illustrates the faulty condition

The fault also appeared within the signature analysis of the current. Figure 3.45 is the FFT spectral of the original signals and at around 25 Hz and 75 Hz unknown harmonics are revealed, which could also be explained by equation (2.4).

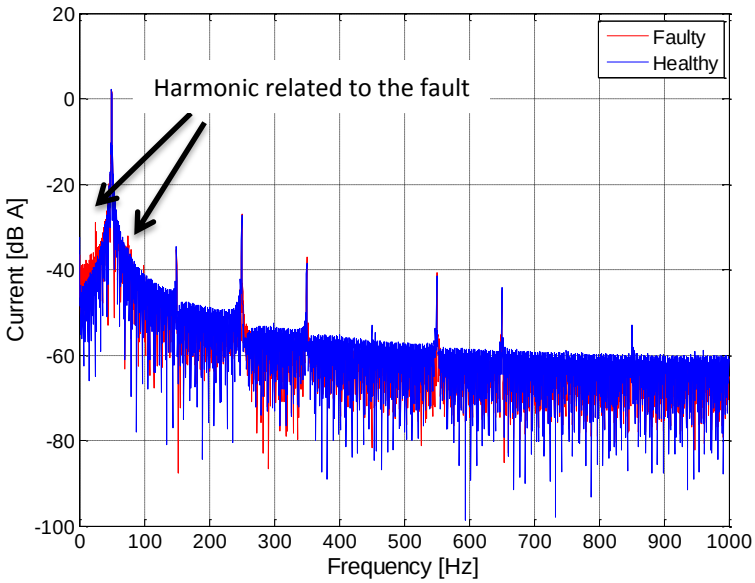

Figure 3.45: FFT of the healthy and faulty conditions

Within spectrogram (time-frequency domain) analysis of the faulty signal, the time and the period of the fault can be seen. This is illustrated in Figure 3.46. This could be represented by the eccentricity frequency [100].

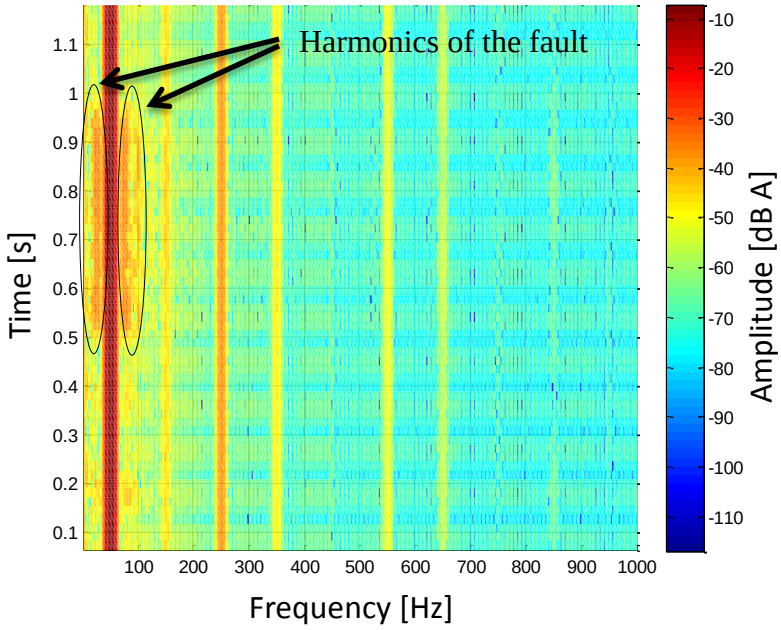

Figure 3.46: Spectrogram of the faulty condition

Park's transform and envelope analyses also indicate the fault. These can be seen as follows:

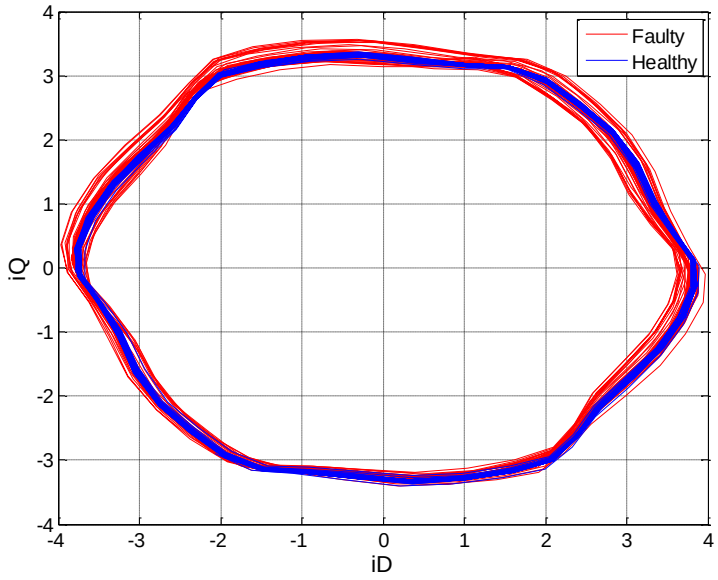

Figure 3.47: Park's transform of the healthy and faulty condition

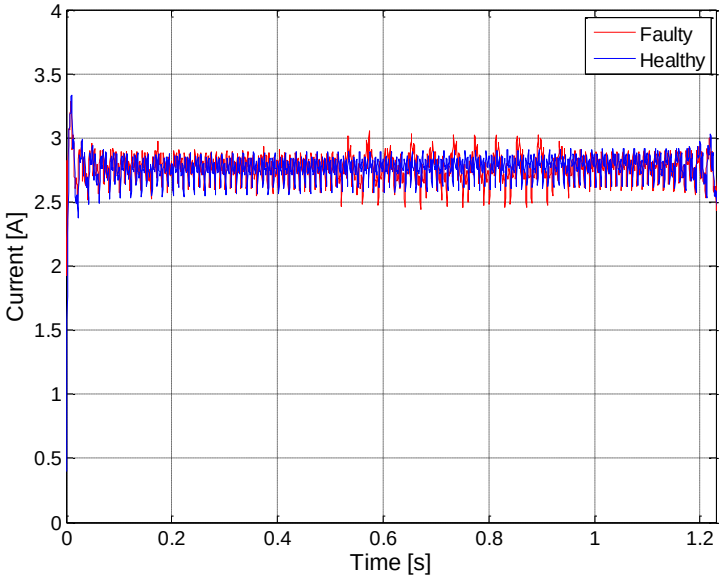

Figure 3.48: Hilbert transform of the healthy and faulty condition

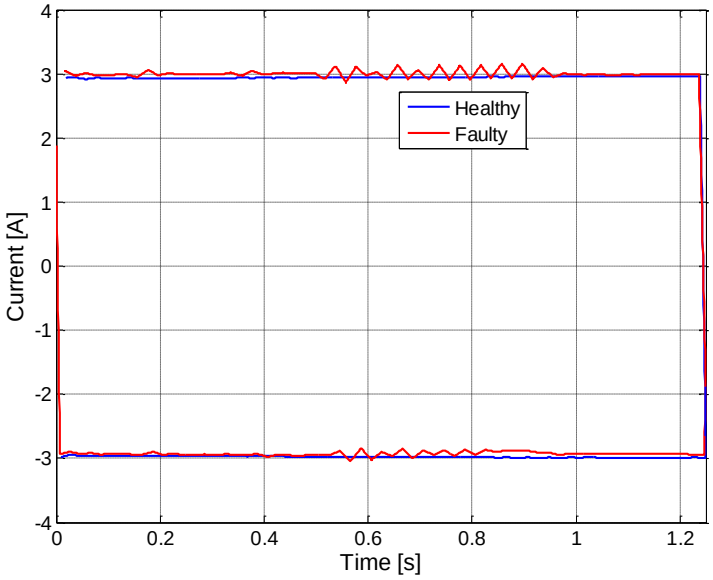

Figure 3.49: Envelopes of the healthy and faulty condition

To confirm that the voltage measurement is not needed to carry out fault detection and diagnosis of the three-phase motor, voltages were measured and analyses are as follows:

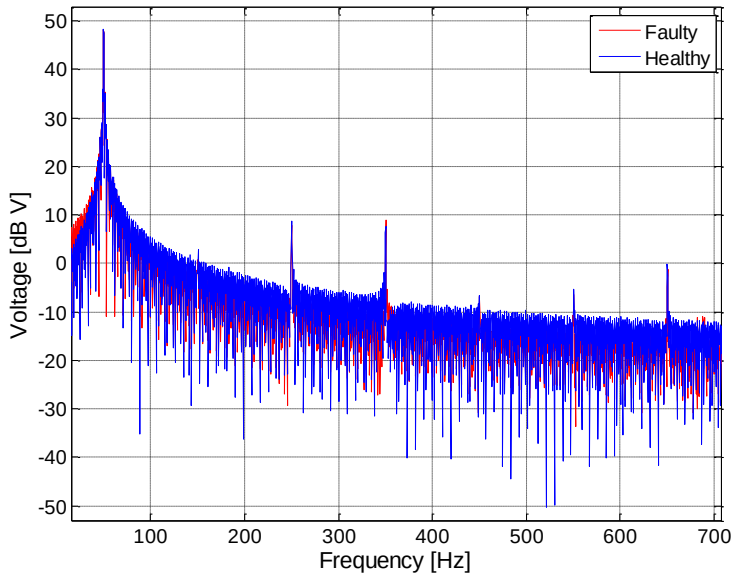

Figure 3.50: Frequency analysis of faulty and healthy condition voltages

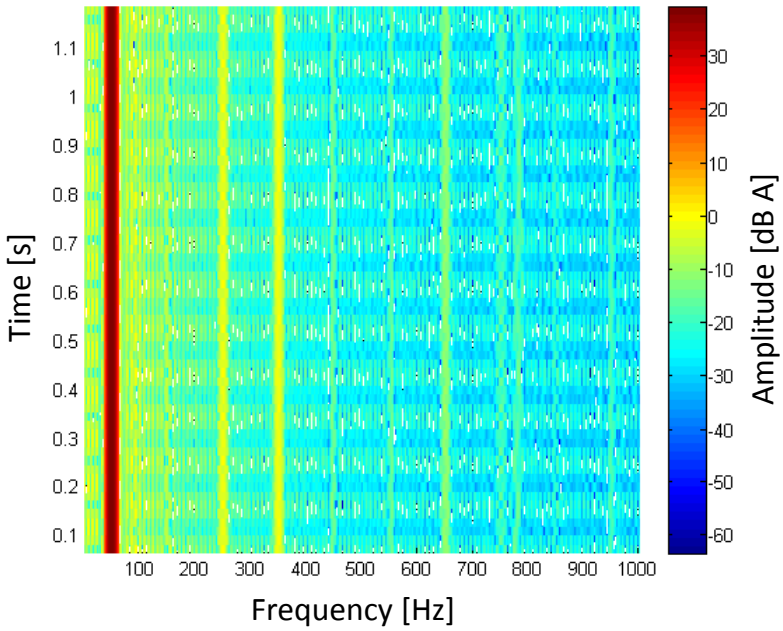

Figure 3.51: Spectrogram of the voltage in healthy condition

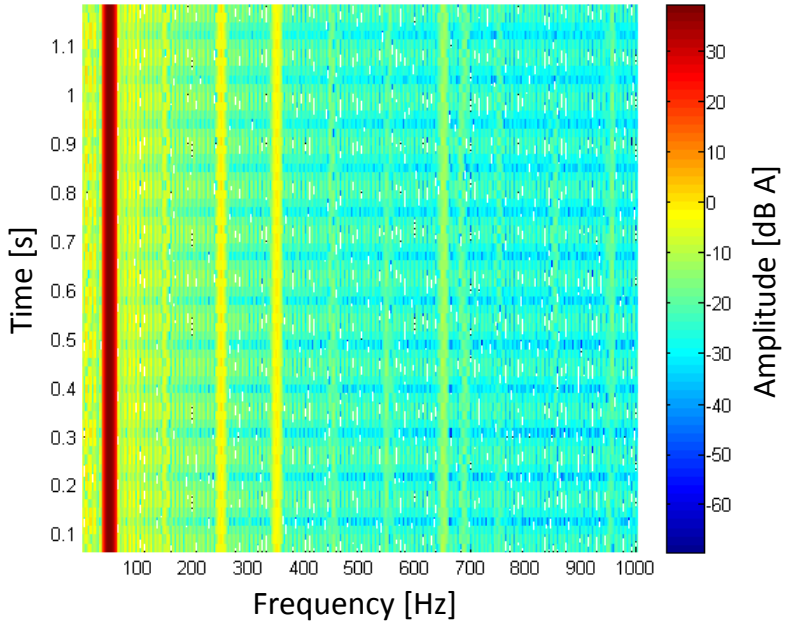

Figure 3.52: Spectrogram of the voltage in faulty condition

As can be seen in Figures 3.50, 3.51 and 3.52 there is no difference between the healthy and faulty conditions by analysis of the voltages.

3.4 Summary

In this chapter various laboratory experiments were described, and the use of applied methods, explained in Chapter 2, were demonstrated. The approaches from the previous chapter have been practically applied and discussed. An experiment was carried out to illustrate healthy and faulty conditions of an induction machine using current signature analysis. The motor current analysis and its advantages and limitations for condition monitoring, and fault detection and diagnosis approaches for induction machines were discussed, for example, a combination of a Park's transform and spectrogram analysis was used to detect corrupted measurements. An induced laboratory-based fault was applied to evaluate the use of motor current signature analysis. Improvements within the data acquisition unit have been described, as has the use of filtering to avoid unimportant high frequency harmonics and noise produced by systems such as PWM-based power, and

choosing an adequate sampling rate to prevent loss of the important harmonics that relate to the behaviour of the system. The use of a wiring diagram and control panel configuration was also studied. The unimportance of voltage measurements for condition monitoring of a three-phase system has been discussed. It also demonstrated the use of lower sampling frequency in motor current signature analysis applications and how the methods can be used to show the behaviour of a three-phase induction machine and its related system.

In the next chapter the achieved methods are applied to monitor the condition of a wind turbine brake hydraulic power unit, which is driven by a three-phase induction machine.

Chapter 4 NEG MICON 750 Brake Hydraulic Power Unit

4.1 Introduction

This chapter describes how condition monitoring of the hydraulic power unit of a wind turbine mechanical brake system was carried out. This is an expanded version of work that has already been published in the Journal of Renewable Energy [101], of which the author was the main contributor, in addition to being the lead author. The mechanical brake, as explained in Section 1.6.2, is a fail-safe braking system that is usually installed on a high-speed shaft. The hydraulic power unit provides active hydraulic pressure to keep the wind turbine brakes disengaged. When the brake command is sent, or if the electric system drops-out, the brakes will immediately engage to stop the rotor. Active hydraulic power, provided by the pump, is used periodically to maintain the pressure in the accumulator to release and keep the pads off the brake disc.

Figure 4.1 is a schematic of the whole braking unit installed on a NEG Micon 750 wind turbine, located at CRES wind farm – Greece [102].

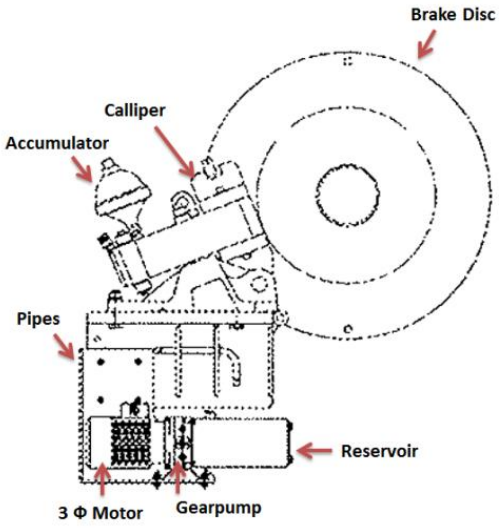

Figure 4.1: SIME-Industry mechanical brake system installed on NEG Micon 750 adapted from reference [103]

Figure 4.2 is the diagram of the wind turbine hydraulic power system. The three-phase motor drives a gear pump that maintains the hydraulic flow within the pipes. An electro value is installed to automatically drop all the pressure if the power goes off or a major failure is detected within the turbine. The pressure limit value also protects the accumulator and pipes in case the pressure goes higher than is expected. A pressure sensor failure or a fault within a controller could cause the pump to operate longer than necessary. After the pressure reaches a certain limit (250 bar in this example) the valve opens and directs the extra pressure to the tank.

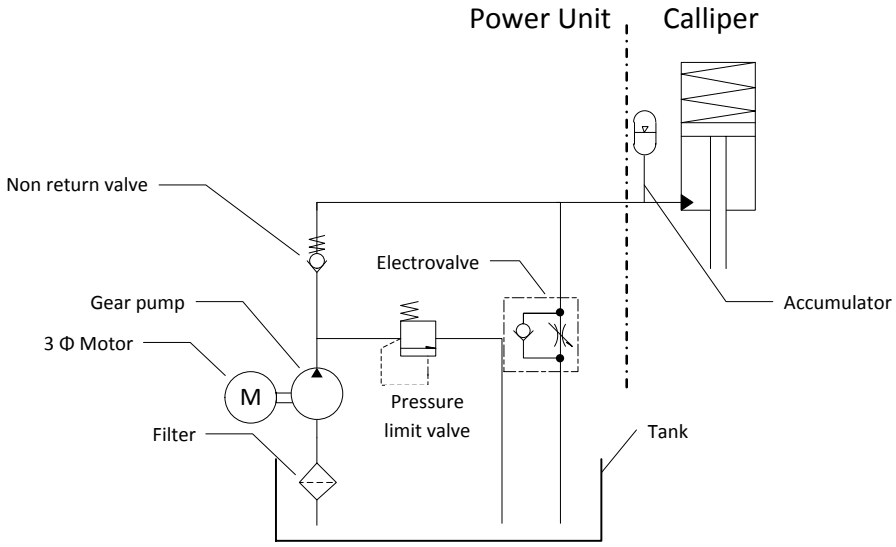

Figure 4.2: Hydraulic system of NEG Micon 750
adapted from reference [103]

Currents flow in the three-phase pump motor only when the pump is charging the accumulator, a process that normally takes just a few seconds. The rest of the time there is no current flowing in the motor. The duration of the event is just a couple of seconds, therefore the analysis can be performed fairly fast. This part of the thesis describes how analysis of three-phase currents of the hydraulic pump motor was used to monitor its condition.

4.2 Measurements and analysis

4.2.1 Data acquisition

The data acquisition system, shown in Figure 3.1, collects data from the sensors. Primary fault detection stages, such as peak detection and moving average calculations, of the sampled currents are also carried out by the digital signal processor of the data logger. Data are then stored on a flash memory card, along with time from a global positioning system module and a real-time clock calendar. Light emitting diodes (LEDs) provide status information. A connection to the wind farm central processing system is also provided by a web interface to present the raw data plus the basic analysis of the performed braking events. The whole system is powered from the local mains supply with a battery back-up to avoid data corruption in the event of power loss.

The custom-built condition monitoring system was installed within the main control panel of the NM-750 wind turbine, which is shown in Figure 4.3. It also illustrates how the currents of the three-phase motor were obtained from the main panel. Samples of the three-phase hydraulic pump motor voltage and currents were collected to monitor its condition. The system measured and logged the three-phase currents at a 2 kHz sampling rate with 16-bit resolution.

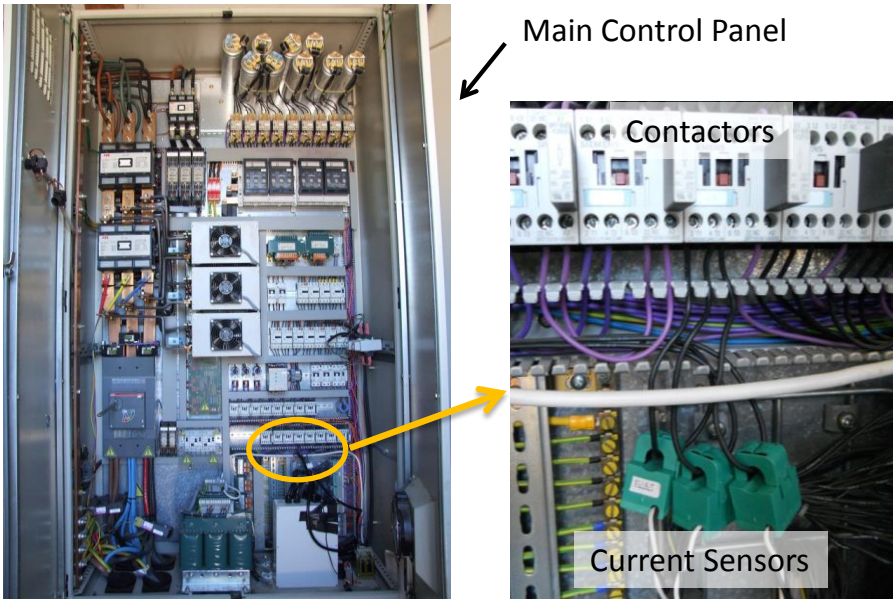

Figure 4.3: The main control panel of the NEG Micon and the UoB data logging system connections for condition monitoring of the three-phase hydraulic power unit current

Figure 4.4 shows an example plot of the three logged current channels following the release of the brake. This was captured using the auto detection mode of the data logging unit.

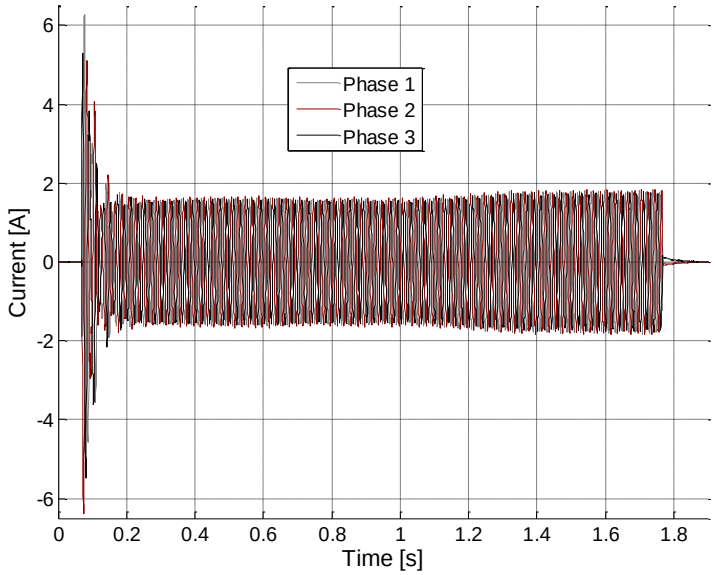

Figure 4.4: Automatically recorded data from the hydraulic unit by UoB data logging unit

4.2.2 Data analysis

4.2.2.1 Time-frequency domain

Currents flow in the three-phase pump motor only when the pump is running and charging the accumulator, a process that takes just a few seconds and results in keeping the callipers disengaged. The rest of the time the currents are zero. The event where the pump operates gets captured automatically by the data logging system. This provides the exact period with a minimised data size, which makes further analysis easier. An example of one of the phase currents during a pumping event is shown in Figure 4.4. Figure 4.5 illustrates the FFT spectrum of the collected current data, shown in Figure 4.4.

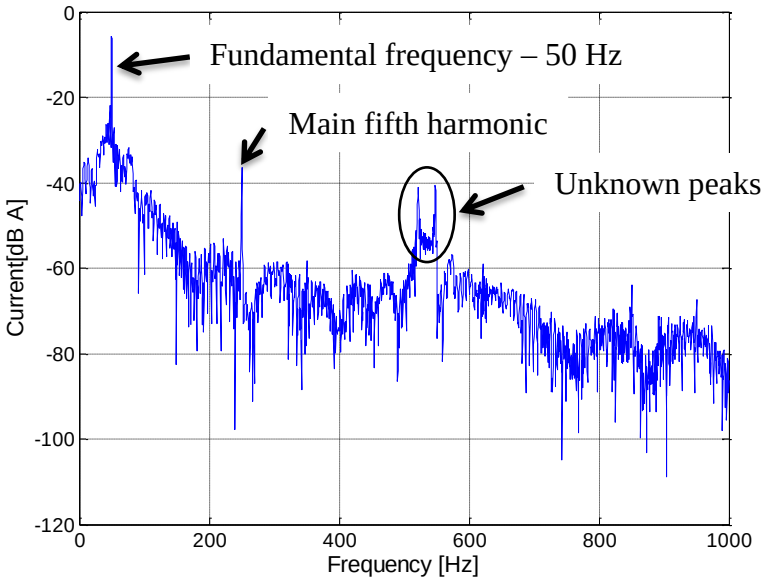

Figure 4.5: FFT of the current of the recorded event

The 50 Hz fundamental and a strong 250 Hz (5^{th} harmonic) are clearly visible. Within the result some notable unexplained spectral features can be seen between 500 and 600 Hz. In order to find out what the unknown peaks could be related to, the signal can be divided into shorter time slices; a spectrum is then prepared for each slice, producing a spectrogram [2]. Figure 4.6 shows the resulting spectrogram for the current illustrated in Figure 4.5.

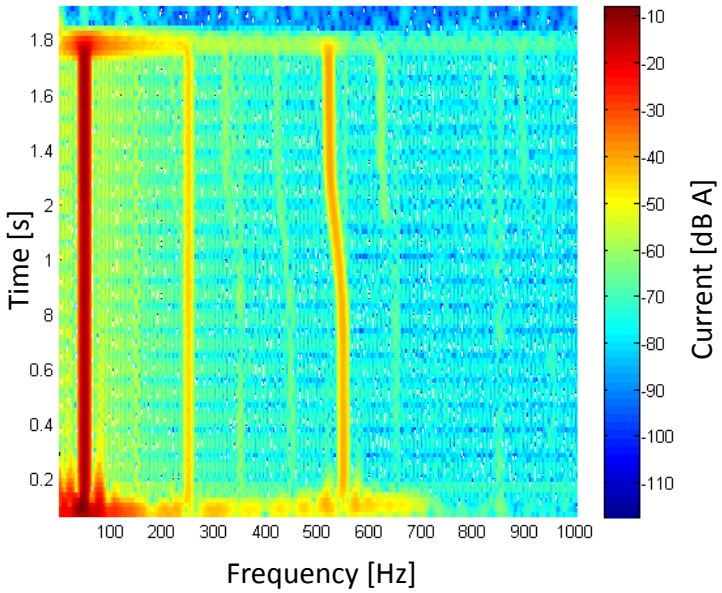

Figure 4.6: Spectrogram of the captured current while the pump was maintaining the pressure

There is an initial transient current in the first 0.2 s. At around 550 Hz there is a significant peak indication in the spectrum where the frequency is changing over time, although the amplitude is reasonably stable. The pump runs until the desired fluid pressure is achieved. Consequently, the torque on the shaft is increased and the speed decreases. This can also be seen in the increase in the current amplitude as shown in Figure 4.4. The 550 to 525 Hz frequency change is believed to be related to -the gear pump. Laboratory tests presented in Chapter 3 showed similar effects.

4.2.2.2 Routine operation of the braking system

During the operation of the turbine, the hydraulic pressure has to be maintained at a certain level (in this case 200 – 210 bar) to keep the callipers detached. Pressure is monitored by a sensor which is observed by the main controller. The controller sends commands to start and stop the motor to preserve the pressure level. This procedure happens frequently, depending on the pressure level and the turbine condition. For example, if the turbine is fully stopped and is about to start, the pressure level is usually less than 10 bar and it has to drive up to

200 bar. However, during normal operation it must keep the callipers away from the disc. Experiments show that this procedure happens at least four times in an hour. Collected data for a month shows several events with differences in time of the pumping period and pressure levels. Figure 4.7 illustrates five different events of the recorded current of the hydraulic power unit. As can be seen, data set 1 (red) has the longest period. This shows that there was a greater drop in pressure before the pumping event happened. Data sets 2 and 3 occurred on the same day, 13 minutes apart. This demonstrates that the pump could run up to four times an hour. Events 4 and 5 were recorded on different days when the turbine was being started and stopped randomly for other test reasons, by the operator. All these events occurred in healthy conditions but with different drops in pressure. In all events, peak values at the end of the operation reached approximately the same level when they achieved the desirable limit.

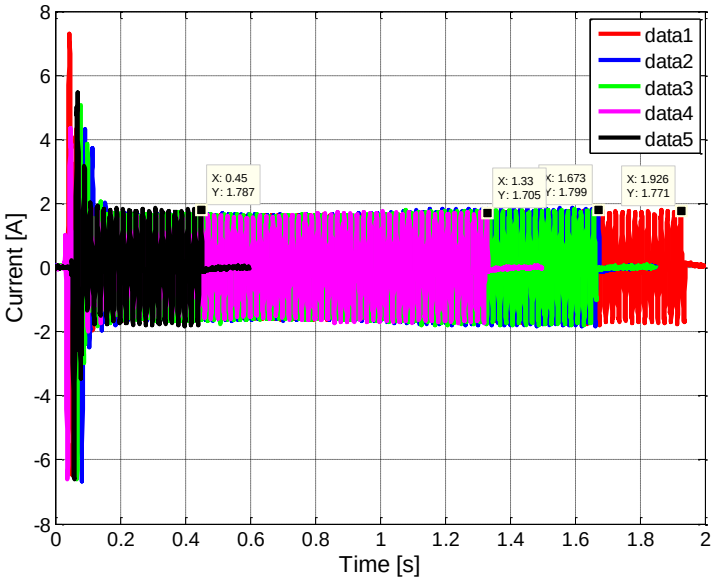

Figure 4.7: Current data from 5 different events

The FFT analysis for the peaks related to the behaviour of the pump and pressure of the above five events, between 520 Hz – 550 Hz, is shown in Figure 4.8. This behaviour demonstrates that in all experiments, after the required pressure limit is reached, the related

harmonics will occur between 520 Hz and 530 Hz. This varies depending on the pressure level at which it exactly stops.

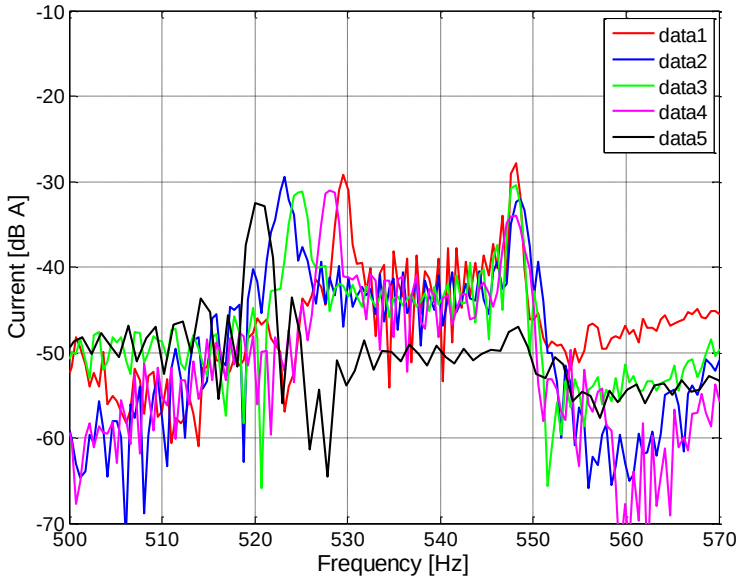

Figure 4.8: FFT spectrum of the 5 current samples

Data set 5 (black), which in time domain has the shortest period, has the smallest peak at around 550 Hz but the peak at the end of the event looks almost the same as the others. The explanation for this could be that the motor reached the higher pressure value faster than the other events, from its starting pressure level. For the other events, depending on the initial pressure level, the peaks at 550 Hz vary. In general, the current signature demonstrates the behaviour of the motor, the gear pump and its pressure level.

4.3 Simulation of the hydraulic power unit

Modelling can be used as a facility to develop designs or improve control algorithms. It also provides an effective way of understanding particular system behaviours [104]. Having an appropriate model will enable faults to be introduced in simulation without damaging the physical system [105].

For the purpose of modelling the brake system, the following subsystems were considered:

- Three-phase power supply including contractor and circuit breaker
- Three-phase asynchronous motor
- Gear pump and the hydraulic pressure
- Sensors and control signals

Some parameters, such as pressure and shaft speed within the hydraulic system, were not measured during the trials, but the fault-free results and the manufacturer information have led to the development of a practical simulation. Simulink and the SimPowerSystems toolbox have been used for modelling [106]. As the parameter of the motor of the hydraulic unit is unknown, Simulink - ABB 370 W asynchronous machine parameters were used to model the three-phase induction machine [107].

Figure 4.9 is the simulated hydraulic unit in Simulink.

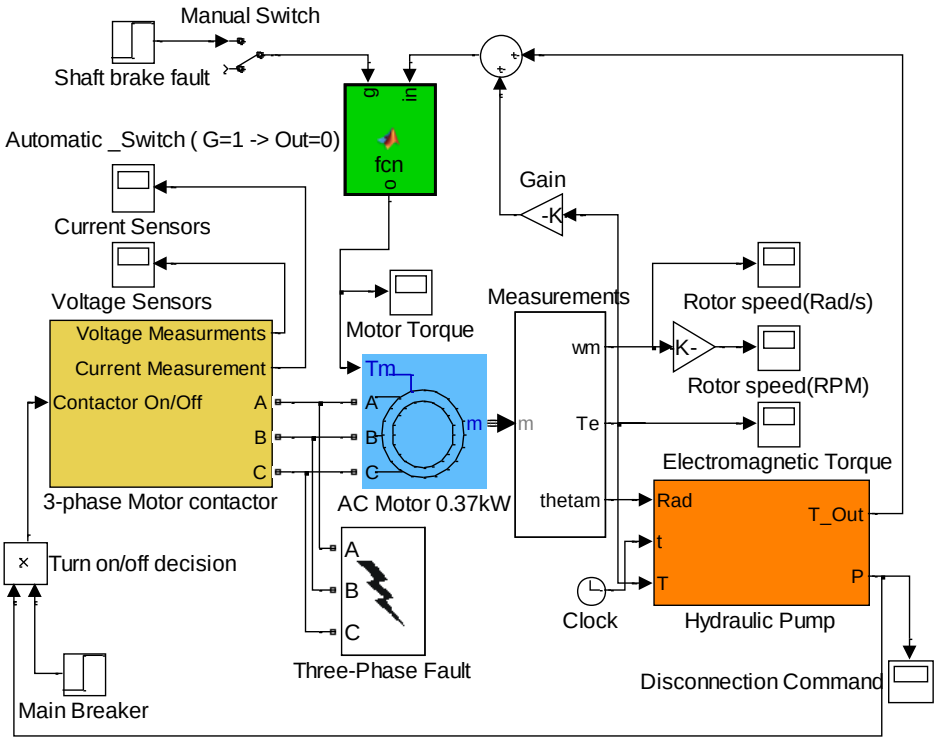

Figure 4.9: Model of the hydraulic brake system in Simulink

The behaviour of the gear pump has been simulated via an embedded function and applied to the motor shaft torque. The torque generated by the gear pump can be seen on the current

signature [67]. A fault-free situation was carried out; the results and signal analysis were used first to improve the subsystem parameters, then to check the model. Figure 4.10 illustrates the output of the simulation that closely matches the field measurements. The condition monitoring procedure can be carried out by splitting the signal into different segments and comparison of the real signal measurements and the free-fault situation will lead to online fault detection. Simulation of the fault and applying the result into the main fault detection and diagnosis system can assess the ability of the algorithm to diagnose the failures. Peaks, envelope assessments and the period of the event are used for classifying the pumping events, shown in Figure 4.10.

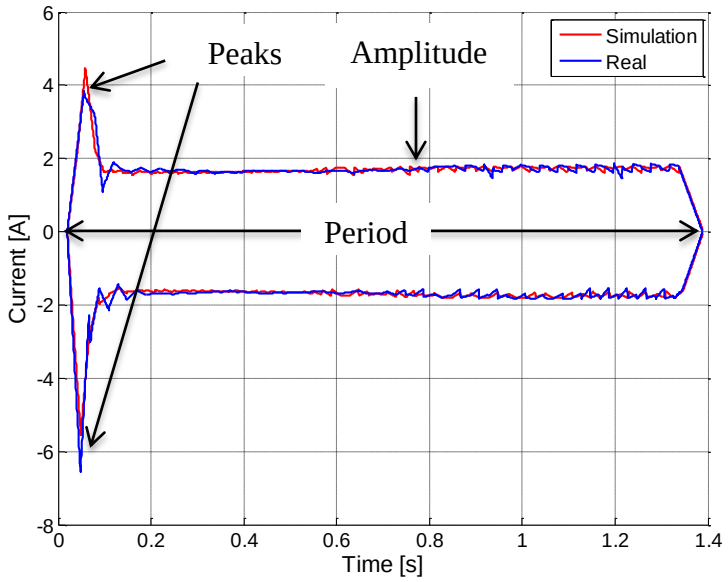

Figure 4.10: Current envelope of the simulation and real data and their categorisation

The resulting FFT and spectrogram for the simulation, which illustrate similar effects, are shown in Figure 4.11 and Figure 4.12.

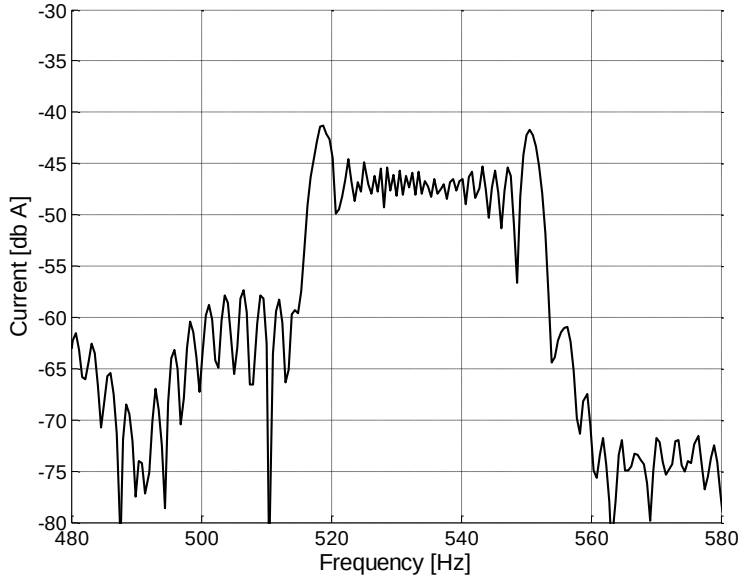

Figure 4.11: FFT spectrum of a phase from the simulation zoomed for the gear pump harmonics

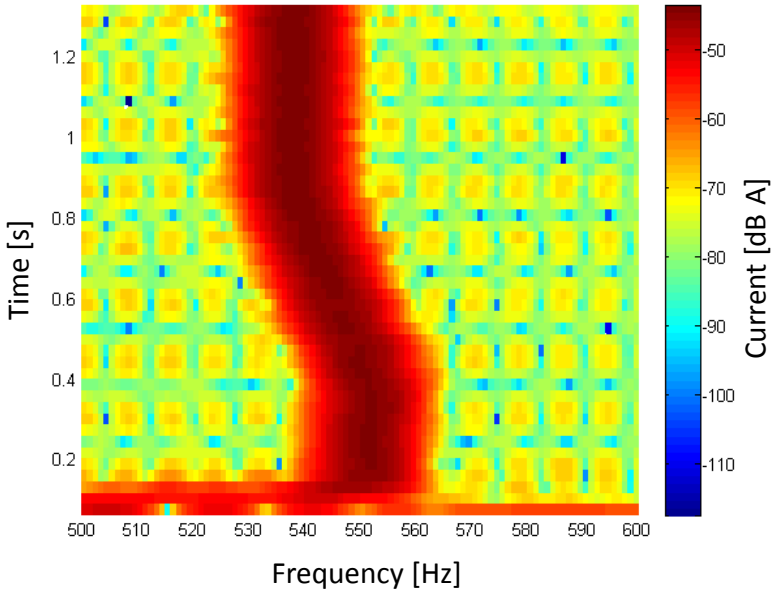

Figure 4.12: Spectrogram of the current from the simulation zoomed for the gear pump harmonics

Three different pressure levels were also simulated to mimic similar conditions to the events that were shown in Figure 4.7. This is also to validate the relation between the FFT analysis and the gear pump behaviour. Figure 4.13 shows the three simulated conditions. The period increases when the starting pressure is lower. Data set 3 has the highest period of all the sets.

This is because the induction motor, driving the hydraulic unit, performed longer than data set 2 and 1.

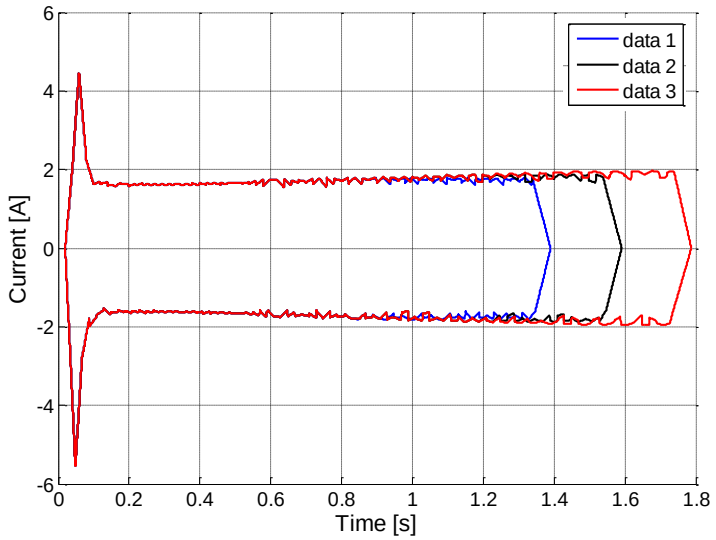

Figure 4.13: Envelope curve of the three simulated conditions

The amount of torque generated by the motor has been monitored within the model and as soon as it reaches a predetermined level, it stops the motor. Increasing the threshold level for the final torque value affects the current signature, where the harmonics related to the gear pump reach a lower frequency value.

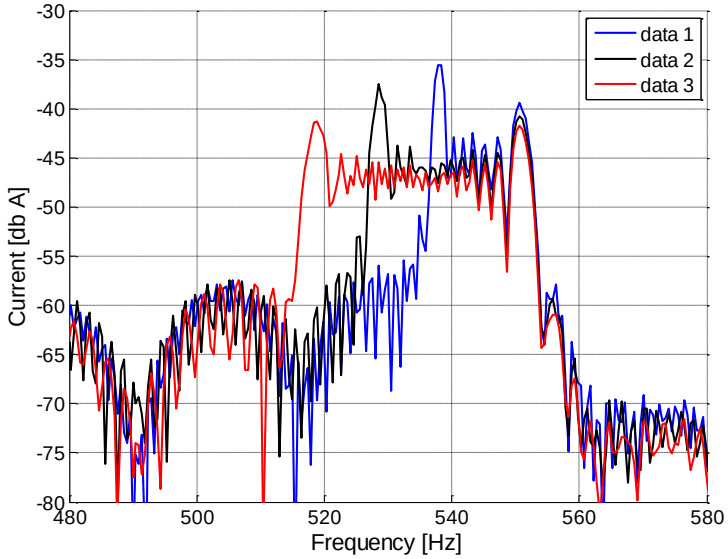

Figure 4.14: FFT spectrum of the three simulated conditions

Leakage in the hydraulic system is a common failure mode [108]. One of the consequences of a leakage in the brake system is that there is a reduction in pressure within the hydraulic pipes and therefore an increase in motor operation time to get to the desired pressure. The consequences of this failure can be observed in Figure 4.15.

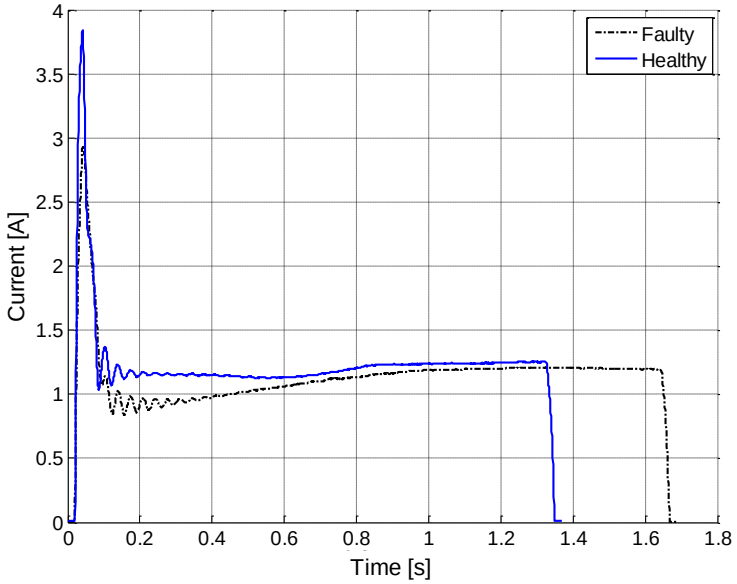

Figure 4.15: Moving RMS for every 5 cycles of the faulty and healthy conditions

A three-phase fault was applied to the system using Matlab Simulink toolbox, SimPower – Three-phase Fault [109] . This is a programmable phase to phase/ground fault the breaker system [110]. A thousand ohms resistance was set up between the first phase and the ground for 0.8 second of the run time. This was to demonstrate a very modest and small current leakage between the ground and a phase, the fault in lower resistance can be easily detected. Figure 4.16 shows the simulated three-phase current driving the motor; on phase 1, higher peaks can be seen from 0.1 second to sometime around 0.9 second. The effect of this asymmetry and how it differs from a healthy condition is illustrated by use of Park's transform, shown in Figure 4.17.

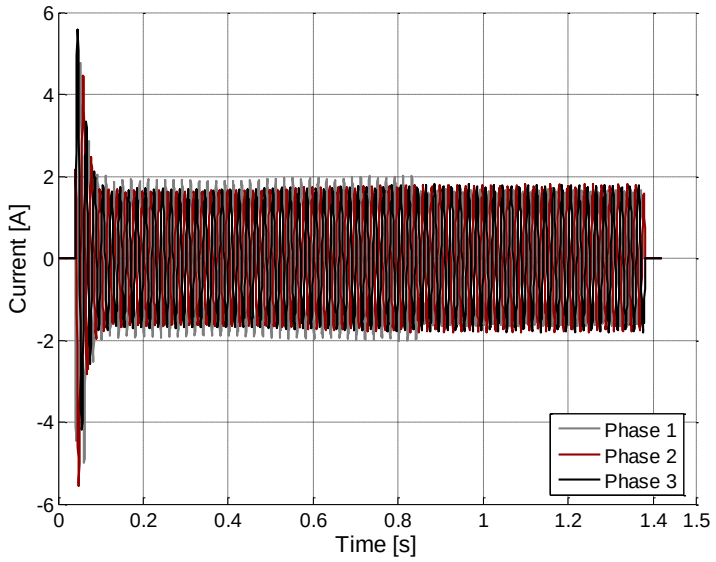

Figure 4.16: Simulated three-phase current with one faulty phase to ground line

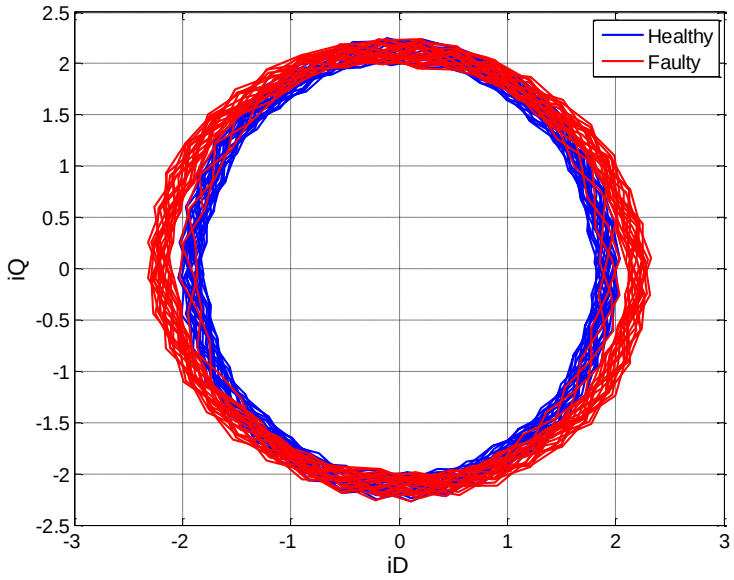

Figure 4.17: Park's transform of a simulated healthy condition and a faulty phase situation

4.4 Summary

An experimental condition monitoring system was developed for the evaluation of the NEG Micon 750 wind turbine brake system. A number of routine tests were carried out to evaluate the performance of the monitoring system. The analyses of these tests revealed a

number of features which could be related to the overall braking system. A model, based on Simulink, with the appropriate fidelity was built to further explore the observed features. It was found that the features could be explained by methods such as motor current signature and envelope analyses.

For more accuracy of the model, measurements of the grid and exact motor parameters would have been advantageous, but were not required in the achieved level of modelling.

Time-frequency domain analysis of the hydraulic unit behaviour was carried out to explain the changes in the frequency over time.

The model was able to adequately represent the behaviour of the gear pump and its effect on the motor torque through the motor current signature. It was then used to simulate a number of faults to observe how the features would appear in the fault detection and diagnosis methods.

Similar mechanical brake systems are found in other wind turbines from manufacturers such as Vestas and Acciona; these are addressed in the next chapter.

Chapter 5 V47 and AW1500 Hydraulic Power Unit

5.1 Introduction

In this chapter, condition monitoring of two hydraulic power units is described. Data were collected from a Vestas 660 kW, V47, and an Acciona Windpower 1.5 MW, AW1500 wind turbine. Measurements were carried out using the same data logging system described in previous chapters, but due to the larger hydraulic power unit in the AW1500, use of higher rate current sensors was used. This chapter explains the use of motor current signature analysis and historical process data approaches in order to monitor the condition of those hydraulic power units.

5.2 Vestas V47-660 hydraulic power unit condition monitoring

5.2.1 Introduction

The V47 is a pitch regulated 660 kW wind turbine. In terms of braking, this turbine has a fail-safe mechanical brake for emergency circumstances and uses the pitch to stop in normal conditions. The pitch controller is also used to regulate the power by changing the angle of the blades to maintain the shaft speed within a 10% margin of the turbine nominal speed rate.

Both the pitch and mechanical brake are driven by a hydraulic power unit, shown in Figure 1.6. The hydraulic unit has to maintain the pressure for operation of both. However, the mechanical brakes in these systems are only used during emergency conditions and for normal maintenance the turbine can be stopped by the pitch controlled air brake.

Instrumentation was carried out on a V47 wind turbine, which is run by Terna Energy located in Evia, Greece [111].

Figure 5.1: Terna Energy wind farm, Evia, Greece
[Author's collection]

5.2.2 Instrumentation

In the design of the V47 turbine, the wiring for the hydraulic unit is within the control box located on the nacelle, therefore the data logging system had to be set up in the nacelle. Figure 5.2 shows how the current transducers were placed within the main control panel.

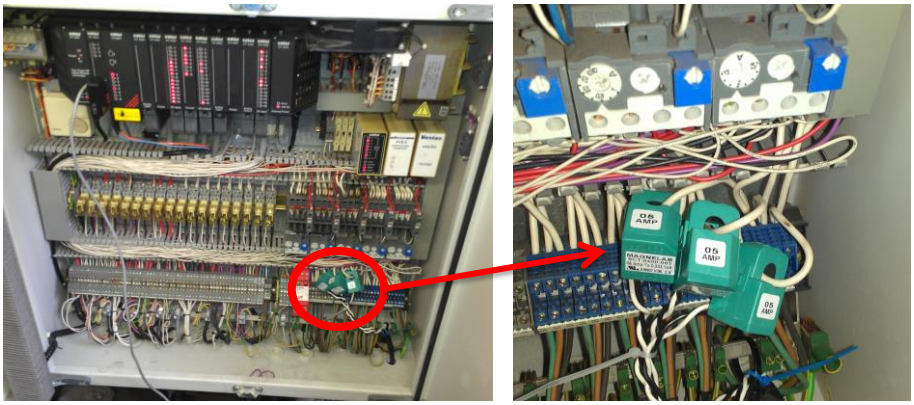

Figure 5.2: V47 nacelle control panel
and the use of the current transducers to monitor the hydraulic unit [Author's collection]

Due to the wind farm data communication network policy, the experimental UoB data logging could not be connected to their local network. Thus, a mini computer system equipped with a 3G modem was installed to transfer the data. For ease of access to the logged data and to complete an online monitoring system, a special program was written (in C#) to

automatically detect the logged events and upload them to a hard drive where they could also be accessed via the internet. Dropbox, a file sharing product, was used for this part. Figure 5.3 shows the set up of instrumentations in the nacelle. Figure 5.4 demonstrates the communication method used in this trial.

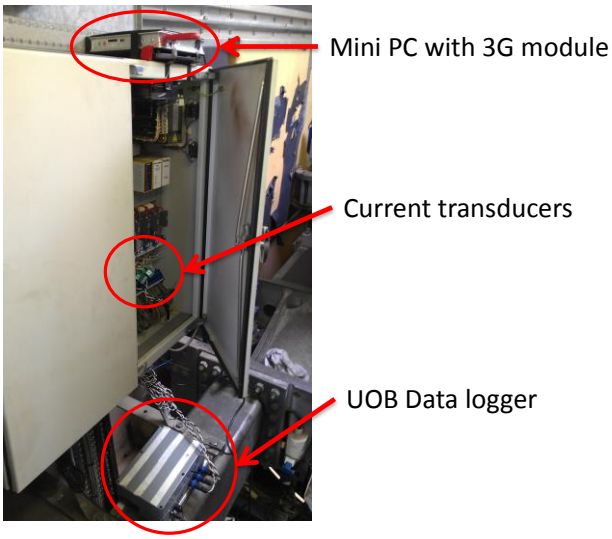

Figure 5.3: Instrumentation used for remote monitoring of the V47 hydraulic power [Author's collection]

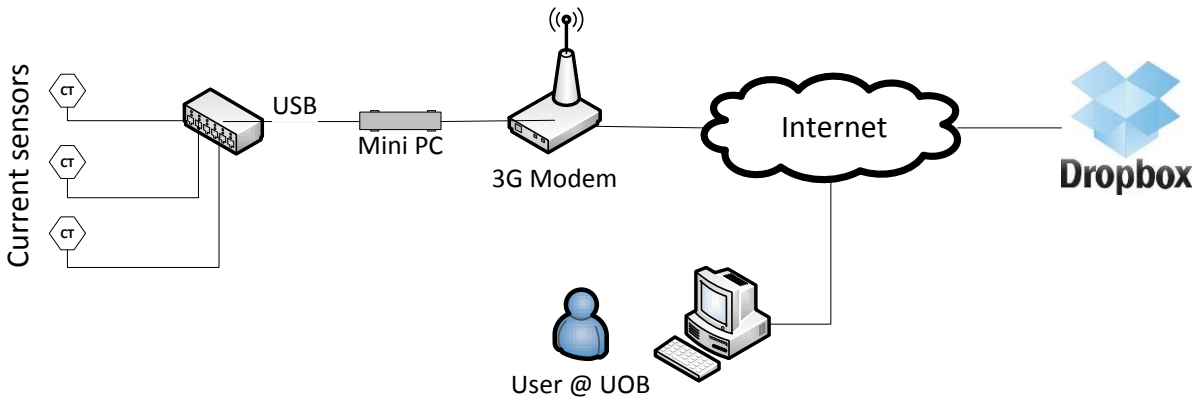

Figure 5.4: Overview of the condition monitoring system for the V47 turbine

5.2.3 Data Analysis

During pitch-controlled braking or normal operation, the hydraulic system continuously maintains the pressure and this causes the unit to pump almost every minute for about 2-3 seconds. A custom built data logger was used to capture the event of the pumping. The event can be seen in Figure 5.5. The pressure was reported from 180 to 200 bar within the operation of the hydraulic unit.

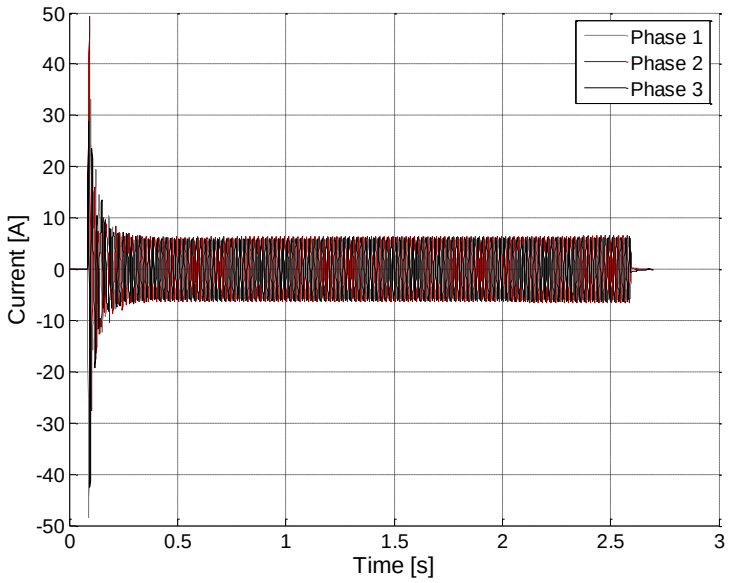

Figure 5.5: Captured event from the V47 hydraulic unit
while braking using pitch controller

As an example, the situation of a failure of a pressure sensor was applied by letting the system pump up to 250 bars; this was an induced fault provided by the wind farm operator. The result of the current measurements can be seen in Figure 5.6. This shows how the current rises as the pressure increases until the pump was stopped by the safety valve. Comparing the two last figures indicates a considerable difference between the captured events. This can be used for early stages of fault detections and later fault diagnosis procedures.

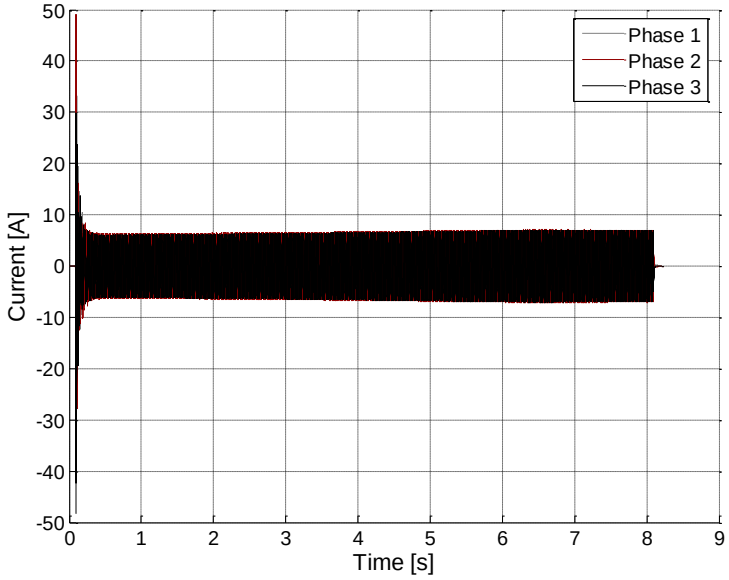

Figure 5.6: The event of pumping up to 250 bar

The events that were captured by the data logger indicate that the hydraulic system was running frequently. It appears that, in normal conditions, the hydraulic system runs once every minute. The moment that the induced fault was simulated on the pressure sensor the duration showed a significant change. Figure 5.7 demonstrates the running duration of the hydraulic unit including the specific time that the sensor fault was applied. For the same events, analysis of the current also shows that the final peak value was steady until the sensor fault was added. The rise in the current within the faulty situation can also be seen in Figure 5.8.

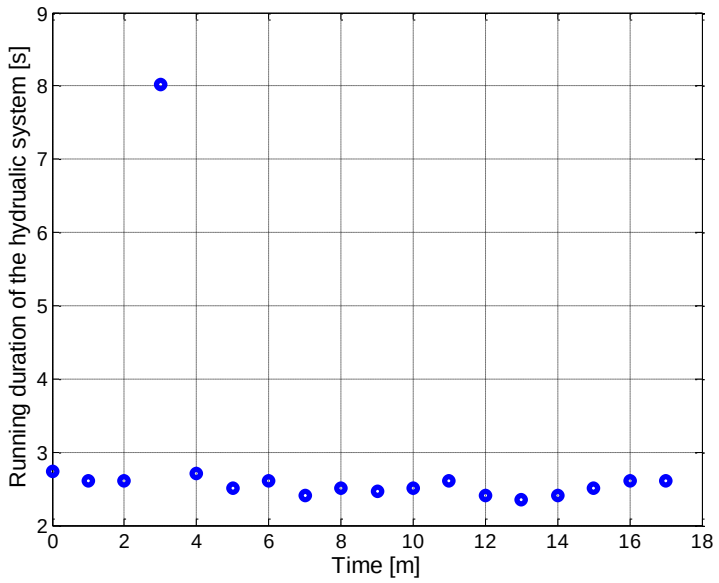

Figure 5.7: Performance duration of the recorded events
within 17 minutes including the sensor failure condition

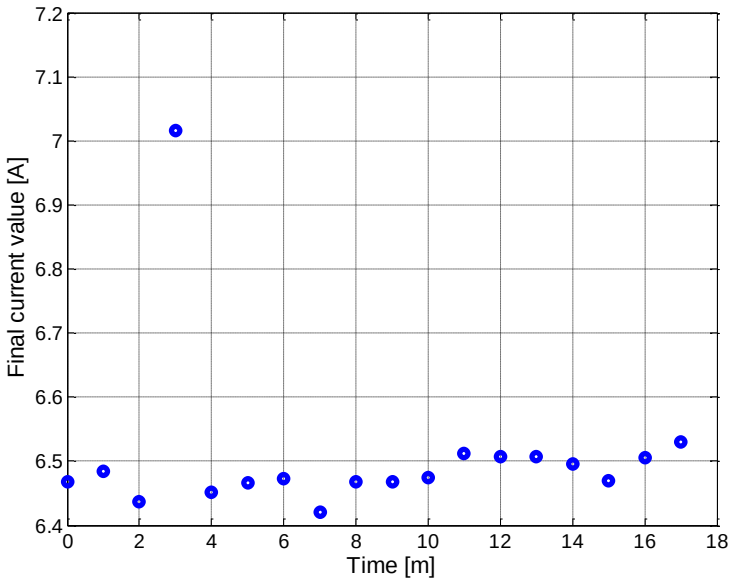

Figure 5.8: Final peak of the current values
for 18 minutes including the sensor failure condition

As all the three-phase were measured, Park's transform can be calculated. The amount of hydraulic pressure level changes within the hydraulic unit, while the motor is pumping, affects the Park's vector. The current value rises when the pressure level increases. Figure 5.9 shows the transformation of a faulty condition compared to a healthy event.

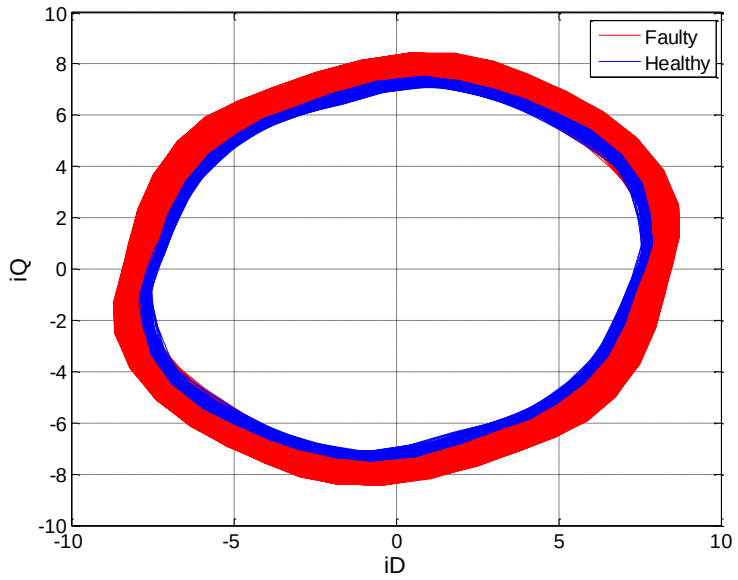

Figure 5.9: Park's vector of a healthy and the faulty conditions

Spectrograms of the current in healthy and faulty conditions are shown in Figure 5.10 and Figure 5.11. The time difference, regardless of slight changes in the amplitude of some frequency components, is the most observable change that can be seen. Alterations within hydraulic pressure and mechanical torque within the system do not appear on these two spectrograms.

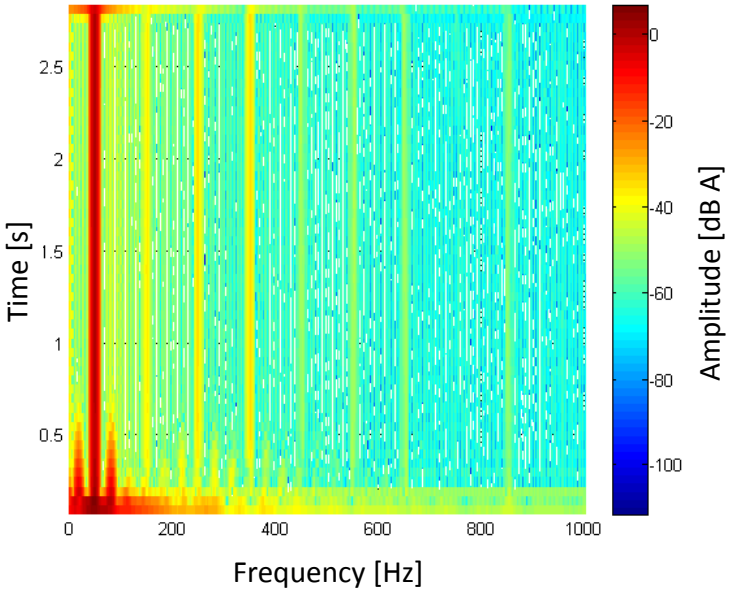

Figure 5.10: Spectrogram of the current from the V47 hydraulic unit in healthy condition

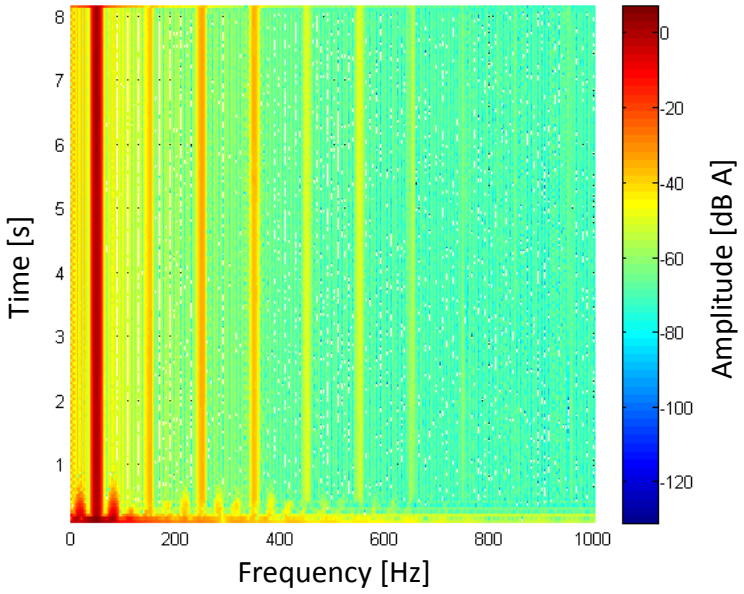

Figure 5.11: Spectrogram of the current from the V47 hydraulic unit in faulty condition

Harmonics that could be related to the pressure and gear pump can be seen by use of digital filters. A high-pass Butterworth filter to focus on frequency over 800 Hz was applied to the sampled data [112]. Figure 5.12 shows the appearance of the harmonics and how the frequency decreases over time.

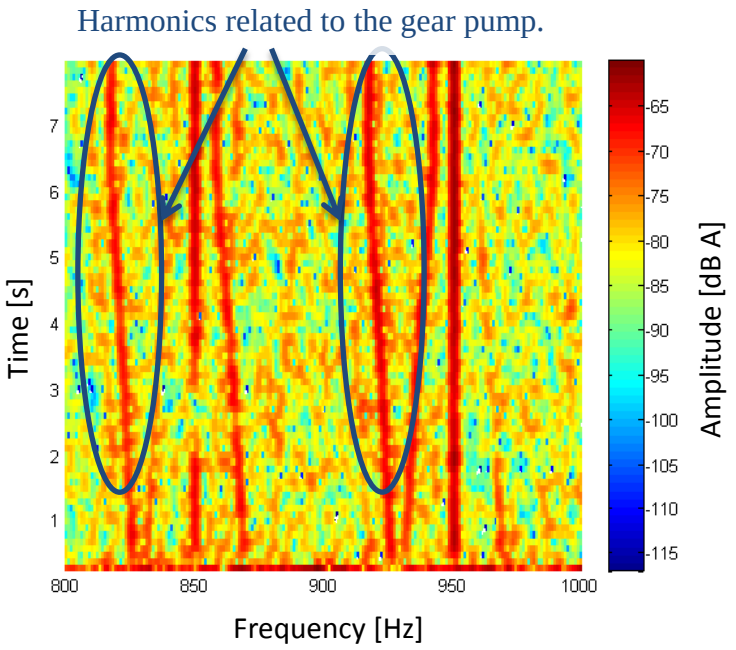

Figure 5.12: Filtered and zoomed form of the faulty current data

The changes in these harmonics are less obvious within the healthy data as the pumping time is shorter and variations within pressure are smaller, illustrated in Figure 5.13.

Harmonics related to the gear pump.

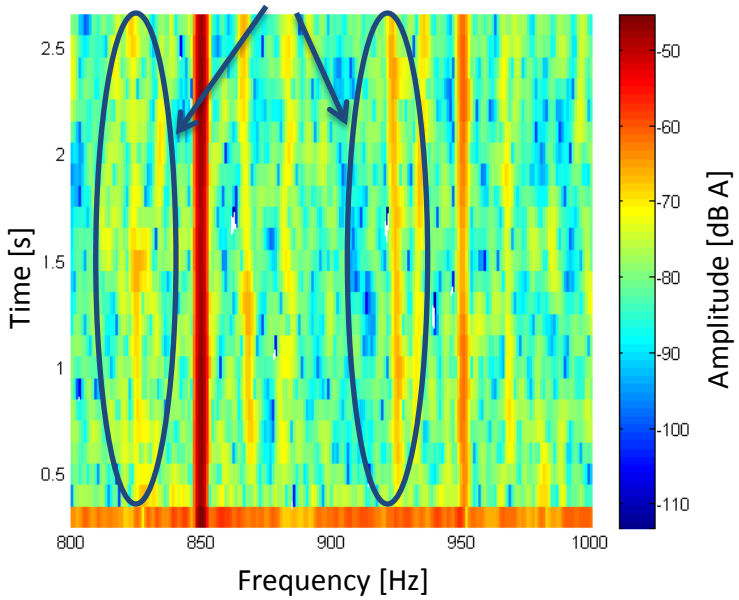

Figure 5.13: Filtered and zoomed form of a healthy current data

5.3 Acciona AW1500 hydraulic system condition monitoring

5.3.1 Introduction

The AW1500 is a pitch-controlled wind turbine, manufactured by Acciona. This turbine is more advanced in braking than the V47 or NEG Micon 750. The AW1500 not only uses the pitch mechanism to brake, it also has an independent fail-safe piston accumulator on blades. Additionally, it is equipped with a mechanical brake on the high speed shaft, and is able to brake electro-mechanically, using the main generator to stop the rotation [113].

The AW1500 uses a hydraulic power unit to drive the pitch and mechanical brake system. The pressure is continuously monitored and logged by the main controller.

Figure 5.14 illustrates the hydraulic power unit that has been monitored and studied in this section. The turbine is located in Acciona wind farm (Subestacion de Vedadillo) in Navarra, Spain. The hydraulic system is driven by an 18.5 kW three-phase motor, with speed up to 1475 rpm. It has two accumulators, a mechanical brake and a pitch system.

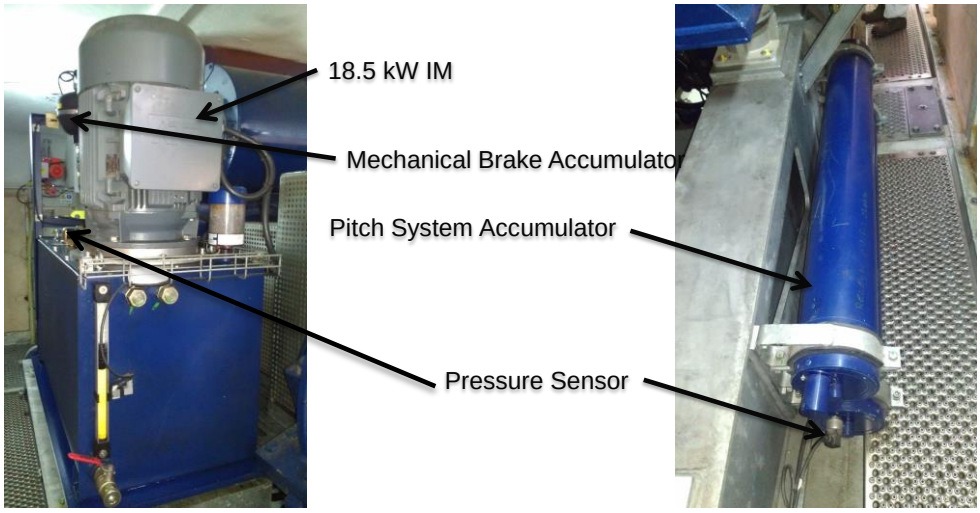

Figure 5.14: AW1500 hydraulic power system
[Author's collection]

5.3.2 Instrumentation

In order to monitor the three-phase current of the hydraulic power unit, three current clamps, rated for 25 A, were installed within the control panel, situated in the nacelle. The logging system was installed on a wind turbine which is a commercial and non-experimental turbine. This was agreed by the operator due to the non-intrusive installation approach of the UoB monitoring system. Figure 5.15 shows how the current clamps were installed.

Figure 5.15: Installation of current clamps within the control box of the AW1500
[Author's collection]

Pumping events were automatically logged on the SD card using the UoB logging unit on the day of the trial. Hydraulic pressure is also continuously logged by the farm operator every minute. Hydraulic data for the wind turbine were provided by the operator and studied in this work.

5.3.3 Data analysis

A trial run was carried out on 3rd September 2012; the average wind speed was around 12 m/s. Wind speed, shaft speed and hydraulic pressure measurements from the wind farm were provided by Acciona for the day of the trial run. The wind speed data can be seen in Figure 5.16.

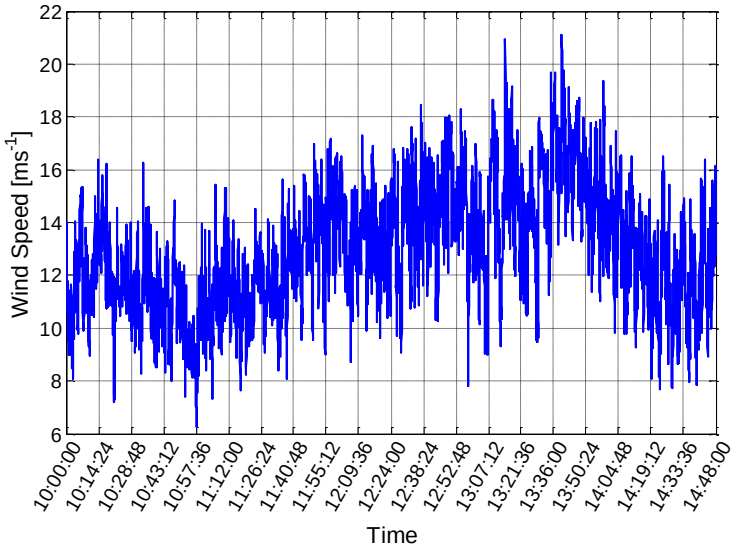

Figure 5.16: Wind speed measurement from the day of the trial provided by Acciona

The hydraulic pressure measurement from the farm shows that the hydraulic unit maintains the pressure between 210 to 230 bar during the operation of the turbine. Moreover, minimum pressure at the pump side did not drop below 170 bar on average. Up to 170 bar is kept in the accumulator, which helps the hydraulic unit to pump less before start up. Higher fluctuation within the pressure level at the starting point indicates the behaviour of the pitch system in order to position the blades to face the right direction for optimised power. In order to place the blade in the correct position, after the turbine is parked, the hydraulic unit needs to run longer to maintain adequate pressure. Subsequently, it causes a greater loss in pressure level during the positioning period.

Figure 5.17 demonstrates how the hydraulic pressure level changes with shaft speed. It also shows a greater loss in hydraulic pressure before the optimised shaft speed.

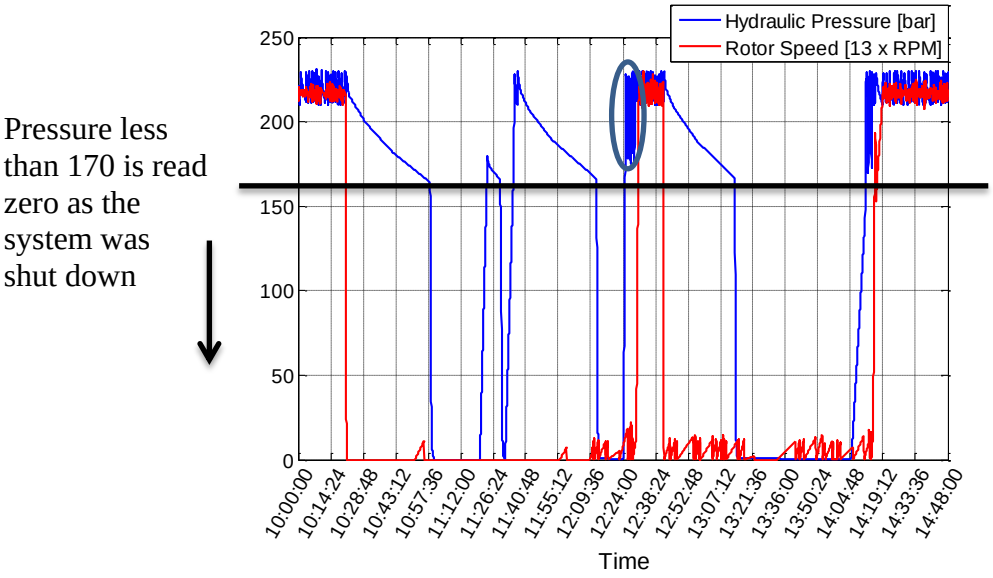

Figure 5.17: Shaft speed along with hydraulic pressure of the AW1500 (x13 of the actual value)

The wind operator manually added more cycles to the yaw drives, which rotate the nacelle, and this created an abnormal situation for the pitch control and positioning system, therefore additional work for the hydraulic unit was required to complete the positioning process. This can be seen by comparing the hydraulic pressure changes in a normal starting up procedure with the manipulated trial run.

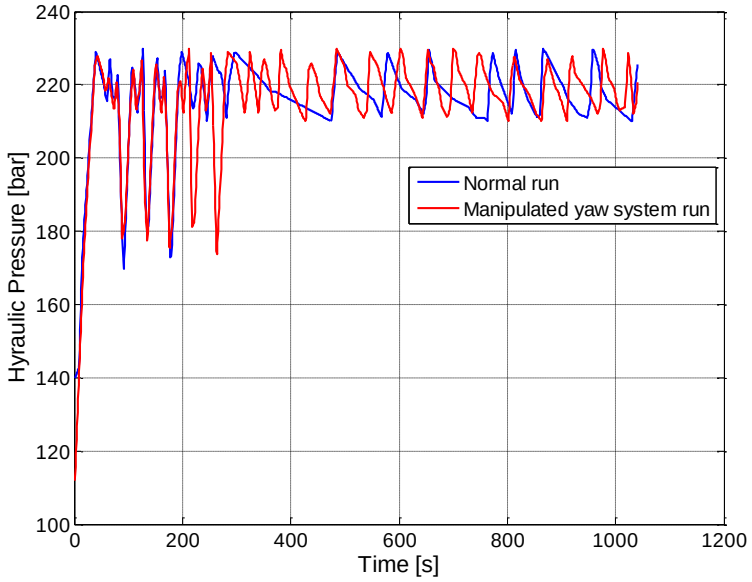

Figure 5.18: Hydraulic pressure in normal and intentional fault conditions

Recorded current data matches the hydraulic measurements. For example, when the override yaw system situation was being applied, the hydraulic power current data also showed how long the hydraulic unit was pumping. Figure 5.19 demonstrates the rise in pressure along with the current, where Hilbert transform was used to generate an envelope of the current data.

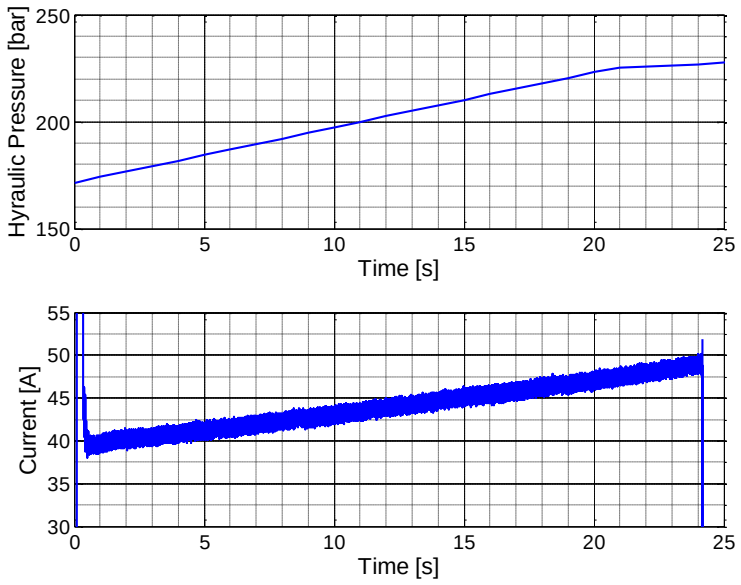

Figure 5.19: Increase in hydraulic pressure and current envelope during the motor running time

The current data has a peak around 250 V due to the size of motor. The three-phase current from the event, where the pressure starts from 174 bar to 228 bar, is shown in Figure 5.20.

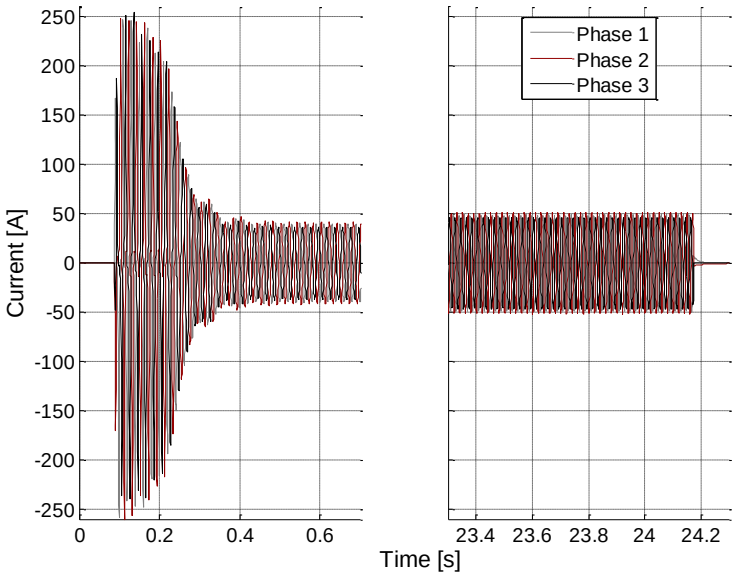

Figure 5.20: Current data, starting hydraulic pressure 174 bar and ending around 228 bar

Spectrogram analysis of the current also shows the changes related to the hydraulic pressure, which would also represent the torque and speed of the motor. This can be seen in Figure 5.21.

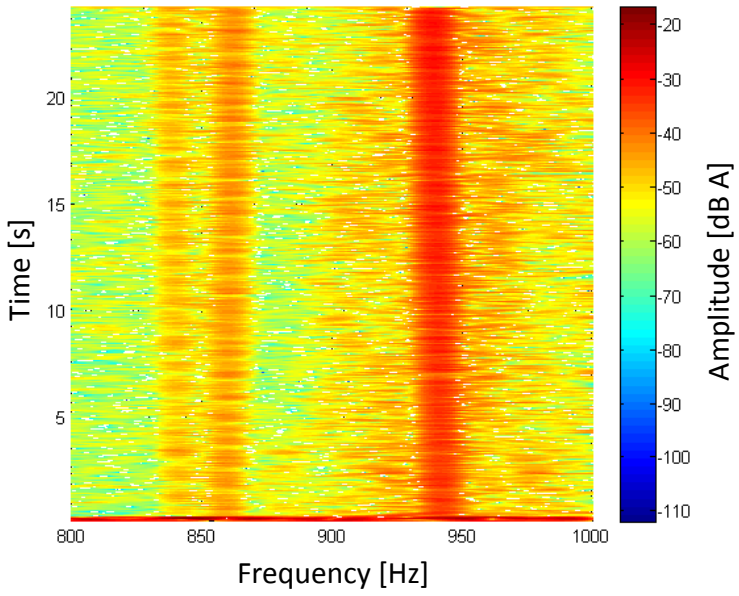

Figure 5.21: Spectrogram of the current
behaviour of the pump can be seen around 945 Hz, the frequency decreases slightly with time

Figure 5.22 shows how the controller triggers the hydraulic pump within the first 100 seconds after the turbine was set to operation mode by the operator. Four hydraulic events were logged by the UoB logging system, each event labelled as a section in Figure 5.22.

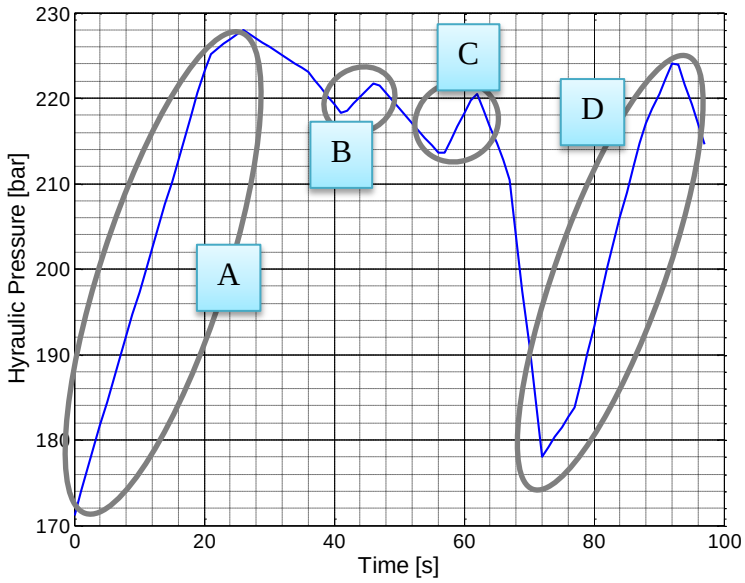

Figure 5.22: Hydraulic pressure for the 100 seconds from the starting point

Current data representing sections A to D are shown in Figure 5.23.

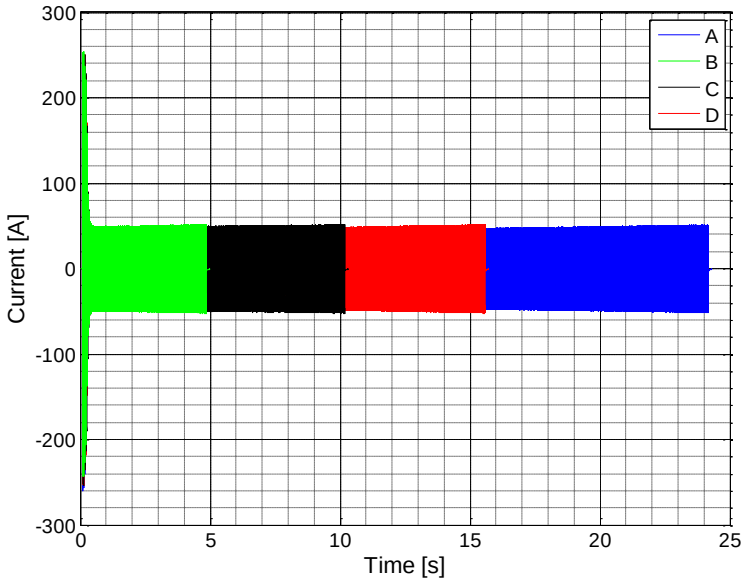

Figure 5.23: Current data for the hydraulic pressure sections

5.4 Summary

This chapter described two case studies in which the motor current analysis techniques were applied to in-service wind turbines. Simple faults were simulated manually by the turbine operators.

In the first case, the V47 turbine, a simulated sensor fault resulted in the motor running for an extended period of time. This was observed from the spectrograms, through the envelope analysis, and through the analysis of the Park's transformation. All indicate that the methods could therefore be used for a relatively simple threshold-based fault detection system.

In the second part, the AW1500 turbine had its yaw drive system manipulated in such a manner that the hydraulic system controlling the blade pitch increased its activity. These features were again observed with the range of motor current analysis techniques.

Both case studies suggest that the simple sensor condition monitoring technique discussed in this thesis has potential application to identify complex faults in parts of the wind turbine system which are remote from the sensor location.

In the next chapter, the use of existing shaft speed measurements is studied to monitor the condition of the air brakes.

Chapter 6 Blade Tip Monitoring

6.1 Introduction

The previous chapter dealt with the condition monitoring of the hydraulic system by using current analysis applied to AC machines used for various actuators. The methodology applied was to use simple sensors on the current lines to monitor a complex system. The same practice is performed in this chapter but on the tip braking system, and instead of a current measurement, rotation speed of the high-speed shaft was used. The rationale is that measurement of the shaft rotation speed is a relatively straightforward task.

As described in Section 1.6.1 , blade tips are used for aerodynamic braking in stall type wind turbines [20]. These are mounted at the end of the blades. The NEG Micon 750 is a wind turbine with blade tips, known as tip brakes. Activated blade tips act as a damper by facing against the direction of the wind to slow down the shaft [114]. Figure 6.1 illustrates NEG Micon brake tips in action.

Figure 6.1: NEG Micon 750 with applied brake tips
[Author's collection]

Confidential reports, from CRES wind farm, show that the only existing method to monitor the condition of the tips is the operator's observation.

In this chapter, analysis of the high-speed shaft data is employed to detect failures within blade tips. The blades and blade tip are considered as a mass spring damper system and speed of the shaft after the activation of the brakes, which could be seen as a step response, was used for condition monitoring purposes.

Shaft speed data was provided by CRES wind farm for this work. The provided data was collected from the high speed shaft with a sampling rate of 256 Hz. Figure 6.2 illustrates the location of the optical sensor on the high-speed shaft within the NEG Micon 750 nacelle.

Figure 6.2: Shaft speed sensor
pointing at the black/white marks on the high speed shaft for speed measurements installed on the NEG Micon, CRES wind farm [Author's collection]

6.2 Data analysis

A braking event imparts an impulsive load on the wind turbine system which excites various modes of vibration. The impulse response (flutter effect) of the brakes and particularly of the blade tips during braking has been studied by analysing the shaft speed. Observations of the

shaft speed were recorded in various wind speed conditions, with normal blade tip operation and also with one blade tip (of three) not working. Figure 6.3 demonstrates three measurements in different wind conditions during a brake application.

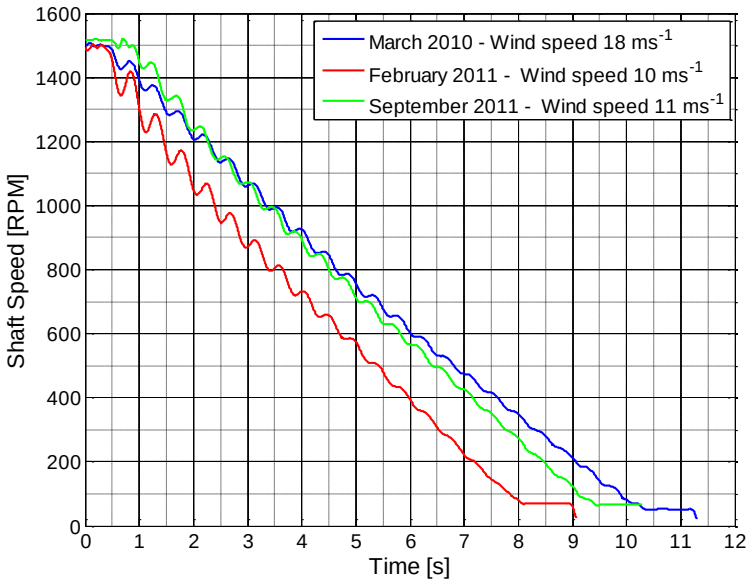

Figure 6.3: High-speed shaft data in three wind speed conditions during braking

A difference in stopping time of about 2 seconds between the highest and lowest wind speed can be observed in Figure 6.3. The data from February is with a faulty blade tip which did not apply during the braking, and with newly installed brake pads. New pads were also present for the measurements in March, with no brake faults. The data from September shows a slower stopping time but with healthy blade tips and slightly worn brake pads. The difference in the stopping time between February and September can be explained by having the pads changed and a lower wind speed. However, the blade tips would be less effective in higher wind speed situations. The frequency analyses of the shaft speed measurement show unusual behaviour of the flutter effect within the step response which illustrates the blade tip failure.

In Figure 6.4 the FFT of the high speed shaft angular velocities are shown, which reveals the natural frequency characteristic of the blades.

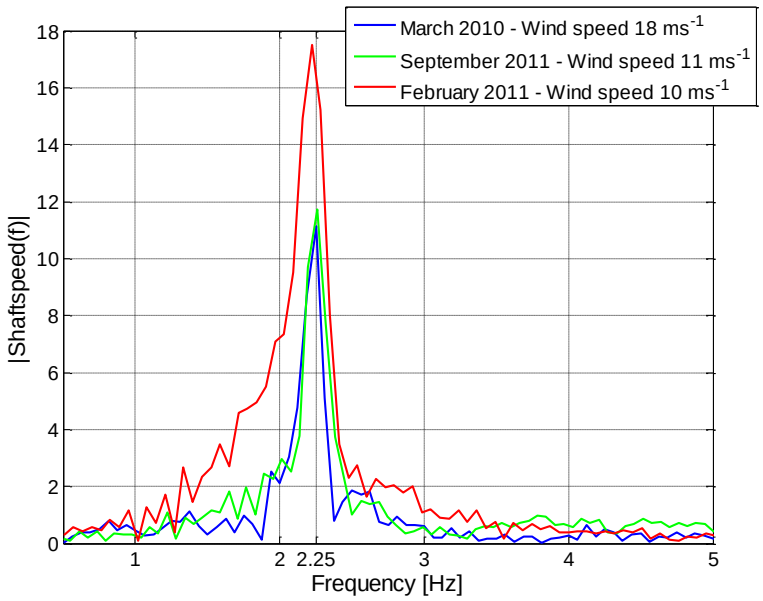

Figure 6.4: FFT analysis of the shaft speeds
for 8 seconds at 256 Hz

Due to the failure in a blade tip, a higher peak can be seen from the data recorded in February; however the frequency is not noticeably changed. The higher peaks are because a blade tip failure affects the damping of the system, which results in a change in the amplitude of the resonant response but with no noticeable change in the resonant frequency. This might be because the frequency of oscillation could be close to the undamped natural frequency, and therefore a reduction in damping may not produce a measurable change in frequency, which is demonstrated in the modelling section. To some extent this phenomenon can also be seen in Figure 6.3 where the February data has larger peak to peak oscillations.

6.3 Modelling

In this section, a dynamic mass spring damper model of the high speed shaft during braking was studied and implemented in Simulink. The aim of this model is to show how changes in damping can affect the fluctuation within shaft speed measurements during braking. A mass spring damper system (second order system) was used to implement the model. One possible, simple approach to explain the flutter effect is a dynamic mass spring damper system, where

the blade tip can be represented by a damper, total blade weight and rotary parts as the mass and the stiffness of the system could be the stiffness of the blades [115].

$$m\ddot{x} + c\dot{x} + kx = f(t) \tag{6.1}$$

where 'x' is the rotational position, 'm' is the mass of the block [kg], 'c' is the damper coefficient and 'k' is the spring constant [$kg \times s^{-2}$].

Equation (6.1) can also be written as:

$$\ddot{x} + 2\zeta\omega_n\dot{x} + \omega_n^2 x = f(t) \tag{6.2}$$

where ω_n and ζ are the natural frequency and the damping ratio of the system, respectively. $f(t)$, is the force applied to the system. By comparing equations (6.1) and (6.2), equations (6.3) and (6.4) can be extracted:

$$\omega_n = \sqrt{\frac{k}{m}} \tag{6.3}$$

$$\zeta = \frac{c}{2\sqrt{mk}} \tag{6.4}$$

In equation (6.5), the relation between undamped and damped natural frequency is shown.

$$\omega_d = \omega_n\sqrt{1 - \zeta^2} \tag{6.5}$$

where ω_d is the frequency of the oscillation of a damped system.

With regards to equation (6.5) the resonance frequency of the system in [Hz] can be written as:

$$f = \frac{1}{2\pi}\sqrt{\frac{k}{m}} \tag{6.6}$$

The damping ratio and natural frequency can be calculated from the measurement of the flutter effect frequency of the step response, which then will provide the ratio of k/m and can be used for modelling and blade tip condition monitoring.

The natural frequency in FFT analysis is 2.25 Hz, therefore the $\frac{k}{m}$ ration is:

$$\frac{k}{m} = (2\pi \times 2.25)^2 \approx 200\ [\text{rad}\times\text{s}^{-1}]^2$$

The overshoots in the shaft measurements can be used to monitor the damping of the blade tips:

$$M_p^{\%} = 100e^{-\frac{\zeta\pi}{\sqrt{1-\zeta^2}}} \tag{6.7}$$

where M_p represents the maximum overshoot [115].

To estimate parameters of a mass spring damper system that represent the shaft speed during the braking event, ARX function in Matlab was used [116]. The ARX function provides a transfer function based on input, output and time slice; to use this function input was assumed as a step function and output was the shaft speed fluctuations without an offset. As the shaft speed changes the reduction of the mean values could not help to eliminate the dynamic offset. To overcome this, intrinsic mode function (IMF) was applied to the shaft speed

measurement [117]. In this method, the data is plotted based on its local mean and consequently the oscillation related to the flutter effect can be decomposed from the speed measurements. Figure 6.5 demonstrates the IMF function procedure. The middle point between the upper envelope and the lower envelope is the new x-axis base point for the signal. The signal based on the new x-axis is shown in Figure 6.6. The presented signal was then used in the ARX function and the parameters that represent *m*, *k* and *c* in a mass spring damper system were estimated. The estimated parameters were applied to a Simulink model of the mass spring damper system, which also estimates the stop time based on the initial shaft speed and braking time measured from the recorded events.

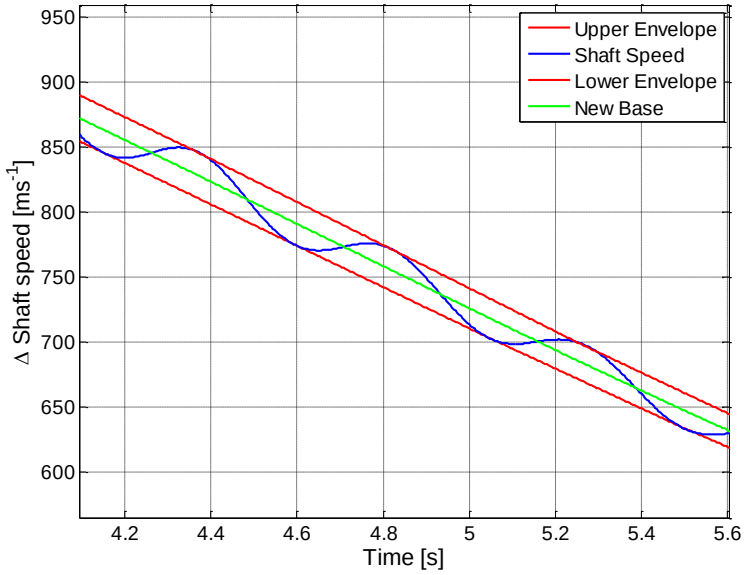

Figure 6.5: The process of IMF

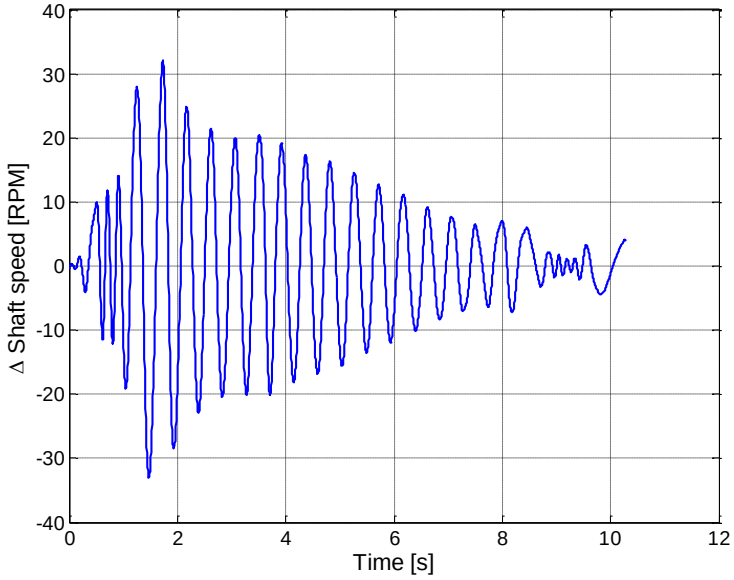

Figure 6.6: IMF level 1 of the shaft speed data

The estimated parameters from the ARX function were passed to the Simulink model which simulates the shaft speed behaviour during the braking period. The model and the parameters can be seen in Figure 6.7.

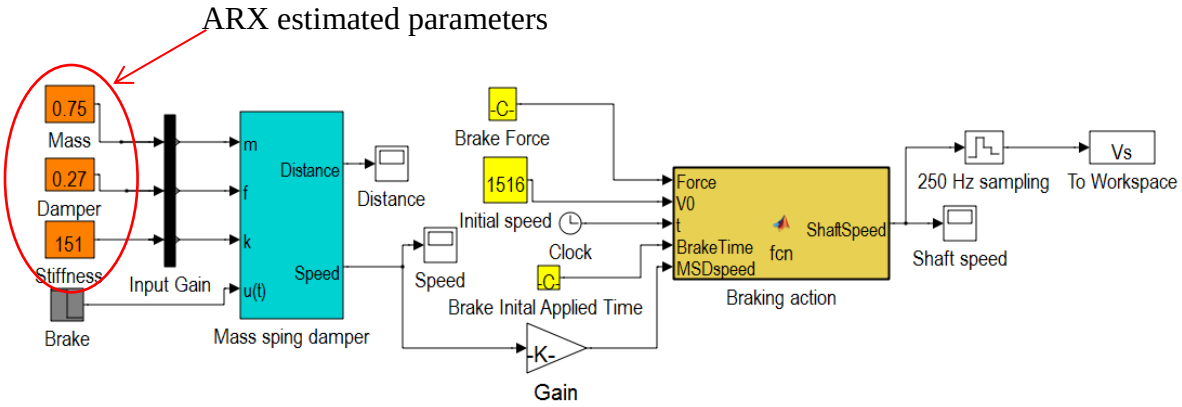

Figure 6.7: Simulink model of the shaft speed with the use of estimated parameters

Figure 6.8 shows the simulated data and the actual measured data from the NEG Micon 750 on September 2011.

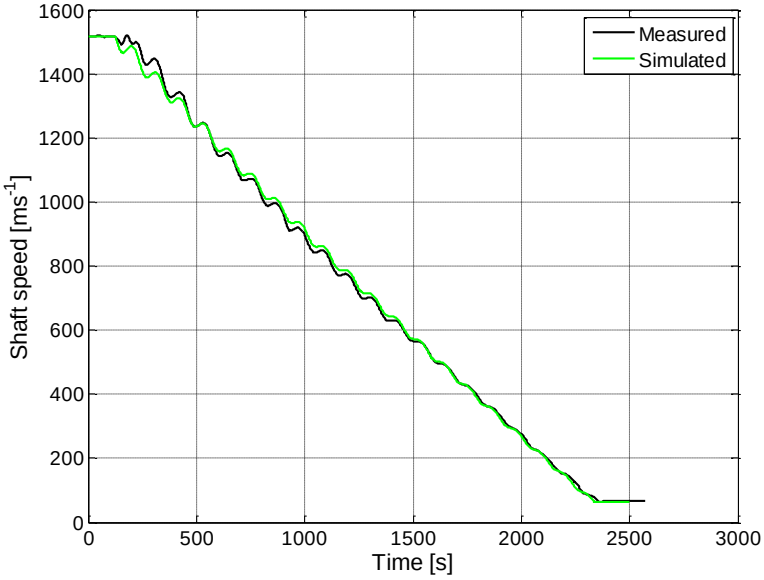

Figure 6.8: Measured high speed shaft velocity versus simulated data

The FFT analysis of the simulated and measured data also confirms that the model can produce data with less than 8% error in final values.

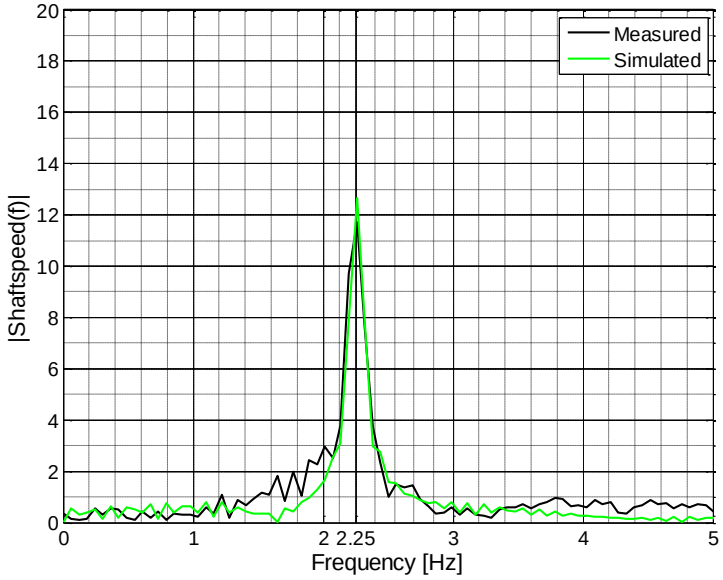

Figure 6.9: FFT of the measured data and the simulation output

To simulate how a failure in blade tip can behave, in the model the value for the damper was reduced to one third of its original value and the FFT results show the difference within

damping amplitude. This can be explained by having less damping and consequently higher overshoot.

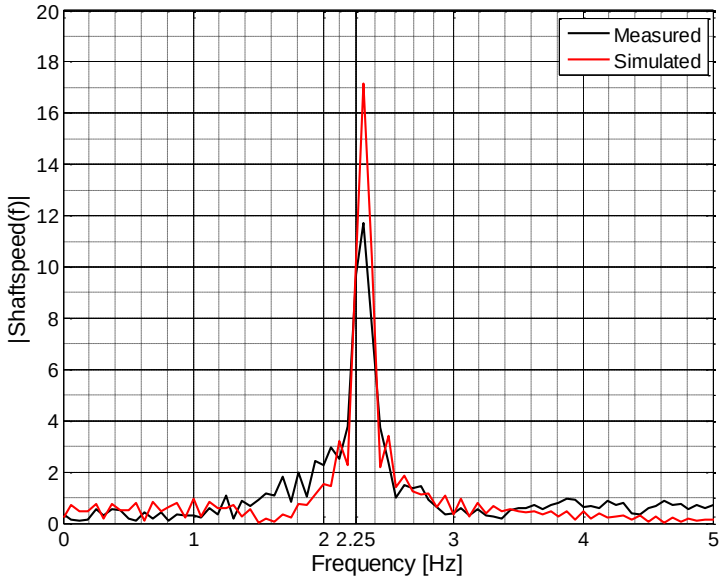

Figure 6.10: FFT of the simulated fault versus the measured data

The idea of detecting icing issues of the blades can also be considered within the model. This can be simplified by considering an additional mass to the blades (25% extra mass was applied). The results show changes within the natural frequency, which is also explainable by equation (6.5).

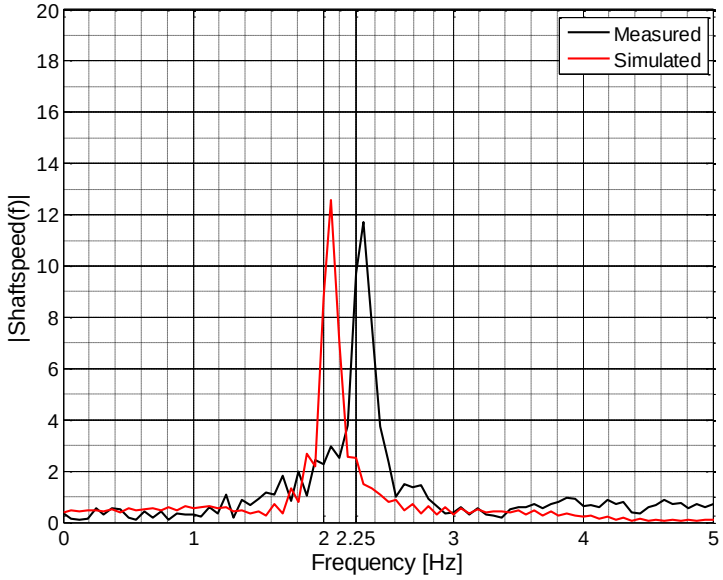

Figure 6.11: Simulated icing fault and healthy measured data

6.4 Summary

Wind turbine shaft speed data are usually recorded by wind farm operators. If the speed is logged with an adequate level of sampling rate and accuracy, then any mechanical irregularity in blades or blade tips can be derived from appropriate analysis of the shaft speed data during a braking event.

To achieve a demonstrable frequency analysis on the natural frequency of the blades, the sampling frequency should be at least twice its resonance frequency so it can then be observed. Adequate sampling rates enable the resonance frequency to be positioned in the centre of the FFT spectrum, therefore monitoring of this frequency could be improved for conditions where the resonance frequency may change. As an example, if the natural frequency is around 2 Hz, to have the natural frequency in the centre of the spectrum, a sampling rate of 8 Hz is required, which is twice the Nyquist frequency. This needs a sensor to be able to measure the shaft speed at around 50 rad/s. This requirement was simply met by

the installed shaft speed measurement system on the NEG Micon 750 wind turbine. Thus no extra instrumentation or sensor was needed for an existing turbine.

It has also been shown that the use of a mass spring damper model to match the real data can help to identify faults through changes to the model parameters. For example, increased overshoot in a mass spring damper system can be caused by reduction in damping or changes in the stiffness and mass. As the natural frequency, which is related to mass and stiffness, is not changed, then it can be concluded that the change in damping causes the higher overshoots. This also explains why the damping ratio has been decreased, which is caused by the failure of the blade tip.

Conditions such as blade icing were simulated then detected by the presented fault detection and diagnosis methods.

The work presented in this chapter has confirmed that the method of using a simple measurement can be applied to other parts of the turbine system. A major risk for turbines operating in cold climates is the accumulation of ice on the blades during operation. The recent methods for ice detection include: piezoelectric vibro-meter, ultrasonic wave analysis, analysis of the output power and other complex approaches; these have some disadvantages such as expensive sensors, difficulties installing the sensors and lack of adequate sensitivity of measurements [118,119].

The presented method in this chapter, which can monitor the dynamics of the blades during impulsive events, has the potential to detect ice build-up that would lead to an increase in rotational inertia of the system.

Chapter 7 Conclusions

7.1 Introduction

This work was motivated by the aspiration of the wind industry to increase the reliability and effectiveness of health monitoring systems for wind turbines. The thesis described the development of cost effective and non-intrusive condition monitoring solutions that could cover the areas that have a lack of automatic health monitoring systems. It also explored the use of existing data collected by wind farm operators to spatially correlate data from the monitored assets within a turbine to improve the efficacy of fault detection and diagnosis approaches.

7.2 Key achievements

In this thesis, the design of a condition monitoring system to enable fault detection and diagnosis for wind turbine brake systems was investigated and evaluated.

It was shown that the use of motor current analysis to monitor the behaviour of systems that are driven by induction motors can be a cost effective technique; this was applied to hydraulic power units. A cost efficient data acquisition system (UoB data logging unit) and the ease of data processing were also advantageous in this work. To assess the approaches in Chapter 2, data was collected from different wind turbines and a number of laboratory tests were carried out.

Using a non-intrusive, low-cost and simple monitoring system meant that wind farm operators provided the necessary permissions to perform the installation of the equipment.

Due to the NIMO project agreement, which was carried out in parallel with this thesis, a number of recorded data sets from the existing wind turbine sensor were requested for this

work and the correlation of the data collected for the UoB data logging unit and the provided data sets was studied:

- The hydraulic pressure data analysis resulted in being able to monitor the behaviour of the pitch controller and detect an induced fault using a yaw system with an historical data processing strategy.
- The high-speed shaft measurements led to calculation of the natural frequency of the blades during braking. This was used to detect a faulty blade tip of a NEG Micon 750 wind turbine; this was confirmed by the wind farm operator technician observation.

These results demonstrate how the use of existing recorded data by wind farm operators can contribute to improvements in the effectiveness of the current condition monitoring systems.

Models and simulation of faults were described in this thesis and were used to explain the use of the collected data, fault detection and diagnosis approaches, and evaluation of the estimation for the system behaviour to improve the condition monitoring system.

The methods proposed and tested in this thesis could have potential application in both retrospectively applying condition monitoring systems to existing turbines, and in the development of more sophisticated systems for new designs. Many of the failures within wind turbines occur in parts of the system where direct measurements are very difficult or even impossible, therefore an indirect method employing simple low-cost technology could offer considerable improvements.

7.3 Further areas for investigation

Only a small number of faults were examined; investigation of other faults, such as gear pump or leakage failure in a hydraulic unit, within the industrial experiments on the hydraulic power units would have allowed for development of a more robust condition monitoring system. Nevertheless, a faulty situation was induced by the wind farm operator and presented in Chapter 5 and a faulty blade tip condition was detected by the discussed fault detection and diagnosis methods in Chapter 6.

The work addressed a narrow range of simulated faults but the results indicated that there is potential to extend and develop a more comprehensive analysis in order to commercialise the method. This would involve a case study approach which would feed into a threshold-based type algorithm which could then look for specific faults deemed of interest to wind turbine operators.

7.4 Publications

Some of the works in this thesis have been presented at academic conferences and published in a journal; some have also been awarded by prizes.

1) Poster prize winner at the BlueBear poster conference, University of Birmingham, June 2010. (Appendix A - BlueBEAR conference poster)
2) Accepted and presented paper at 8th International Conference on Condition Monitoring and Machinery Failure Prevention Technologies (CM2011), "Fault Detection and Diagnosis within a Wind Turbine Mechanical Braking System", Cardiff, 2011. (Appendix B - CM2011 conference paper)
3) Awarded scholarship to attend and present at the PHM Society Doctoral Consortium, "Distributed fault detection and diagnosis for wind farms", Montreal, September, 2011. (Appendix C - PHM society doctoral consortium)

4) Published journal paper: M. Entezami, S. Hillmansen, P. Weston, M.Ph. Papaelias, Fault detection and diagnosis within a wind turbine mechanical braking system using condition monitoring, Renewable Energy, Volume 47, November 2012, Pages 175-182, ISSN 0960-1481, 10.1016/j.renene.2012.04.031.(Appendix D - Renewable Energy journal paper)
5) Poster prize winner at the Institution of Engineering and Technology (IET) poster conference, "Distributed fault detection and diagnosis for wind farms", Coventry University, March 2012. (Appendix E - IET conference poster)
6) Poster prize winner at the Midlands Energy Graduate School (MEGS) annual conference, "Condition monitoring of wind turbine brake systems", University of Birmingham, September 2012. (Appendix F - MEG III conference poster)

References

[1] World Wind Energy Association, "World Wind Energy Report 2011", WWEA, Bonn, 2012.

[2] Directgov, "National Renewable Energy Action Plan for the United Kingdom", Renewable Energy Directive, 2009/28/EC 2008. [Online]. https://www.gov.uk/government/uploads/system/uploads/attachment_data/file/47871/25-nat-ren-energy-action-plan.pdf

[3] C. A Walford, "Wind Turbine Reliability: Understanding and Minimizing Wind Turbine Operation and Maintenance Costs", Global Energy Concepts, LLC, Albuquerque, New Mexico, Government Report 2006.

[4] P. J. Tavne, J. Xiang, and F. Spinato, "Reliability Analysis for Wind Turbines", *Wind Energy*, vol. 10, no. 1, pp. 1-18, July 2006.

[5] EDS Consulting, "Land Use Planning for Wind Energy Systems in Manitoba ", EDS Consulting, Winnipeg, Intergovernmental Report 2009.

[6] J. A. Andrawus, "Maintenance optimisation for wind turbines", The Robert Gordon University, Aberdeen, PhD Thesis 2008.

[7] A. Zaher, S. McArthur, and D. Infoeld, "Online wind turbine fault detection through automated SCADA data analysis", *Wind Energy*, vol. 12, pp. 574-593, January 2009.

[8] T. W. Verbruggen, "Wind Turbine Operation & Maintenance based on Condition

Monitoring WT-Ω", ECN Wind Energy, Final report 2003.

[9] F. D. Bianchi, H. D. Battista, and R. J. Mantz, *Wind turbine control systems: principles, modelling and gain scheduling design*. London, UK: Springer, 2007.

[10] S. Mathew, "Wind energy conversion systems", in *Wind Energy: Fundamentals, Resource Analysis and Economics*. Heidelberg, Netherlands: Springer, 2006, ch. 4, pp. 90-92.

[11] D. Darling. The Encyclopedia of Alternative Energy and Sustainable Living. [Online]. http://www.daviddarling.info/encyclopedia/W/AE_wind_turbine.html

[12] G. Feng, Z. Liu, B. Daorina, and Z. Gon, "Experimental Research on Vertical Axis Wind Turbine", *IEEE Power and Energy Engineering Conference*, pp. 1-4, March 2009.

[13] M. Bhutta, N. Hayat, A. Farooq, and Z. Ali, "Vertical axis wind turbine – A review of various configurations and design techniques", *Renewable and Sustainable Energy Reviews*, vol. 16, no. 4, pp. 1926–1939, May 2012.

[14] M. Singh, "Dynamic Models for Wind Power Plants", University of Texas, Austin, PhD Thesis 2011.

[15] NEG Micon, NM48/750 Techincal Specifications, 1999, Datasheet.

[16] J. Gertler, *Fault detection and diagnosis in engineering systems*. United States of America: CRC Press, 1998.

[17] C. Roberts, "Methods for fault detection and diagnosis of railway actuators", University

of Birmingham, Birmingham, PhD Thesis 2006.

[18] J. Ribrant and L. M. Bertling, "Survey of Failures in Wind Power Systems With Focus on Swedish Wind Power Plants During 1997–2005", *IEEE Transactions on Energy Conversion*, vol. 22, no. 1, pp. 167-173, March 2007.

[19] Y. Sun, Y. Lin, L. Wei, and D. Zhang, "The Digital Soft Braking for Wind Turbine", in *ICEEE International Conference E-Product E-Service and E-Entertainment*, Henan, 2010, pp. 1-6.

[20] Det Norske Veritas and Riso National Laboratory, *Guidelines for design of wind turbines*, 2nd ed. Copenhagen, Denmark: Jydsk Centraltrykkeri, 2002.

[21] International Electrotechnical Commission (IEC) Standard, Wind turbine generator systems - Part1: Safety requirements, 2004, BS EN 61400-1:2004.

[22] M. Friedrich and R. Andersen, "Method for Stopping a Wind Turbine in Two Stages", US Patent 2010/0068057 A1, March 18, 2010.

[23] D. Lekou and I. Zalacain, Private communication, 2012, CRES and ACCIONA Windfarm operators.

[24] Vestas Wind Systems A/S, "Vestas General Specification Brochure", Technology R&D, General Description, Class 1 0010-7152 V00, May 2010.

[25] L. D. Willey, "Design and development of megawatt wind turbines", in *Wind Power Generation and Wind Turbine Design*, Wei Tong, Ed. Southampton, UK: WIT Press, 2010, ch. 6, pp. 206-231.

[26] Garrad Hassan & Partners Ltd., "Electrodynamic braking of large wind turbines", EC Fourth Framework Programme ETSU W/45/00519/REP, 1999.

[27] J. P. Lyons, A. Andreas, M. Esser, and P. S. Bixel, "Method and System for Wind Turbine Braking", United States Patent 5,907,192, May 25, 1999.

[28] L. Staudt, "Design and development of small wind turbines, rotor overspeed control", in *Wind Power Generation and Wind Turbine Design*, Wei Tong, Ed. Southampton, UK: WIT Press, 2010, ch. 7, pp. 264-271.

[29] K. L. Cousineau and C. L. Christenson, "Non-volatile over speed control system for wind turbines", United States Patent 6,265,785 B1, July 24, 2004.

[30] P. Lading, O. Sangill, and D. Welner, "Hydraulic Braking System", US Patent 6,254,197 B1, July 3, 2001.

[31] Twifles Limited. (2011, May) Braking calculations and braking terms. [Online]. http://warnernet.com/litportal/pdfs/P-1648-TF_USpg41-44.pdf

[32] H. Stiesdal, "The wind turbine components and operation", Bonus Energy A/S, Brande, Bunos-Info Newsletter Autumn 1999.

[33] F. Jepsen, A. Soborg, and Z. Yang, "Disturbance control of the hydraulic brake in a wind turbine", in *IEEE Energy Conference and Exhibition (EnergyCon)*, Manama, 2010, pp. 530-535.

[34] Z. Wang, S. Liu, L. Luan, and H. Xiao, "Study on the influence of the temperature rise and frictional coefficient of brake shoe on braking of wind turbine", *Advanced Materials Research*, vol. 443-444, pp. 1045-1049, January 2012.

[35] E. A. de Cesare and I. Lopez Lacasta, "Passive fire protection system for wind turbines", European Patent 10006700.8, January 12, 2011.

[36] (2011, December) Berwickshire News. [Online]. http://www.berwickshirenews.co.uk/news/local-headlines/brake_failure_to_blame_for_collapsing_of_wind_turbine_1_2007887

[37] D. Brownlow. (2012) Wind Turbine Safety. [Online]. http://www.windbyte.co.uk/safety.html

[38] K. Rajambal, B. Umamaheswari, and C. Chellamuthu, "Electrical braking of large wind turbines", *Renewable Energy*, vol. 30, no. 15, pp. 2235-2245, 2005.

[39] W. J. Bonneau et al., "Pitch control battery backup methods and system", EP1763126 A1, 14 March, 2007.

[40] TWI Ltd. (2010, January) Development and Demonstration of a Novel Integrated Condition Monitoring System for Wind Turbines. [Online]. http://www.nimoproject.eu/

[41] F. R. Giordano, W. P. Fox, S. B. Horton, and M. D. Weir, *First Course in Mathematical Modeling*. Belmont, CA, United States of America: Cengage Learning, 2008.

[42] Z. Hameed, Y. S. Hong, Y. M. Cho, S. H. Ahn, and C. K. Song, "Condition monitoring and fault detection of wind turbines and related algorithms: A review", *Renewable and Sustainable Energy Reviews*, pp. 1-39, January 2009.

[43] I. M. Taylor and M. A. Labrador, "Improving the energy consumption in mobile phones by filtering noisy GPS fixes with modified Kalman filters", in *IEEE Wireless*

Communications and Networking Conference, March 2011, pp. 28-31.

[44] Y. Lu, E. G. Collins, and M. F. Selekwa, "Parity Relation Based Fault Detection, Isolation and Reconfiguration for Autonomous Ground Vehicle Localization Sensors", Florida A&M University - College of Engineering, Tallahassee, Conference paper ADA432374, 2004.

[45] R. Isermann, "Supervision, fault-detection and fault-diagnosis methods — An introduction", *Control Engineering Practice*, vol. 5, no. 5, pp. 639-652, May 1997.

[46] V. Venkatasubramanian, R. Rengaswamy, and S. N. Kavuri, "A review of process fault detection and diagnosis: Part II: Qualitative models and search strategies", *Computers & Chemical Engineering*, vol. 27, no. 3, pp. 313-326, March 2003.

[47] R. Parekh. (2003, December) AC Induction Motor Fundamentals. Application Note AN877. [Online]. http://www.microchip.com

[48] D. Kacprzak. Induction motor, University of Auckland, School of Engineering. [Online]. http://www.ece.auckland.ac.nz/~kacprzak/PE2.html

[49] S. Jeevanand, B. Singh, B. K. Panigrahi, and V. Negi, "State of art on condition monitoring of induction motors", *IEEE International Conference on Power Electronics, Drives and Energy Systems (PEDES)*, pp. 1-7, December 2010.

[50] S. Nandi and H. A. Toliyat, "Fault diagnosis of electrical machines - a review", in *Electric Machines and Drives International Conference*, 1999, pp. 219-221.

[51] Y. Zhongming and W. Bin, "A review on induction motor online fault diagnosis", in *Power Electronics and Motion Control Conference*, Slovakia, 2000, pp. 1353-1358.

[52] R. Mistry, W. R. Finley, and S. Kreitzer, "Induction Motor Vibrations", *IEEE Industry Applications Magazine*, vol. 16, no. 6, pp. 37-46, December 2010.

[53] B. Li, G. Goddu, and M. Y. Chow, "Detection of common motor bearing faults using frequency-domain vibration signals and a neural network based approach", *American Control Conference*, vol. 4, pp. 2032-2036, January 1998.

[54] R. R. Gonzalez-Carrato, F. P. García Márquez, and J. M. P. Pérez, "A Novel Predictive Maintenance Method for Wind Turbines Based On Wavelets Transforms", Ingenium Research Group, Universidad Castilla-La Mancha, Ciudad Real, 2012.

[55] M. Neelam, "Condition Monitoring and fault diagnosis of induction motor using motor current signature analysis", National institute of technology, Kuruksherta, PhD Thesis 2010.

[56] H. Hafezi and A. Jalilian, "Design and Construction of Induction Motor Thermal Monitoring System", in *41st International Universities Power Engineering Conference*, Newcastle upon Tyne, 2006, pp. 674-678.

[57] M. J. Picazo-Rodenas, R. Royo, J. Antonino-Daviu, and J. Roger-Folch, "Energy balance and heating curves of electric motors based on Infrared Thermography", in *IEEE International Symposium on Industrial Electronics (ISIE)*, 2011, pp. 591-596.

[58] K. Bacha, H. Henao, M. Gossa, and G. Capolino, "Induction machine fault detection using stray flux EMF measurement and neural network-based decision", *Electric Power Systems Research*, vol. 78, no. 7, pp. 1247–1255, July 2008.

[59] M. L. Sin, W. L. Soong, and N. Ertugrul, "Induction machine on-line condition

monitoring and fault diagnosis – a survey", in *Australasian Universities Power Engineering Conference*, Christchurch, 2003, pp. 1-6.

[60] N. Mehala and R. Dahiya, "Motor Current Signature Analysis and its Applications in Induction Motor Fault Diagnosis", *International journal of systems applications, engineering & development*, vol. 2, no. 1, pp. 29-35, 2007.

[61] J. H. Jung, L. Jong-Jae, and B. Kwon, "Online Diagnosis of Induction Motors Using MCSA", *IEEE Transactions on Industrial Electronics*, vol. 53, no. 6, pp. 1842-1852, December 2006.

[62] D. Basak, A. Tiwari, and S. P. Das, "Fault diagnosis and condition monitoring of electrical machines - A Review", in *IEEE International Conference on Industrial Technology*, Mumbai, 2006, pp. 3061-3066.

[63] S. H. Chetwani, M. K. Shah, and M. Ramamoorty, "Online condition monitoring of induction motors through signal processing", *IEEE Electrical Machines and Systems, ICEMS*, vol. 3, pp. 2175- 2179, September 2005.

[64] S. Nandi, H. A. Toliyat, and X. Li, "Condition Monitoring and Fault Diagnosis of Electrical Motors—A Review", *IEEE TRANSACTIONS ON ENERGY CONVERSION*, vol. 20, no. 4, pp. 719-729, December 2005.

[65] P. Vicente, J. Rodriguez, M. Negrea, and A. Arkkio, "A general scheme for induction motor condition monitoring", *IEEE International Symposium on Diagnostics for Electric Machines, Power Electronics and Drives*, pp. 1-6, September 2005.

[66] W.T. Thomson and M. Fenger, "Current signature analysis to detect induction motor

faults", *IEEE, Industry Applications Magazine*, vol. 7, no. 4, pp. 26-34, 2001.

[67] C. Kar and A. R. Mohanty, "Monitoring gear vibrations through motor current signature analysis and wavelet transform", *Mechanical Systems and Signal Processing*, vol. 20, no. 1, pp. 158–187, January 2006.

[68] D. Stranneby and W. Walker, *Digital signal processing and applications*, 2nd ed. UK: Elsevier, 2004.

[69] M. Abdesh Shafiel Kafiey Khan and M. Azizur Rahman, "Wavelet Based Diagnosis and Protection of Electric Motors", in *Fault Detection*. NL, Canada: In-teh, 2010, ch. 12, pp. 255-280.

[70] F. Karami, J. Poshtan, and M. Poshtan, "Broken bar fault detection in induction motors based on modified winding Function", *IEEE International Conference on Control Applications*, pp. 1951-1956, Septempber 2010.

[71] N. Thrane, J. Wismer, H. Konstantin-Hansen, S. Gade, and Brüel&Kjær. Practical use of the "Hilbert transform". Application Note. [Online]. http://www.bksv.com/doc/bo0437.pdf

[72] The Mathworks Inc. (2012) Gridded and Scattered Sample Data. [Online]. http://www.mathworks.co.uk/help/techdoc/math/bsou4rj.html

[73] D. M. Meko. (2011) Applied Time Series Analysis - GEOS 585A. University of Arizona Course. [Online]. http://www.ltrr.arizona.edu/~dmeko/geos585a.html#cLesson5

[74] The Mathworks Inc. (2010) Input-Output Polynomial Models. [Online].

http://www.mathworks.com/access/helpdesk/help/toolbox/ident/ug/bq2fhe8.html

[75] H. Austerlitz, "Analog/Digital Conversions", in *Data Acquisition Techniques Using PCs*.: Academic Press, 2002, ch. 4, pp. 73-75.

[76] J. Park and S. Mackay, "Plugin data acquisition boards", in *Practical Data Acquisition for Instrumentation and Control Systems*. Great Britain: Newnes, 2003, ch. 5, pp. 141-151.

[77] I. Aydin, M. Karakose, and E. Akin, "A new method for early fault detection and diagnosis of broken rotor bars", *Energy Conversion and Management*, vol. 52, no. 4, pp. 1790-1799, April 2011.

[78] B. Ayhan, H. J. Trussell, M. Chow, and M. Song, "On the use of a lower sampling rate for broken rotor bar detection with DTFT and AR-based spectrum methods", *IEEE Transaction on Industrial Electronics*, vol. 55, no. 3, pp. 1421-1434, March 2008.

[79] D. Stranneby and W. Walker, "The analog-digital interface", in *Digital Signal Processing and Applications (Second Edition)*. United Kingdom: Elsevier, 2004, ch. 2, pp. 41-68.

[80] Marposs. (2004) Industrial computers: Frequent asked questions. Document. [Online]. http://www.marposs.com/ftp/files/faq_indpc_115_en.pdf

[81] M. Colnaric, D. Verber, and W. A. Halang, "Real-time Characteristics and Safety of Embedded Systems", in *Distributed Embedded Control Systems : Improving Dependability with Coherent Design*, 1st ed. United Kingdom: Springer, 2007, pp. 3-28.

[82] Microchip Technology Inc. (2012, April) Watchdog Timer (WDT) and Power-Saving Modes. Reference Manual. [Online]. http://ww1.microchip.com/downloads/en/DeviceDoc/70196D.pdf

[83] Magnelab Inc. Split-Core AC Current Sensor SCT-0400. [Online]. http://www.magnelab.com/products/Current-Voltage-Sensors/Split-Core-AC-Current-Sensor-SCT-0400

[84] LEM. (2011, November) LA 25-NP. [Online]. http://www.lem.com/docs/products/la%2025-np.pdf

[85] National Instrument. (2012) NI USB-6210. [Online]. http://sine.ni.com/nips/cds/view/p/lang/en/nid/203223

[86] Linear Technology Corporation. (2004) LTC1857/LTC1858/LTC1859. Datasheet. [Online]. http://cds.linear.com/docs/en/datasheet/185789fa.pdf

[87] P. Pillay and Z. Xu, "Motor current signature analysis", in *IEEE, Industry Applications Conference,Thirty-First IAS Annual Meeting*, 1996, pp. 587-594.

[88] LEM. (2012) AV 100-2000. [Online]. http://www.lem.com/docs/products/av%20100-2000%20sp1.pdf

[89] V. Arun, B. Shanthi, and S. P. Natarajan, "Unipolar PWM control technique having inverted sine carrier for an asymmetric reduced switch multilevel inverter", *International Journal of Engineering Science and Innovative Technology*, vol. 2, no. 3, pp. 486-493, May 2013.

[90] E. D. Gates, "AC Circuits", in *Introduction to Electronics*. USA: Cengage Learning,

Inc, 2011, ch. 2, pp. 142-145.

[91] A. H. Robbins and W. C. Miller, "Filters and the Bode plot", in *Circuit Analysis With Devices: Theory and Practice*.: Delmar Cengage Learning, 2003, ch. 22, pp. 800-810.

[92] Analog Devices, Inc., "The data conversion handbook", in *Fundamentals of Sampled Data Systems*, W. A. Kester, Ed. United States of America: Newnes, 2005, ch. 2, pp. 57-82.

[93] K. Smith and R. Alley, "Electrical Circuits: An Introduction", in *Transformers for three-phase systems*. Cambridge: Cambridge University Press, 1992, ch. 5, pp. 269-275.

[94] E. R. Collins and J. Jiang, "An Experimental Investigation on Third Harmonic Current Distortion in Single-Phase Induction Motors", *13th International Conference on Harmonics and Quality of Power, ICHQP*, pp. 1-7, September 2008.

[95] ESH Testing Limited, "ESH 100 kN low cycle fatigue machine", Brierley Hill, Operating manual SN996259, 2002.

[96] B. A. Shenoi, "Infinite Impulse Response Filters", in *Introduction to Digital Signal Processing and Filter Design*.: John Wiley & Sons, Inc., 2006, ch. 4, pp. 231-238.

[97] Torquemeters Ltd, "110 kW Train Simulation Rig for University of Birmingham", Northampton, Operating Manual SN42384, 2012.

[98] I. Y. Önel, K. Burak Dalci, and İ. Senol, "Detection of bearing defects in three-phase induction motors using Park's transform and radial basis function neural networks", *SADHANA - Springer*, vol. 31, no. 3, pp. 235–244, June 2006.

[99] S. V. Vaseghi, "Impulsive noise", in *Advanced Signal Processing and Noise Reduction*.: John Wiley, 2000, ch. 12, pp. 355-377.

[100] C. Marcelo, J. P. Fossatti, and J. Ign, "Fault Diagnosis of Induction Motors Based on FFT", in *Fourier Transform - Signal Processing*, Salih Salih , Ed.: InTech, 2012, ch. 7, pp. 157-182.

[101] M. Entezami, P. Weston, S. Hillmansen, and M. Papealias, "Fault Detection And Diagnosis Within A Wind Turbine Mechanical Braking System Using Condition Monitoring", *Renewable Energy*, vol. 47, pp. 175-182, April 2012.

[102] The Centre for Renewable Energy Sources and Saving. CRES Windfarm. [Online]. http://www.creswindfarm.gr/site1/index_en.htm

[103] SIME INDUSTRIE, Disc brake - TE2L supply unit, 1995, Technical Datasheet.

[104] F. R. Giordano, W. P. Fox, S. B. Horton, and M. D. Weir, *A First Course in Mathematical Modeling*, 4th ed. Belmont, USA: Cengage Learning, 2009.

[105] B. Liang, B. S. Payne, A. D. Ball, and S. D. Iwnicki, "Simulation and fault detection of three-phase induction motors", *Mathematics and Computers in Simulation*, vol. 61, no. 1, pp. 1-15, November 2002.

[106] K. L. Shi, T. F. Chan, Y. K. Wong, and S. L. Ho, "Modelling and simulation of the three-phase induction motor using Simulink", *International Journal of Electrical Engineering Education*, vol. 36, pp. 163–172, April 1999.

[107] The Mathworks Inc. (2012) Estimate electrical parameters of double cage asynchronous machine based on standard manufacturer specifications. [Online].

http://www.mathworks.co.uk/help/physmod/powersys/ref/power_asynchronousmachineparams.html

[108] A. Yazdanpanah Goharrizi and N. Sepehri, "A Wavelet-Based Approach for External Leakage Detection and Isolation from Internal Leakage in Valve-Controlled Hydraulic Actuators", *IEEE Transaction on Industrial Electronics*, vol. PP, no. 99, p. 1, November 2010.

[109] The Mathworks Inc. (2013) Implement programmable phase-to-phase and phase-to-ground fault breaker system. [Online]. http://www.mathworks.co.uk/help/physmod/powersys/ref/threephasefault.html

[110] Y. G. Paithankar and S. R. Bhide, "Introduction", in *Fundamentals Of Power System Protection*.: Prentice Hall Of India Pvt. Limited, 2004, pp. 1-7.

[111] Terna Energy S.A. [Online]. http://www.terna-energy.com/

[112] The Mathworks Inc. (2012) Butterworth filter design. [Online]. http://www.mathworks.co.uk/help/signal/ref/butter.html

[113] Acciona Energy. (2012) Acciona Windpower. [Online]. http://www.acciona-energia.com/media/360246/AW%201500_2012.pdf

[114] (2003, July) Danish Wind Industry Association (DWIA). [Online]. http://wiki.windpower.org/index.php/Turbine_Safety

[115] B. Kulakowski and J. Gardner, "Analytical Solutions of System Input–Output Equations", in *Dynamic Modelling and Control of Engineering Systems*, 3rd ed. Cambridge, UK: Cambridge University Press, 2007, ch. 4, pp. 92-104.

[116] The Mathworks Inc. (2013) Estimate parameters of ARX or AR model using least squares. [Online]. http://www.mathworks.co.uk/help/ident/ref/arx.html

[117] N. E. Huang and S. S. Shen, "Introduction to the Hilbert Huang Transform and its related mathematical problems", in *Hilbert-Huang Transform and Its Applications*.: World Scientific, 2005, ch. 1, pp. 4-13.

[118] M. C. Homola, P. J. Nicklasson, and P. A. Sunds, "Ice sensors for wind turbines", *Cold Regions Science and Technology*, vol. 46, no. 2, pp. 125-131, November 2006.

[119] N. Harper. (2011, July) Windpower engineering development. [Online]. http://www.windpowerengineering.com/maintenance/detecting-ice-on-wind-turbine-blades/

Appendix A - BlueBEAR conference poster

UNIVERSITY OF BIRMINGHAM

Centre for Railway Research and Education

Distributed Fault Detection and Diagnosis for Wind Farms

Mani Entezami - PhD Student - School of Electronic, Electrical and Computer Engineering

Background

Since 1980, progress in electrical, mechanical and control engineering has continued to drive enhancements within the wind energy industry. This results in more powerful and efficient components, such as large towers and blades.

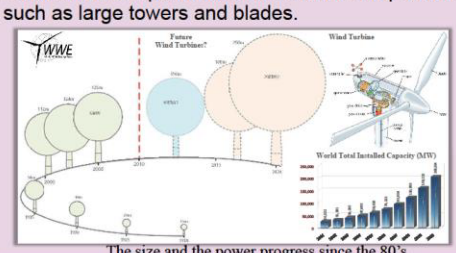

The size and the power progress since the 80's

Motivation

Analyses of wind farm maintenance costs show that up to 40% of the outlay is related to unexpected component failures that lead to costly unscheduled amendments. Wind farm operators constantly aspire to minimise these expenses.

The consequences of not having a proper health monitoring system for the gearbox oil temperature

Aim

To develop a Condition Monitoring System (CMS) for wind turbines that predicts critical and detects incipient failures. The benefit will be advanced-failure detection which results in better planned maintenance, shorter downtimes and decreased revenue losses. Furthermore, this could either be used to enhance safety or achieve a more affordable level of safety.

Acknowledgement

I am indebted to Dr. S. Hillmansen, Dr. C. Roberts and my colleagues in the Railway Research Group for their constant support. This project is partially funded by the European Commission FP7 project NIMO. www.nimoproject.eu

Contacts

Objectives

- Review wind turbine failures and model-based Fault Detection & Diagnosis (FDD) literature.(A)
- Develop a model for a wind turbine to enable FDD algorithms to be tested with simulated faults. (B)
- Extend the model to consider multiple wind turbines in a wind farm. Assess the simulation in order to improve the efficacy of the algorithms.(A,B)
- Develop a requirements specification for a wind farm condition monitoring system, based around a distributed embedded system. (C)

Project Plan

Mathematical Modelling and Simulations (A)

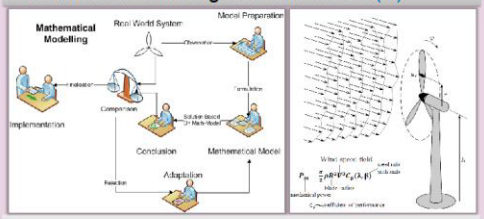

Fault Detection and Diagnosis (B)

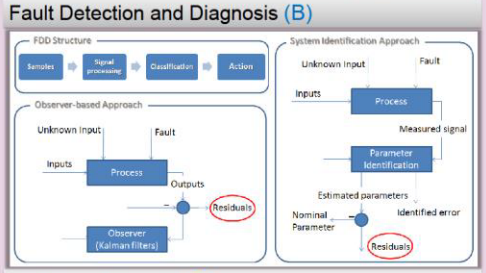

Distributed System (C)

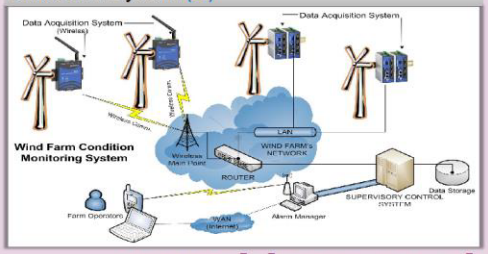

www.bham.ac.uk

Appendix B - CM2011 conference paper

The Eighth International Conference on Condition Monitoring and Machinery Failure Prevention Technologies

Fault detection and diagnosis within a wind turbine mechanical braking system

Mani Entezami, Dr Stuart Hillmansen, Dr Paul Weston and Dr Mayorkinos Papaelias

University of Birmingham, Birmingham, West Midlands, B15 2TT, United Kingdom
+44 (121) 414 7522

Abstract

Renewable energy is one of the most imperative aspects for solving the current worldwide energy crisis. Presently, wind energy is the most developed of these renewable technologies due to the vast number of wind turbines used across the world and the many projects currently in progress. Analyses of wind farm maintenance costs show that up to 40% of the outlay is related to unexpected component failures that lead to costly unscheduled amendments. Wind farm operators constantly aspire to minimise these expenses. Moreover, situations involving major failures of the braking system may result in catastrophic damage, jeopardising investments, reputation and the certainty of wind energy.

Early fault detection by carrying out regular inspection of the system components helps to prevent and lessen the number of major breakdowns. The benefit will be advanced-failure detection, resulting in superior planned maintenance, shorter downtimes and decreased revenue losses. Furthermore, this could be used to either enhance safety or achieve a more affordable current level of safety.

1 Introduction

One of the over-speed control methods for a wind turbine is mechanical braking. The mechanical brake is a steel disc brake usually installed on the high-speed shaft. Braking is achieved by engagement of the brake calliper to the disc. Wind turbine brakes experience extreme stresses, so special alloys are used in brake disc manufacture, capable of withstanding temperatures up to 700 °C. The braking system is a fail-safe system – brakes are applied if the power fails, or if the hydraulic pressure is out of the normal range.

The mechanical brake is generally applied after the blade furling and electromagnetic braking (if available) have reduced the shaft speed, as the mechanical brakes would wear down rapidly if used to stop the turbine from full speed. However, in an emergency, the mechanical brakes can be used alone. It is essential that wind turbines automatically stop if a critical component malfunctions. For instance, if the generator overheats or disconnects from the electrical grid, the braking system will stop the rotor. In most countries, wind turbines are required by law to have two independent fail safe brake mechanisms to stop the turbine

promptly when required [1]. The braking system used in this paper is installed on the NEG Micon750 wind turbine.

1.1 The NEG Micon 750 (NM750) mechanical braking system

The NM750 is a 750 kW wind turbine with a fail-safe hydraulic braking system, shown in Figure 1 and Figure 2. This system uses active hydraulic pressure to keep the wind turbine brakes disengaged (inactive). When the brake command is sent, or if the electric system drops-out, the brakes will immediately be engaged to stop the rotor. The brake disc is located on the high speed shaft, and the calliper, consists of two swing arms, is mounted on a steel bracket bolted to the gearbox housing. The brake pads are installed at one end of the arms, either side of the disc.

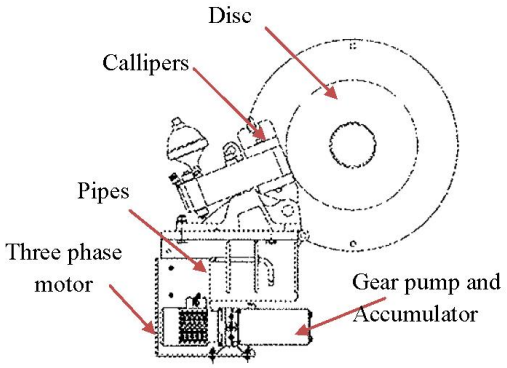

Figure 1: NM750 Mechanical Brake (SIME-Industry)

The brake force is provided by accumulated and passive hydraulic power at one side of the hydraulic piston. The passive pressure is continuously ready to force the brake pads against the brake disc.

Figure 2: Hydraulic/Accumulator system and Callipers

Active hydraulic power, provided by the pump, is used periodically to maintain the pressure in the accumulator to release and keep the pads off the brake disc. In any circumstances if the

active part is removed, the passive accumulated power will engage the brake to stop the turbine.

In this paper, the design of a condition monitoring system (CMS) based on the voltages and the currents of the three-phase hydraulic pump motor, is described. The prospects for fault detection and diagnosis are considered and a Simulink model, are also described.

2 Instrumentation and data acquisition

The CMS is being developed, consisting of various parts, shown in Figure 3a. A data acquisition system acquires data from the sensors; data are stored on a flash memory card along with time from a GPS system and real-time clock calendar. LEDs provide status information. A connection to a SCADA system and a web interface will be realised in the final version. The whole system is powered from the local mains supply, but with a battery back-up to avoid data corruption in the event of power loss.

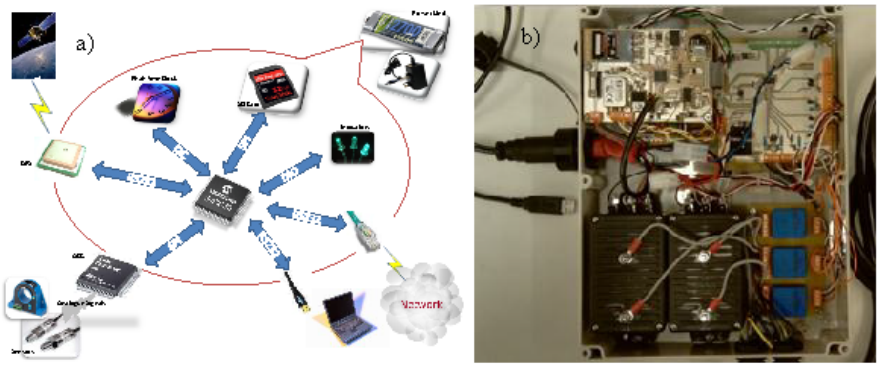

Figure 3: (a) The overview of the deliverable system (b) Custom-built data logger for three-phase motor condition monitoring

Custom-built instrumentation was installed within the main control panel of the 750 kW NEG Micon wind turbine located at the "Centre for Renewable Energy Sources" (CRES), Athens, Greece, shown in Figure 3b. Samples of the three-phase hydraulic pump motor voltage and currents were collected to monitor its condition. Figure 4 illustrates how the voltages and currents of the three-phase motor were obtained from the main panel.

The instrumentation measured and logged the three-phase currents and two phase-phase voltages at 2 kHz sampling rate with 16-bit resolution. The equipment logged the measured signals for one day. Figure 5 shows an example of the three logged current channels following the release of the brake.

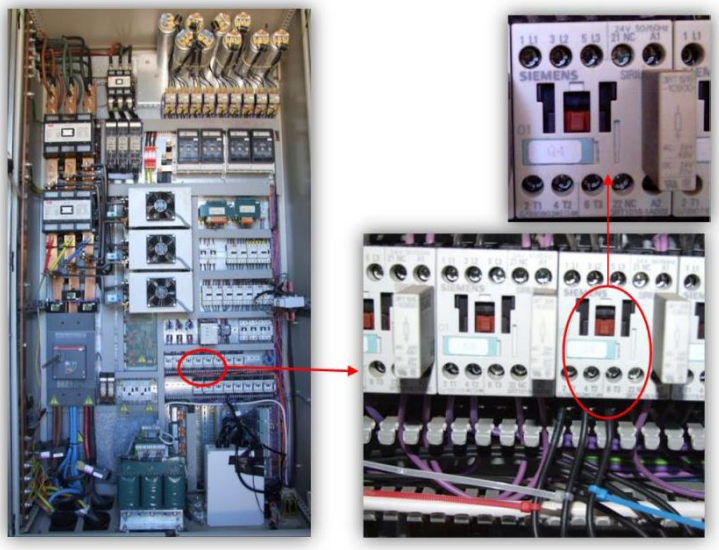

Figure 4: The main contactor for the brake hydraulic system inside the main control panel

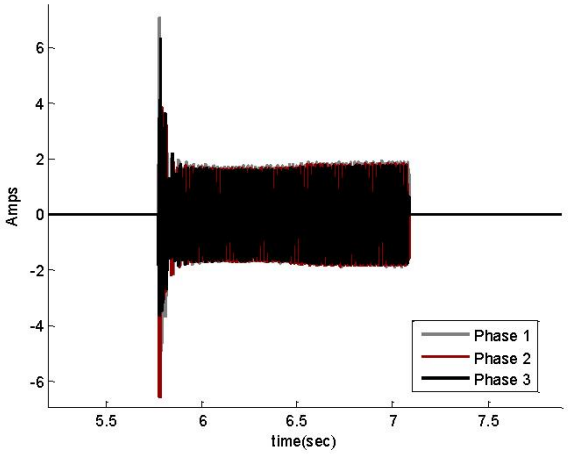

Figure 5: An example of a recorded current data

2.1 Current data validation

Before the logging equipment was installed, some tests were performed using a current clamp and Fluke Scopemeter. Acquired data were used to check the instrumentation results. Figure 6 shows the data from one test. Comparisons found results to be consistent with data recorded by the CMS.

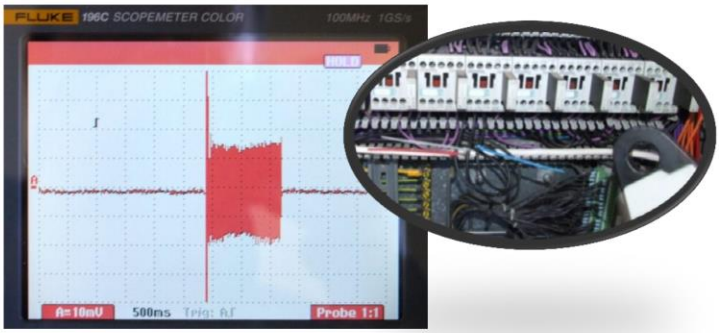

Figure 6: Current data from the three phase motor, sampled by Fluke logger

3 Data analysis

Analyses of the measured voltages showed that their amplitudes and frequencies remain fairly constant. This is to be expected as the voltage comes directly from the local electricity grid. The currents were found to be significantly more useful than the voltages for further analysis. This section describes the types of analyses that have been performed on the current data collected on the trial day.

Currents flow in the three-phase pump motor only when the pump is running and charging the accumulator, a process that takes only a few seconds. The rest of the time the currents are close to zero. For further analyses, the events where the pump was running were extracted from the recorded data. An example of one of the phase currents during a pumping event is shown in Figure 7.

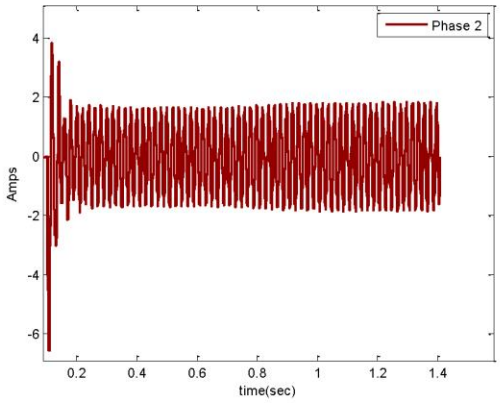

Figure 7: A detected event from the measured currents

Frequency analysis using the Discrete Fourier Transform (DFT) is the most frequent signal processing method used for three phase motor condition monitoring as several mechanical and electrical characteristics can be determined from current signals [2]. Figure 8 illustrates

the spectrum of the current shown in Figure 7. Within the results some notable unexplained spectral power can be seen between 500 and 600 Hz.

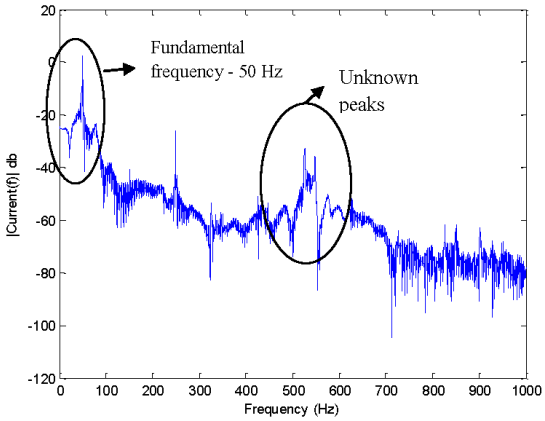

Figure 8: Spectrum of a measured current phase

The signal can be divided into shorter time slices, and a spectrum prepared for each slice, producing a spectrogram [2]. Figure 9 and Figure 10 show the resulting spectrogram for the current previously shown in Figure 7. The 50 Hz fundamental and a strong 250 Hz (5th harmonic) are clearly visible all the time. There is an initial transient current in the first 0.2 s. Around 550 Hz there is a significant peak in the spectrum whose frequency is changing over time although its amplitude is reasonably stable. The pump runs until the desired fluid pressure is achieved. Consequently, the torque on the shaft is increased and the speed decreases. This can also be seen in the increase in the current amplitude. The 550 to 525 Hz frequency change is believed to be related to this change in shaft speed. A laboratory test has been performed and shown a similar effect.

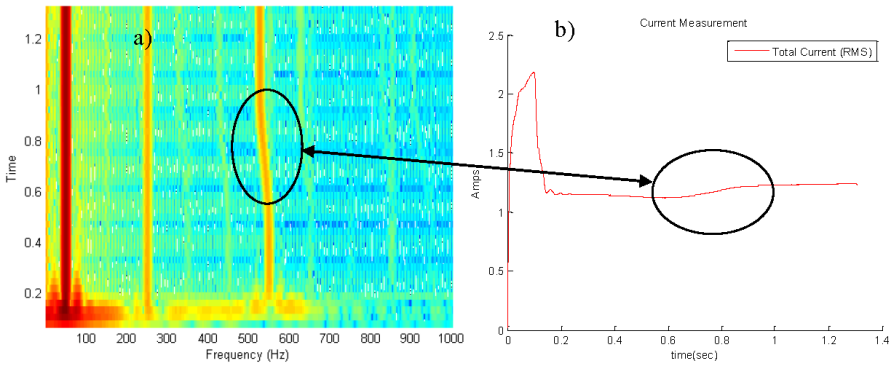

Figure 9: (a) Spectrogram of the current (b) the 0.1 s moving RMS graph of the current

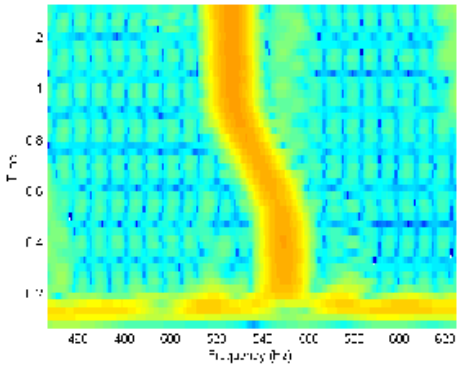

Figure 10: Zoomed spectrogram

4 Fault detection and modelling

In this section, possible ways of fault detection and diagnosis (FDD) are discussed. Modelling the brake system and implementing FDD methods in the model are also presented.

4.1 Fault detection and diagnosis

Model-based and model-free techniques are being considered for the purpose of Fault Detection and this will also be applied to perform fault diagnosis processing. Recent improvements in current sensor technology combined with advances in data processing have led to novel techniques in the field of three phase motor monitoring by the use of spectral analysis of the stator current signal [3]. Time-domain analysis, such as looking at the envelope of a signal, identifies changes within the machinery and its characteristics. Vibration monitoring approaches could also be used for incipient fault detection. However, stator current monitoring has been established as being able to detect such faults without requiring access to the motor [3]. Depending on the severity and importance of the fault, a model-free Fault Detection System (FDS) has to take appropriate actions [4]. FDS structure is shown in Figure 11.

Figure 11: Structure of a model free fault detection system

The faults can be categorised with different levels of urgency (for instance: caution; warning; or, alarm) and system responses.

Figure 12a illustrates the general idea of the model-based methods and Figure 12b shows an expert system approach. This can be used to generate residuals and allow detection of changes in the system behaviour and lead to fault detection and possible diagnosis. This will represent the knowledge of a human expert by classifying a sequence of rules from which conclusions can be made. This could consist of simple *if* and *then* statements [5].

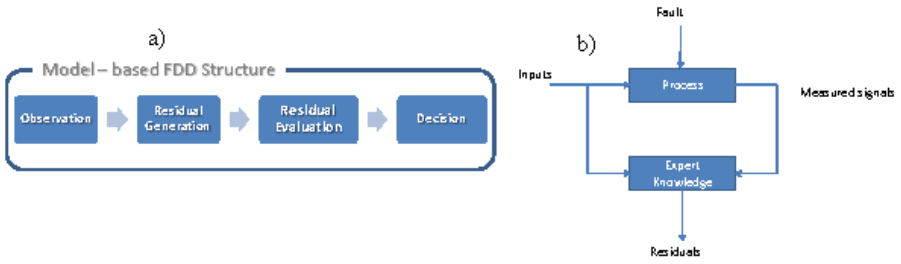

Figure 12: (a) Model-based FDD structure and some of the methods [6] (b) Expert system approach [6]

Other model-based fault detection mechanisms have also been reviewed and will be tested in future work, for instance using system identification and Kalman filters [7] [8]. The use of the Kalman filter supports estimations of past, present and future states, even when the exact parameters of the modelled system are unknown.

4.2 Faults in brake system

Figure 13 demonstrates some of the possible fault-tree of the brake system. The red blocks represent faults within the three-phase system, such as three phase supply and motor. These faults can mostly be detected and diagnosed by using model-based FDD methods and current signature analysis (CSA). The blue blocks are the faults that could happen within the hydraulic part, such as gear pump and its surrounding parts. As the gear pump is considered as a load for the motor, therefore it is likely that some of the faults that are found in the gear pump and the hydraulic pipes will be detectable. The green blocks indicate processes that are unlikely to be detected using CSA. Further instrumentation is required to monitor these parts of the system, which involve the physical engagement of the brake discs.

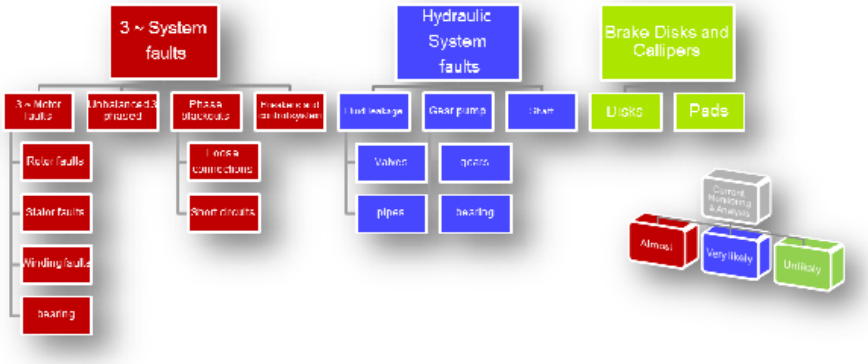

Figure 13: Some of the possible braking system faults and their likelihood of detection by CSA

4.3 Modelling and FDD methods

Modelling can be used as a facility to develop designs or improve control algorithms. It also provides a better way of understanding particular system behaviours. However, modelling

has its limitations; an acceptable model will lead to valuable outcomes and conclusions [9]. Having an appropriate model will enable faults to be introduced in simulation without damaging the physical system [10]. Figure 14 demonstrates the process of the system modelling.

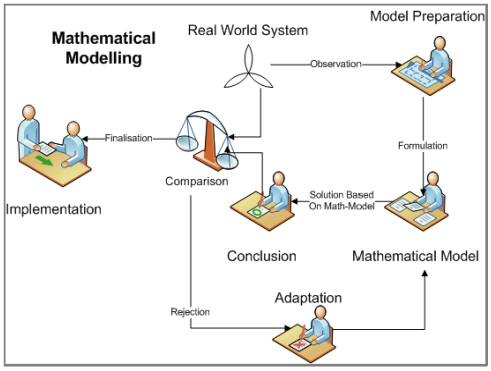

Figure 14: Process in system modelling [9]

For the purpose of modelling the brake system, following subsystems were considered:

- Three-phase power supply including contractor and circuit breaker
- Three-phase asynchronous motor
- Gear pump and the existing hydraulic pressure
- Sensors and control signals

Some parameters, such as pressure and shaft speed within the hydraulic system, were not measured during the trial experiment but the fault-free results and the manufacturer information have led to achieve a practical simulation procedure. Simulink and the SimPowerSystems toolbox have been used for modelling [11].

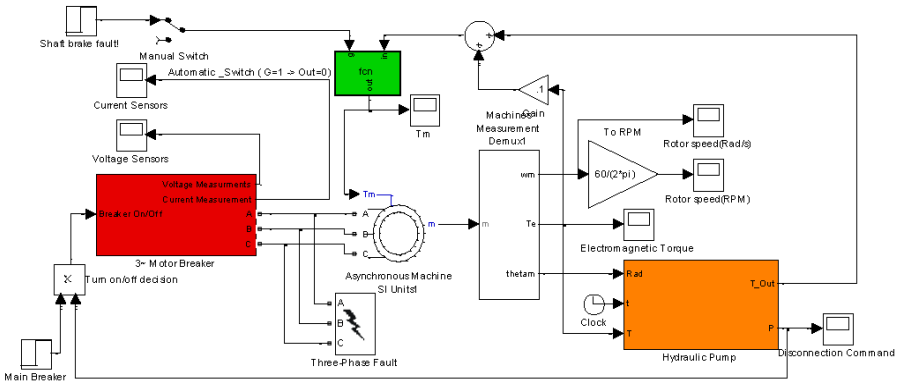

Figure 15: Model of the hydraulic brake system

The behaviour of the gear pump has been simulated via an embedded function and applied to the motor shaft torque.

A fault-free situation was carried out; the results and its signal analysis were used first to improve the subsystem parameters, and then to check the model. Figure 16 (a) and (b) illustrate the most recent output of the simulation that closely matches the field measurements.

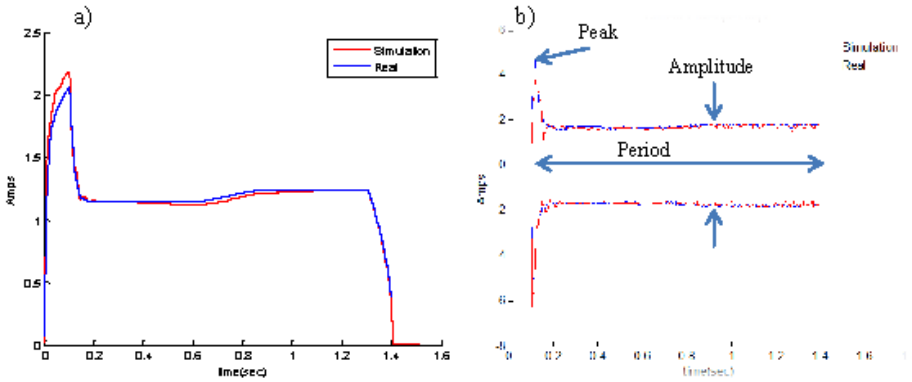

Figure 16: (a) Current (0.1s moving RMS) comparison (b) Current envelope of the Simulation vs. Real data and their categorisation

The condition monitoring procedure can be carried out by splitting the signal into different segments and in conclusion the comparison of the real signal measurements and the free-fault situation will lead to online fault detection. Simulation of the fault and applying the result into the main FDD system can assess the ability of the algorithm to diagnose the failures. Peaks, envelope assessments and the period of the event are used for classifying the pumping events, demonstrated in Figure 16b. the resulting spectrogram for the simulation which illustrates the similar effects is shown in Figure 17.

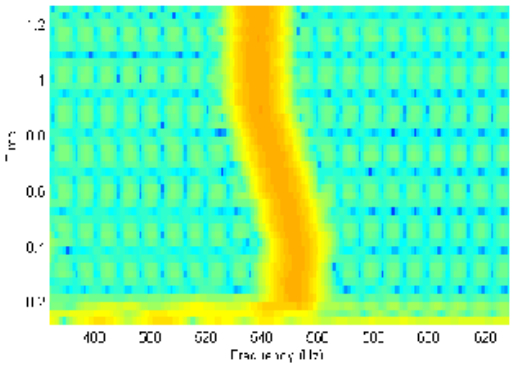

Figure 17: Zoomed spectrogram of the simulated results

Any changes within these segments can be considered as a fault and then further FDD approaches will be applied to diagnose the fault. For further improvements in the fault detection process, the total RMS values of every five cycles of the signal are compared.

Leakage in the hydraulic system is one of the common failure modes [12], the consequence of a leakage in the brake system is that there is a reduction in pressure within the hydraulic pipes and therefore an increase in motor operation time to get to the desired pressure. The results of this failure can be observed in Figure 18. The difference between the new results and the fault-free data can be considered as a fault. Further approaches and appropriate analyses will be applied for diagnosis purposes.

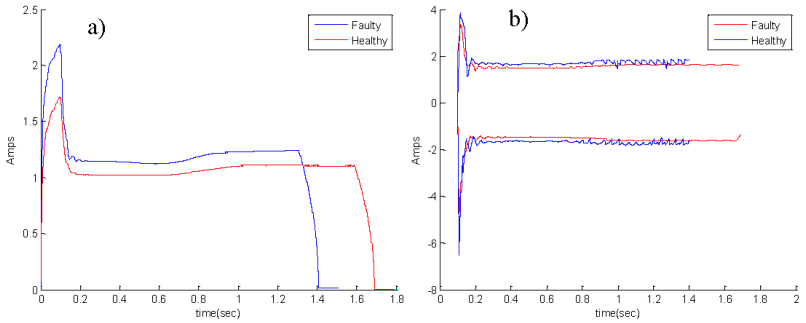

Figure 18: the possible faulty situation due to a leakage (a) total RMS measurement (b) envelope assessments

5 Future work and conclusion

An experimental condition monitoring system on the NM750 wind turbine brake system was constructed for the purpose of development of the further requirements for the advanced fault detection and diagnosis stages. The results of the experiment have led to the implementation of an acceptable model, the testing of a few failure modes, and the study of different FDD mechanisms. It has been mentioned that the current measurements cannot be applied for the FDD in some part of the system. To overcome this, a non-contact temperature and displacement measurements of the disc pads and callipers will be considered for further studies and finally investigating the possible improvement in the FDD algorithms. Shaft and wind speed will be applied in the next stages of performance monitoring of the brake system. The final phase will involve a whole wind farm.

Acknowledgements
We thank the CRES, AVN and SIME Industries for the provided information and support.
This project is partially funded by the European Commission FP7 project NIMO.
www.nimoproject.eu

References

[1] (2003, Jul.) The Danish Wind Industry Association (DWIA). [Online]. http://guidedtour.windpower.org/en/tour/wtrb/safety.htm

[2] E. Mohamed and B. Hachemi, "A Review of Induction Motors Signature Analysis as a Medium for Faults Detection," *IEEE Tran. on Industrial Elec.*, vol. 47, no. 5, pp. 984-993, Oct. 2000.

[3] G. Kliman and J. Stein, "Induction motor fault detection via passive current," in *Int. Conf. Electrical Machines*, Cambridge, 1990, pp. 13-17.

[4] B. Lu, Y. Li, X. Wu, and Z. Yang, "A review of recent advances in wind turbine condition monitoring and fault diagnosis," *IEEE Conf. on Power Elec. & Machines in Wind Apps.*, p. 1, Aug. 2009.

[5] E. Styvaktakis, M. H. J. Bollen, and I. Y. H. Gu, "Expert System for Classification and Analysis of Power System Events," *IEEE Power Engineering Review*, vol. 17, no. 2, pp. 423-428, Apr. 2002.

[6] Z. Hameed, Y. S. Hong, Y. M. Cho, S. H. Ahn, and C. K. Song, "Condition conitoring and faul detection of wind turbines and related algorithms: A review," *Renewable and Sustainable Energy Reviews*, vol. 13, no. 1, pp. 1-39, Jan. 2009.

[7] J. Rose and I. A. Hiskens, "Estimating wind turbine parameters and quantifying their effects on dynamic behavior," *IEEE Pow. & Energy Soc. Gen. Meeting*, p. 1, Jul. 2008.

[8] F. Karami, J. Poshtan, and M. Poshtan, "Model-Based Fault Detection in Induction Motors," *IEEE International Conf. Control Applications*, pp. 1957-1962, Sep. 2010.

[9] F. R. Giordano, W. P. Fox, S. B. Horton, and M. D. Weir, *A First Course in Mathematical Modeling*, 4th ed. Belmont, USA: Cengage Learning, 2009.

[10] B. Liang, B. S. Payne, A. D. Ball, and S. D. Iwnicki, "Simulation and fault detection of three-phase induction motors," *Mathematics and Computers in Simulation*, vol. 61, no. 1, pp. 1-15, Nov. 2002.

[11] K. L. SHI, T. F. CHAN, Y. K. WONG, and S. L. HO, "MODELLING AND SIMULATION OF THE THREE-PHASE INDUCTION MOTOR USING SIMULINK," *Int. J. Elect. Enging. Educ*, vol. 36, p. 163–172, 1999.

[12] A. Yazdanpanah Goharrizi and N. Sepehri, "A Wavelet-Based Approach for External Leakage Detection and Isolation from Internal Leakage in Valve-Controlled Hydraulic Actuators," *IEEE Transaction on Industrial Electronics*, vol. PP, no. 99, p. 1, Nov. 2010.

Appendix C - PHM society doctoral consortium

phmsociety

Distributed Fault Detection and Diagnosis for Wind Farms

PHM 2011 Annual Conference
Montreal, Quebec, Canada
September 25-29, 2011

Mani Entezami
School of Electronic, Electrical & Computer Engineering
University of Birmingham
Dr Stuart Hillmansen, Prof Clive Roberts

UNIVERSITY OF BIRMINGHAM

Background

Since 1980, progress in electrical, mechanical and control engineering has continued to drive enhancements within the wind energy industry. This results in more powerful and efficient components, such as large towers and blades. Analyses of wind farm maintenance costs show that up to 40% of the outlay is related to unexpected component failures that lead to costly unscheduled maintenance. Wind farm operators constantly aspire to minimise these expenses.

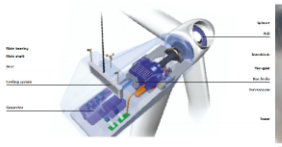

NEG MICON 750KW
Wind Turbine

The consequences of not having a proper health monitoring system for the gearbox oil temperature

Aim

To develop a Condition Monitoring System (CMS) for wind turbines that predicts critical, and detects incipient failures. The benefit will be advanced-failure detection which results in better planned maintenance, shorter downtimes and decreased revenue losses. Furthermore, this could either be used to enhance safety or achieve a more affordable level of safety.

Objectives

- Initial review of wind turbine failure modes and faults, and identification of suitable sub-systems for the latter case studies.**(A)**
- Develop a model for a wind turbine and the specified sub-system to enable FDD algorithms to be tested with simulated faults. **(B)**
- Develop a requirements specification for a wind farm condition monitoring system, based around a distributed embedded system.**(C)**
- Improvement in the model using the trial tests on the turbine.**(D)**
- Extend the model to consider multiple wind turbines in a wind farm. Assess the simulation to improve the efficacy of the algorithms. **(E)**

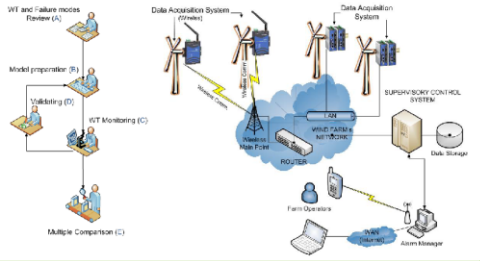

Acknowledgments

I would like to thank PHM Society for organising such an event and sponsorship. I would also like to thank Railway Research Group at University of Birmingham for their friendship and constant support. This project is partially funded by the European Commission FP7 project NIMO. (www.nimoproject.eu)

Work to Date

(A) Mechanical Brake System and possible Faults

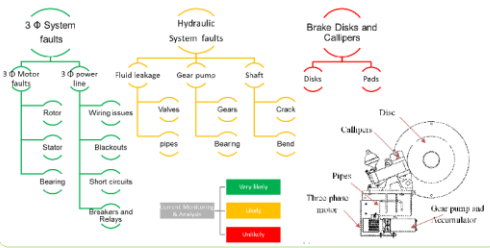

(B) System Modelling and Fault Detection and Diagnosis approaches

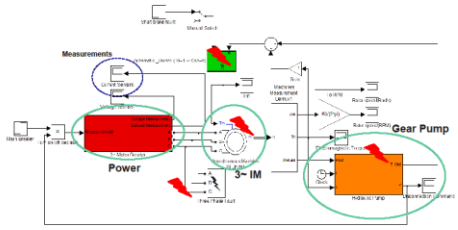

(C) Embedded Data Logger

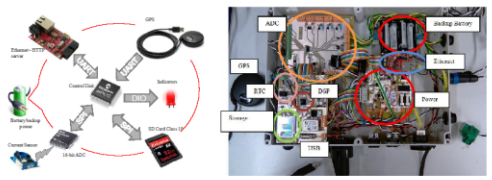

(D) Preliminary Analysis and Feedbacks

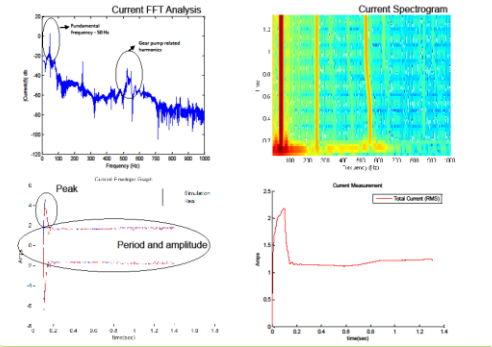

For more information, please contact

Annual Conference of the Prognostics and Health Management Society, 2011

Distributed Fault Detection and Diagnosis for Wind Farms

Mani Entezami[1]
Supervisors: Dr Stuart Hillmansen[1] **and Prof Clive Roberts**[1]

School of Electronic, Electrical and Computer Engineering, University of Birmingham, Birmingham, West Midlands B15 2TT, United Kingdom

ABSTRACT

Analyses of wind farm maintenance costs show that up to 40% of the outlay is related to unexpected component failures that lead to costly unscheduled amendments. Situations involving major failures of the braking system or the gearbox may result in catastrophic damage, jeopardising investments, reputation and the certainty of wind energy. Early fault detection by carrying out regular inspection of the system components helps to prevent and minimise the number of major breakdowns. This project will address the problem of automatic detection and diagnosis of faults within wind farms. The central thesis to be tested is that spatially correlated data, from the monitored assets within each turbine, can be used to improve the efficacy of fault detection and diagnosis algorithms. The benefit will be advanced-failure detection, resulting in superior planned maintenance, shorter downtimes and decreased revenue losses. This could also be used to either enhance safety or achieve a more affordable current level of safety.

1 INTRODUCTION

The project involves wide research, cooperation within the industry, plus sharing information and experiences to obtain detailed features of the trial products that will be designed to fulfil the requirements set by the wind energy industry. This involves collecting real samples from wind farms, as well as modelling and analysing the system. In order to proceed, investigation of the significant failures within the system and focusing on a particular sub-system and its related faults are required. Furthermore, specifying a suitable condition monitoring system (CMS) and fault detection and diagnosis (FDD) methods for operational turbine parts is being studied and executed. Subsequently, laboratory based simulations and evaluations will also be conducted to provide trial demonstrations under customary conditions. Consequently, comparison of the data being collected from a wind farm will be used to improve the FDD methods.

2 AIMS AND OBJECTIVES

The proposed work will be delivered through the completion of several well defined objectives:

- A general review of the FDD literature. To include model based approaches, parameter estimation and other pertinent methods.
- Develop a model for a wind turbine to enable FDD algorithms to be tested with simulated faults.
- Extend the model to consider multiple wind turbines in a wind farm. Assess the simulation in order to improve the efficacy of the algorithms.
- Develop a requirements specification for a wind farm condition monitoring system, based around a distributed embedded system.
- Determine the performance of the CMS during field trials.

3 CURRENT PROGRESS

As a part of a European Framework 7 project, Novel Integration Condition Monitoring of Wind Turbines (NIMO) [1], the opportunity of condition monitoring of the braking system is being considered in this thesis. In most countries, wind turbines are required, by law, to have two independent fail-safe brake mechanisms to stop the turbine promptly when required, especially with regards to over-speed control.

3.1 Brake System Health Monitoring

Figure 1 illustrates the mechanical brake system and the parts that will be monitored. Active hydraulic power, provided by the pump, is used periodically to maintain the pressure in the accumulator to release and keep the pads off the brake disc. At this stage the CMS of the three-phase pump has been carried out.

Appendix E - IET conference poster

Distributed Fault Detection and Diagnosis for Wind Farms

UNIVERSITY OF BIRMINGHAM

Mani Entezami
Dr Stuart Hillmansen, Prof Clive Roberts
School of Electronic, Electrical & Computer Engineering
University of Birmingham

Background

Since 1980, progress in electrical, mechanical and control engineering has continued to drive enhancements within the wind energy industry. This results in more powerful and efficient components, such as large towers and blades. Analyses of wind farm maintenance costs show that up to 40% of the outlay is related to unexpected component failures that lead to costly unscheduled maintenance. Wind farm operators constantly aspire to minimise these expenses.

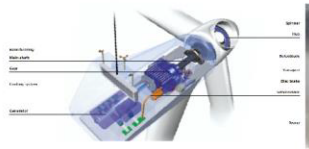

NEG MICON 750KW Wind Turbine

The consequences of not having a proper health monitoring system for the gearbox oil temperature and the brake system

Aim

To develop a Condition Monitoring System (CMS) for wind turbines that predicts critical, and detects incipient failures. The benefit will be advanced-failure detection which results in better planned maintenance, shorter downtimes and decreased revenue losses. Furthermore, this could either be used to enhance safety or achieve a more affordable level of safety.

Objectives

- Initial review of wind turbine failure modes and faults, and identification of suitable sub-systems for the latter case studies.**(A)**
- Develop a model for a wind turbine and the specified sub-system to enable FDD algorithms to be tested with simulated faults. **(B)**
- Develop a requirements specification for a wind farm condition monitoring system, based around a distributed embedded system.**(C)**
- Improvement in the model using the trial tests on the turbine.**(D)**
- Extend the model to consider multiple wind turbines in a wind farm. Assess the simulation to improve the efficacy of the algorithms. **(E)**

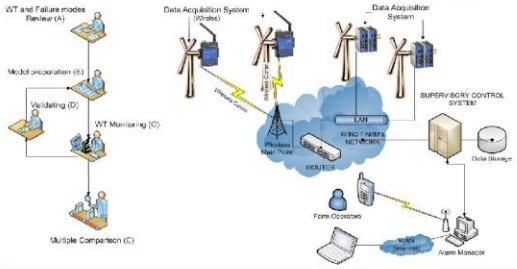

Acknowledgments

I would like to thank the IET for organising such an event. I would also like to thank Railway Research Group at University of Birmingham for their friendship and constant support. This project is partially funded by the European Commission FP7 project NIMO. (www.nimoproject.eu)

Work to Date

(A) Mechanical Brake System and possible Faults

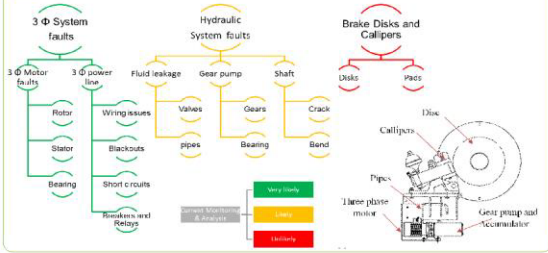

(B) System Modelling and Fault Detection and Diagnosis approaches

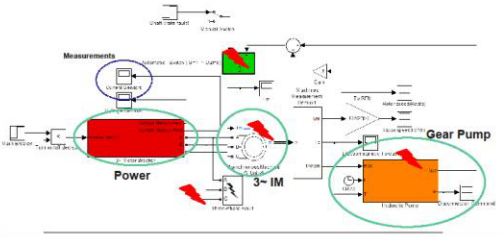

(C) Embedded Data Logger

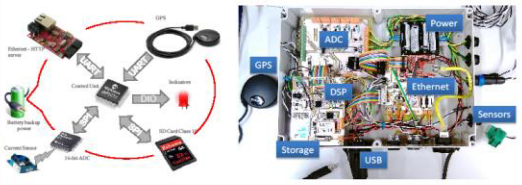

(D) Preliminary Analysis and Feedbacks

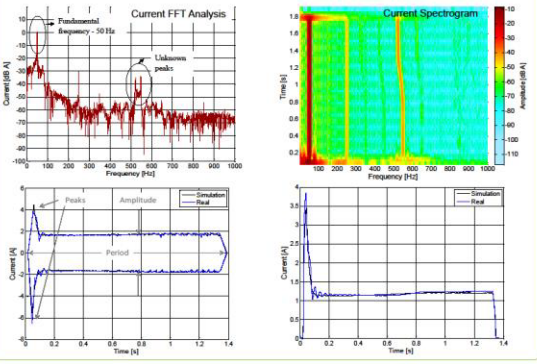

For more information, please contact
Mani Entezami at

Appendix F - MEG III conference poster

UNIVERSITY OF BIRMINGHAM

Condition Monitoring of Wind Turbine Brake Systems

Background

Since 1980, progress in electrical, mechanical and control engineering has continued to drive enhancements within the wind energy industry. This results in more powerful and efficient components, such as large towers and blades. Analyses of wind farm maintenance costs show that up to 40% of the outlay is related to unexpected component failures that lead to costly unscheduled repairs. Wind farm operators constantly seek to minimise these expenses.

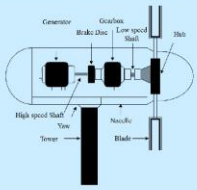

Typical Horizontal-Axis Wind Turbine

A brake failure on a Wind Turbine in Ardrossan

Wind Turbine Brake Systems

It is essential for wind turbines to stop operating in the case of failure of critical components and, importantly, at wind speeds over a critical limit. Failure to brake the wind turbine rotation may result in loss of whole structure . The three main types of braking system are: aerodynamic, mechanical and electrical.

NEG MICON 750 blade tips

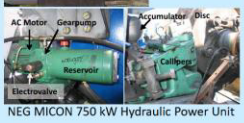

NEG MICON 750 kW Hydraulic Power Unit

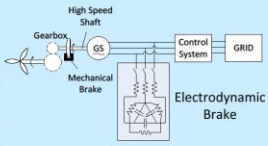

Electrodynamic Brake

Aim

This work addresses the problem of automatic detection and diagnosis of faults within wind turbine brake systems using a three-phase motor as a sensor. A non-intrusive method of monitoring three phases, using low cost current transformers, has been carried out. Moreover, the analyses of existing shaft speed measurements, already provided by the wind farm operator, have been performed to analyse the performance of the brakes and detect structural faults within blades.

Acknowledgments

I would like to thank the MEG for organising such an event. I would also like to thank Railway Research Group at University of Birmingham for their friendship and constant support. This project is funded by the European Commission FP7 project NIMO (www.nimoproject.eu).

Faults and Fault Detection Methods

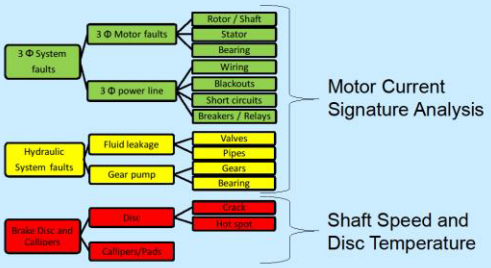

Data Logger and Modelling

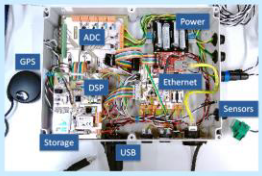

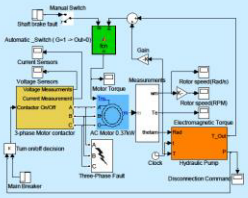

Analysis and Results

Measured Current Data

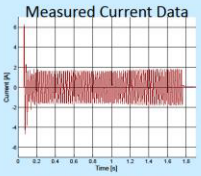

Current FFT Analysis

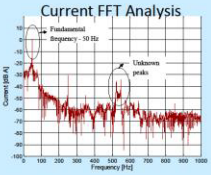

Envelope Analysis

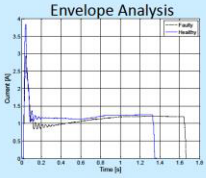

Current Spectrogram

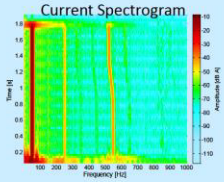

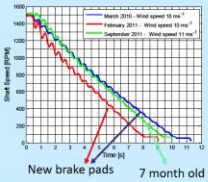

New brake pads

7 month old brake pads

Natural Frequency Analysis

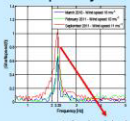

A faulty blade tip

Mani Entezami
Dr. Stuart Hillmansen, Prof. Clive Roberts

SEVENTH FRAMEWORK PROGRAMME NIMO